An investigation of finite element model updating of the Pioneering Spirit

Arthur Schout

Technische Universiteit Delft

Cover image: The Pioneering Spirit during the removal of the Brent Delta platform weighing in at 24,000 tons, at the time the heaviest single lift ever performed. Part of the structural model is superimposed, this model is used to predict the structural behavior of the vessel. *[images from Allseas]*

An investigation of finite element model updating of the Pioneering Spirit

by

Arthur Schout

to obtain the degree of Master of Science
at the Delft University of Technology,
to be defended publicly on Monday August 27, 2018 at 16:00.

Student number:	4025415	
Project duration:	October 16, 2017 – August 27, 2018	
Thesis committee:	Prof. dr. ir. M.L. Kaminski	TU Delft
	Dr. ir. P.T.L.M. van Woerkom	TU Delft
	Ir. R.W. Bos	TU Delft
	Ir. F. Rodenburg	Allseas, Daily supervisor
	Ir. T. van der Horst	Allseas, Daily Supervisor

This thesis is confidential and cannot be made public until August 27, 2023.

An electronic version of this thesis is available at `http://repository.tudelft.nl/`.

Abstract

Correctly predicting the structural behavior of the Pioneering Spirit is vital for ensuring the structural integrity of the ship and the cargo. A detailed finite element model is used to predict the structural behavior of the Pioneering Spirit. The finite element method is based on fundamental principles in solid mechanics. However, when using finite element models considerable differences between the predicted and observed behavior of a structure can occur, even when best industry practices are used to create such models. Because of these differences there is a need to validate the detailed finite element model of the Pioneering Spirit.

Finite element model updating is a method that can validate finite element models. In this method the discrepancy between the measured behavior and the observed behavior is minimized by modifying model assumptions and parameters. Currently a number of sensors is installed on the Pioneering Spirit, which can be used to find the measured behavior. Whether or not the measured behavior is detailed enough to be used in the validation of the finite element model is the subject of this research.

To investigate this a simplified finite element model of the Pioneering Spirit was created using beam elements, this model provides the predicted behavior. Then sensitivity-based finite element model updating was implemented and applied to the beam model. Simulated measurements were used to show that the beam model can be updated using the current sensor setup. When actual measurements were used to update the beam model it was found that the beam model does not correlate with the measured behavior, making it impossible to update the beam model in a meaningful way.

The detailed model does correlate with measured behavior. By assuming that the method will work similarly for the detailed model as it did for the beam model, it can be concluded that the detailed model can be validated using the current sensor setup for a static case. For a dynamic case this is not possible.

Acknowledgement

I want to thank Allseas for providing me with the opportunity and resources to conduct this research project. I want to thank my supervisors Freek and Tim for their support, advise and readiness to answer my questions throughout the project. Finally I want to thank my family and friends for their support.

Arthur Schout
Delft, August 2018

List of Figures

List of Tables

Contents

"La dernière chose qu'on trouve en faisant un ouvrage, est de savoir celle qu'il faut mettre la première."

Blaise Pascal

1 Introduction

In this chapter the motivation for conducting the research in this thesis is presented. Then the problem formulation is given as well as the approach to solve this problem. Finally the outline of the thesis is given.

1.1. Motivation

In all industries there is a constant drive to improve products and lower the cost of production. To achieve this goal two approaches can be distinguished; improve the current operations with incremental innovations or come up with a radical new way of operating that fundamentally changes and significantly improves the operations of an industry. The latter approach is intrinsically more risky, no matter how thorough a concept is thought through on paper, unforeseen upheavals during the execution are unavoidable. Once the initial upheavals have been resolved the rewards of this approach are greater due to the considerable competitive advantage of the new concept. It is through these radical ideas of the past that humans have been able to develop and attain their current standard of living.

The Pioneering Spirit (PS) is an example of a radically different concept in the offshore heavy lift industry. It is a ship with an unconventional shape - see cover image - and with a set of sophisticated systems allowing her to lift entire platforms in a controlled, fast and safe manner. Because of the new systems and unconventional shape of the ship new procedures have been and are being developed to guarantee safe operation of the PS at all times.

One of the critical aspects during lifting and transporting a platform is the structural integrity of the ship and the platform. Platforms are designed to withstand their self-weight and environmental loads, however, when transported by the PS they have to withstand additional transport loads. And as a results additional reinforcements - solely for transport - are needed. These transport loads are caused by motions of the supports of the platform during transit. One can distinguish two types of loading; loads due to accelerations of the supports and loads due to the relative motion between the supports. The accelerations are caused by a combination of the the rigid body motions and the deformations of the ship. The relative motion between the supports is only due to ship deformations. The rigid body motions of a ship in deep-water waves can be predicted accurately using potential theory, for which several commercial software packages are available. The prediction of ship deformations in waves is more challenging. A hydro-elastic approach would be most appropriate, whereby the fluid loads and structural deformations are coupled. However, this is still an active field of research and no standard approach is available that can accurately solve the fully coupled hydro-elastic problem[15]. An approximate approach - called hydro-structural - is easier to apply. It assumes no coupling between the fluid forces and the structural deformations and fluid loads are determined for a rigid ship which are quasi-statically applied to the ship. This is the approach that is currently used to determine the deformations of the PS in waves. Both the hydro-elastic and hydro-structural approach require an accurate structural model of the ship to produce meaningful results, a validated structural model would contribute to this.

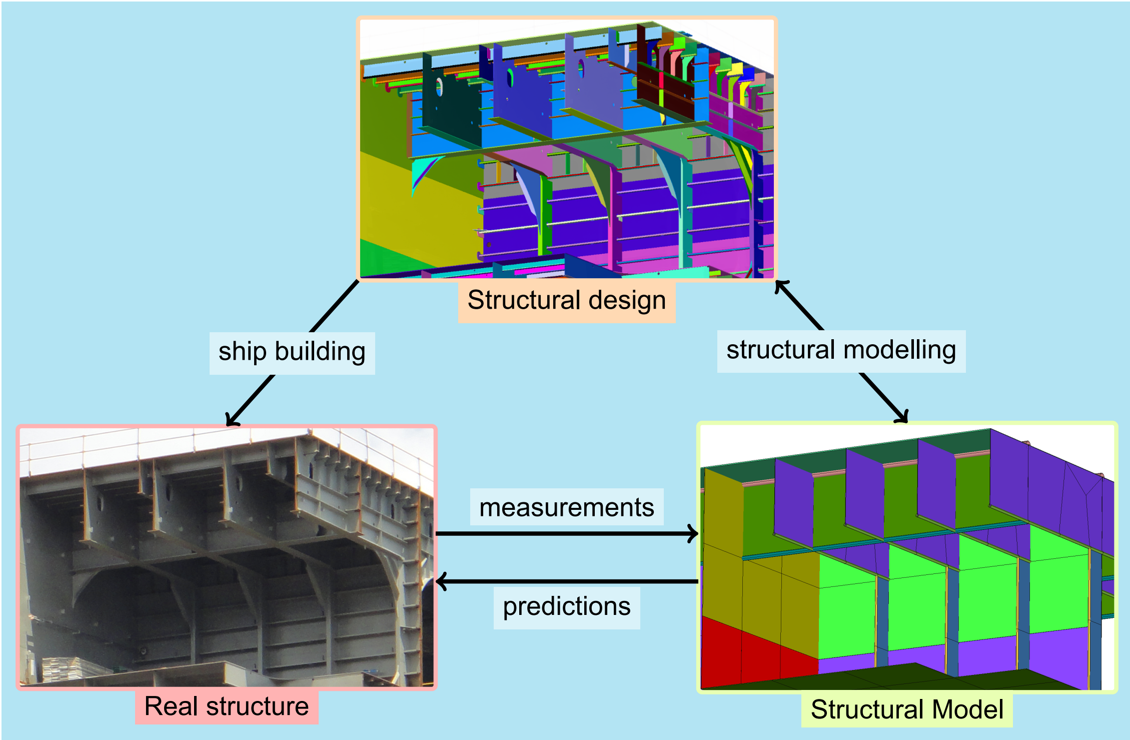

Figure 1.1: Representation of a the part of the Pioneering Spirits structure in three different fields: reality(left), structural design (top) and structural model (right) and their relations. *[images from Allseas]*

A Finite Element (FE) model of the PS is available, providing a discrete description of the mass, damping and stiffness properties of the structure. The description of the structural mass is known with confidence because of good bookkeeping of all masses within the ship. Structural damping remains difficult to assess but in general proportional damping is a good approximation for structural damping. For proportional damping the damping characteristics are determined by using a linear combination of the mass and stiffness. The structural stiffness has been modeled using techniques that are the current state of the art and using a methodology as given in guidelines of classification societies; for example the DNV guideline [14]. Without validation the stiffness will remain uncertain. This is partly due to the simplifications that are made when constructing FE models of ships. A validation of the stiffness is expected to improve the confidence in the predictions of the deformations of the ship. Which in turn leads to greater confidence in the transport loads on platforms, and possibly a reduction in the transport reinforcements on a platform.

Structural design, models and reality

Structural design, structural modeling and the actual structure are three intertwined fields explained below using figure 1.1.

What is structural design?

Creating a structural design of a ship is the art of shaping material according to the loads that should be carried. And at the same time taking into account the boundaries given by the requirements of the ship designer, the customer, classification societies and fabrication efficiency. As such the structural design of a ship is not a goal in itself, rather it serves an already available functional ship design, embodied by a general arrangement.

How to create a structural design?

In order to design a structure its function needs to be known, from there a concept design can be made which contains the following structural aspects: the topology, material choice,

initial dimensions and the joints. The structural concept is then subjected to a structural analysis. For this reasonable loadings need to be assumed, this yields a number of the structural responses. These responses are used to check whether or not the structural design has the required load carrying capacity to fulfill its functions. An actual design process involves the execution of these steps several times in a so called design spiral, whereby each step further refines the structural design.
There is an interplay between the structural design and the structural model, see figure 1.1, the design will be adapted if the structural model predicts failure of a component. The structural model may get more refined each iteration, and can range from simple hand calculations to analytical calculations to a detailed and complex FE model. When a satisfactory structural design has been found it is used to create a set of construction drawings, which are used in the building of the ship. During the building errors are made; welds may be missed, structural parts forgotten or misplaced. Apart form these errors inevitable misalignments are present in the build structure. Also the structural properties of a ship may change in time, for example due to fatigue. The build structure is thus different from the design. In creating a structural model of a ship simplifications are made. The previous statement holds for all model types but now the focus is on FE models, the de facto standard to study the behavior of complex structures. Simplifications are necessary to reduce the complexity of FE models of ships, observe the differences between the design/real and the model in 1.1. The simplification are made by taking into account the relevant physical behavior that the model should predict, see [14] for an overview the modeling simplifications. Apart from simplification on the structural model, simplifications are made for the highly complex hydro-mechanical loading. Any FE model can contain errors, the larger the model the greater the chance of errors and the more difficult to detect errors. On top of that the structural model is mostly based on the structural design which is different from the actual structure. As a result there is considerable uncertainty in the predictions of a structural model, and a need arises to validate a structural model. This can be done by comparing the behavior of the real structure and the structural model, such a comparison will most likely indicate a disparity between the two. Now the idea is that the disparity can be reduced by altering the properties of the structural model. How to reduce this disparity is what is the subject of this thesis, and in particular its application to the Pioneering Spirit. The goal of this research is thus to investigate the validation of the stiffness of the Pioneering Spirit.

1.2. Formulation of the problem and approach

To validate a numerical method like the finite element method the predicted behavior is compared to observed behavior of the modeled structure[1]. The observed behavior is extracted from experimental data, this data can come from two sources: a small-scale model test or full-scale measurements. The difference between the predicted and observed behavior is called the residual, and it can be a goal on its own to conclude that the structural model is valid by checking the magnitude of the residual. If the residual is large it is often desirable to alter the structural model in such a way that its behavior is consistent with the experimental behavior. Such techniques use a parametric description of the model; the predicted behavior is a function of a set of parameters. These parameters are altered until the residual is minimized, if this is the case the resulting model is updated. The predicted behavior of the updated model is then compared to measured behavior not used when updating the model. If the predicted behavior of the updated model is better than the initial model, the updated model is considered validated. This is the approach that will be used in this research.

Validation of a structural model by using measurements is a form of system identification and more particular the subfield of Structural-Identification (St-Id). St-Id aims to improve physics based models of structures using measurements to bridge the gap between the observed static or dynamic behavior and the predicted behavior. It does this by estimating physical parameters of a model, this makes it an inverse problem. In general it can be said that there is no single solution to an inverse problem, and in many cases the problems are ill-

[1]Comparing the results of a numerical method to the solution of the same analytical model is another way to validate a numerical model, however, this is limited to simple geometries.

posed and no solution may exist at all. Apart from that the problems may be ill-conditioned, resulting in a solution that is sensitive to small changes in the data. This together with the inherent errors - from various sources - present in models and measurement data make St-Id a challenging task. One method of St-Id is Finite Element Model Updating (FEMU), this is a technique that can be used to validate a Finite Element model. It is a well-known technique and it has been implemented in commercial software packages.

For the validation of a structural model experimental data is needed, in case of the PS the experimental data comes from a number of strain gauges and accelerometers that are already mounted on the ship. Whether or not a model can be validated meaningfully depends - among others - on the richness of the measured data [12], which is related to the number and the position of the measurements.

The question now arises whether or not the structural model of the PS can be validated with the current sensor setup. The research question may be posed as:

Can finite element model updating be used to validate the structural stiffness of the Pioneering Spirit using the current sensor setup?

To answer this question FEMU could be applied to the available detailed FE model of the Pioneering Spirit. The detailed model is implemented in a commercial FE-software FEMAP, applying FEMU to this model requires extensive interaction with FEMAP. Also it will be computationally expensive; FEMU requires multiple matrix manipulations to find a solution, and the matrices for the FEMAP model are large. Instead of using the FEMAP model a simplified model could be used. This would considerably lower the computational cost and implementing FEMU would be easier since no interaction with FEMAP is required. To more easily apply FEMU and to reduce the computational cost it was decided to use a simplified FE model. This model should be able to model the observed behavior of the PS. It is assumed that the observed behavior from the sensors is the global behavior. For the dynamic behavior this assumption seems reasonable, for most structures only the first few vibration modes contribute significantly to the response. For the static behavior this assumption is more debatable since the static loading can vary greatly from one location to the other.

After constructing the simplified model it is checked whether or not it can model the global behavior of the ship. Then the simplified FE-model is then used to implement the FEMU methods, these methods are first tested on a simple cantilever beam to verify that implementation is correct. When the implementation has been verified the simple ship model will be used for updating. The updating can be done for two cases: one set of measurements which captures the static behavior of the ship, and a second set of measurements that captures the dynamic behavior of the ship. Before actual measurements will be used, simulated measurements are used in order to check if the method works for this geometry as well.

In summary the following research approach will be used:

1. A simplified FE model that is capable of modeling the global behavior of the structure accurately is constructed.

2. FEMU is implemented and is first applied to a simple test problem to verify the code and understand the concepts in FEMU. The effects of sensor noise, the number of measurements and the locations of measurements are investigated.

3. Using simulated data the simplified beam model is updated.

4. The simplified model is updated to the actual measured data, both for the static and the dynamic case.

The finite element method is a numerical method and after setting up a problem a linear set of equations - in the form of a matrix equation - is found. Solving these matrix is a task which computers are particularity good at, and in this thesis the linear algebra software `MatLab` is used. The FE-model and FEMU methods have been implemented in this software.

1.3. Thesis outline

In chapter 2 the theory applied in this research is given, it consists of two sections. In the first section FEMU is discussed. In the second section some important topics of structural analysis are explained, as well as some assumptions of the models in this thesis. In chapter 3 the theory of chapter 2 is applied to a test case; the cantilever beam. The results are presented and discussed, by doing so this chapter elucidates the FEMU concepts presented in chapter 2. Then in the first part of chapter 4 the beam model of the ship is explained, and then FEMU is applied to this model. The results of this are presented and discussed. In chapter 5 a summary of this thesis is given, the research question is answered and the recommendations are presented.

"Strain and Stress are two universal concepts - everybody understands them, but nobody knows which one comes first."

Unknown

2 Theory

In this chapter the theory used in this research and some modeling assumptions are discussed. The theory presented here is not new, but shows what theory was mastered during the research and it makes this thesis a self-contained document. The chapter is divided in two sections, the first section deals with FEMU and in the second section the structural modeling techniques are explained. To aid the understanding several figures have been created to visually explain some concepts.

2.1. Model updating

In this section the relevant FEMU theory will be explained. Starting with a definition of FEMU and putting it in the context of the larger field of system identification. Then models and models spaces are discussed, a fundamental concept in FEMU. Next a few FEMU methods are explained and the most suitable method is chosen. After which relevant topics on errors are discussed including: model errors and measurement error. In the rest of this section concepts pertaining to the sensitivity-based FEMU method are discussed: parameters, sensitivities, the objective function, the updating procedure and - to finish - poor results in FEMU.

2.1.1. FEMU definition

Finite element model updating is a method that tunes a model to experimental data, by reducing the difference between the predicted and observed behavior. By updating a finite element model one aims to reduce the errors present in the model, resulting in a model with a behavior that more closely resembles the real/physical system. When a model is successfully updated - that is its behavior is closer to reality - the model can be considered as being validated, see 2.3 for an overview. FEMU is part of the field of science called system identification and for a proper understanding of the uses and limitations of FEMU an understanding system identification is necessary.

2.1.2. System Identification in Structural dynamics

In this section the limits of system identification in the field of structural dynamics are discussed, relying mostly on the analysis presented by Berman in [3]. According to Berman, the goal of structural system identification is to obtain a model of a structure that is representative of the physical characteristics (E-modulus, dimensions, masses etc.) and the dynamic behavior. The resulting model can be thought as validated, and may be used to predict the behavior of the system in conditions not present in the measured data. In short system identification aims to cast measurements of physical phenomena into a representative mathematical model.

It would be most convenient to obtain a model from using measurement data only. Berman proved that it is not possible to identify an analytical model that has physical meaning by solely using measurements. He also concluded that there are an infinite number of models

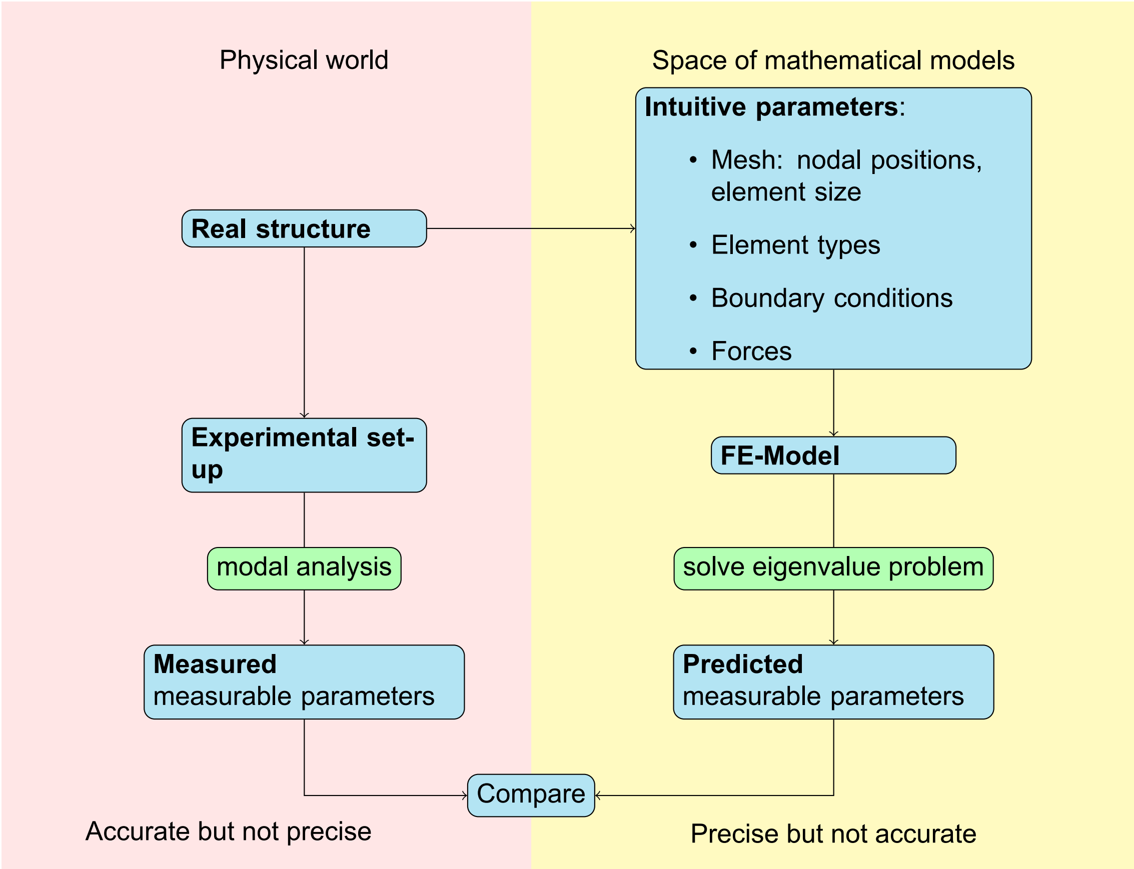

Figure 2.1: Overview of showing how real structures can be identified using an intuitive model.

that can reproduce the behavior of the measured data. Since using only measured data is not a fruitful approach to find a correct model, an alternative approach is needed. One way would be to first construct an intuitive model, based on the real structure, and then alter this model based on measurement data. In constructing an intuitive model *intuitive* parameters are used, like E-moduli and cross-sectional dimensions. These *intuitive* parameters depend on the number and coordinates of the nodes, DOF's, element types etc. of the model. The *intuitive* parameters can be determined with a high degree of precision, they may however be inaccurate due to incorrect modeling assumptions or faulty measurements on the real structure. The *intuitive* parameters that are the ones to be identified. From the measured data *measurable* parameters can be extracted, the measured data is accurate but not precise. Examples of *measurable* parameters are: the response (transient or steady-state), normal modes, natural frequencies. The question arises whether or not the *measurable* parameters can be used to identify the *intuitive* parameters. The *measurable* parameters are independent of a set of defined DOF's in the model, they depend only on the point of the measurement. These parameters are of a different class than the *intuitive* parameters, so some transformation between the two different classes of parameters is needed to compare them. In figure 2.1 an overview is shown depicting how measured parameters and intuitive parameters are compared, the direction of the arrows indicates the direction of the process which are all one-way. A transformation from one class of parameters to the other class involves either a matrix inversion, the solution of a differential equation or the solution of an eigen-problem. A transformation from *intuitive* to *measurable* parameters is possible, a transformation in the opposite direction from *measurable* to *intuitive* parameters however is not possible. One reason for this is that the *measurable* parameters are not precise due to the inherent measurement errors and the transformation from one class to the other is sensitive to noise, see example on the next page.

Berman concluded that the most promising way to identify a structural dynamic system is by altering a prior constructed intuitive model by using measured data, this conclusion has lead to the development of model updating techniques. One of these techniques, FEMU is used in this research.

Example of identifiability [3]

Identification of the stiffness matrix, $\mathbf{K}$, experimentally is not possible. However its inverse the flexibility matrix can be measured by applying a unit load at one DOF and zero at the other DOF's, this is done for all DOF's. The resulting displacement are then the entries of the flexibility matrix, $\mathbf{K}^{-1}$, for a dynamic system at zero frequency the stiffness matrix and the flexibility matrix are given by (2.1) and (2.2) respectively. In these equations ω_i^2 is the natural frequency belonging to mode shape $\boldsymbol{\phi}_i$ and $\mathbf{M}$ is the mass matrix. From this is can be seen that the flexibility matrix (2.2) is dominated by the low frequency modes, the converse is true for the stiffness matrix (2.1) it is dominated by the high frequency modes. The contribution of the high frequency modes to the entries of the flexibility matrix will be small. And for the highest modes the measurement noise is almost always greater leading to a misrepresentation of the contribution of the high frequency modes in the flexibility matrix. Although the flexibility matrix can be measured and then inverted to obtain the stiffness matrix. This is not useful since the high frequency modes are not correctly represented in the measured flexibility matrix but they are the most important modes in the stiffness matrix.

$$\mathbf{K} = \sum_{i=1}^{n} \omega_i^2 \mathbf{M} \boldsymbol{\phi}_i \boldsymbol{\phi}_i^T \mathbf{M} \tag{2.1}$$

$$\mathbf{K}^{-1} = \sum_{i=1}^{n} \frac{1}{\omega_i^2} \boldsymbol{\phi}_i \boldsymbol{\phi}_i^T \tag{2.2}$$

2.1.3. Models

In this section the model type used in this thesis is described and then a somewhat abstract description of the FEMU process w.r.t. models is given, in line with the description found in [10].

Models in this thesis.

This research deals with the validation of models that describe the behavior of structures. In the most general sense a model is: *"a description of the assumed relationship between input and output variables of a system, taking the (known or assumed) properties of that system into account"*[10]. In this research this relationship is given by a finite element model. In FE models a continuous structure is approximated by a number of lumped masses and massless elastic components. When the number components model approached infinity it is assumed that the discrete system approaches the continuous system. In practice the structural behavior that is of interest is limited to a certain frequency range, and to model this behavior accurately a limited amount of components can be used in the model. Another assumption of the models is linearity. Linearity means that if an input force is multiplied by a factor the response will be multiplied by the same factor. And summing the response of two different input forces will yield the same result as the response of the system to the two summed input forces.

Models in FEMU

In theory there are infinitely many discrete models that can describe the behavior of a structure[3], the set of all models that can describe a given structure is called S_1[1]. In FEMU a model from

[1] In theory this set is infinitely large, however this set also contains models which can not be implemented realistically, see figure 2.2. For instance models with n DOF's with $n \to \infty$. Such models are left out of S_1 leading to a bounded set of models

S_1 is picked, such a model $\mathbf{G}$ can be seen as a function that maps an input vector $\mathbf{x}$ to an output vector $\mathbf{y}$. This mapping is a function of a number of model parameters $\boldsymbol{\theta}_M$, in case of FEMU, this can be written down as in (2.3).

$$\mathbf{y} = \mathbf{G}(\boldsymbol{\theta}_M, \mathbf{x}) \tag{2.3}$$

The output $\mathbf{y}$ can contain quantities that are directly measurable from the response of the system like strains, accelerations and displacements. Or they can be derived properties like mode shapes and natural frequencies these are often useful output quantities, because they are independent of the input $\mathbf{x}$, and in some cases the input $\mathbf{x}$ to the system is not known accurately. For a clearer description the input $\mathbf{x}$ will be left out of relation (2.3).

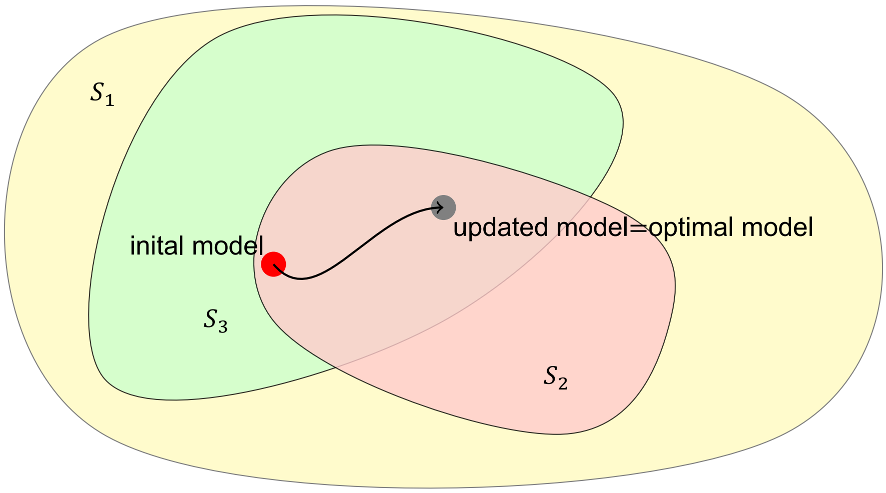

Figure 2.2: Illustration of FEMU process when the optimal model is found.

The parameters are defined by the vector $\boldsymbol{\theta}_M$, which is an element of the set $D_M \subseteq \mathbb{R}^{N_{\theta_M}}$, where $N_{\boldsymbol{\theta}_M}$ is the number or parameters. For a given parameter choice D_M defines the feasible parameters settings. Note that $\mathbf{G}(\boldsymbol{\theta}_M)$ represents not a single model, but a class of models for which (2.4) holds. This class is called S_3 and S_3 is determined by the parametrization of the model, that is the number and the type of parameters used in $\boldsymbol{\theta}_M$.

$$S_3 = \{S_3(\boldsymbol{\theta}_M) | \boldsymbol{\theta}_M \in D_M\} \tag{2.4}$$

All the possible models for a given parametrization, with $\boldsymbol{\theta}_M \in D_M$, are found in the space S_3, which is a subspace of S_1. So for each model there is a mapping from the space of the model parameters D_M to the output space $\mathbb{R}^{N_y}$ of the model.

$$S_3 : D_M \subseteq \mathbb{R}^{N_\theta} \mapsto \mathbb{R}^{N_y} : \boldsymbol{\theta}_M \mapsto \mathbf{y} = \mathbf{G}(\boldsymbol{\theta}_M) \tag{2.5}$$

In FEMU an optimal parameter vector $\boldsymbol{\theta}_M^*$ is sought that minimizes a certain objective function F, which quantifies the misfit between the model predictions $\mathbf{y}$ and the experimental data $\mathbf{d}_m$. The FEMU problem can then be cast into an optimization problem (2.6). The latter expression in (2.6) shows for a given model class S_3 and a set of experimental data, the objective function only depends on the values of the model parameters $\boldsymbol{\theta}_M$.

$$\boldsymbol{\theta}_M^* = \min_{\boldsymbol{\theta}_M \in D_M} F\left(\mathbf{y} = \mathbf{G}(\boldsymbol{\theta}_M), \mathbf{d}_m\right) = min\, F\left(\boldsymbol{\theta}_M\right) \tag{2.6}$$

The set S_1 contains another subset S_2, which contains all models which correlate well with the experimental data. One of these models with parameter setting $\boldsymbol{\theta}_M^*$ is the optimal model which gives the best description of the parameters and the behavior of the structure. It is this model that is to be found from the model with the initial parameters setting $\boldsymbol{\theta}_M^{init}$. An overview of the sets is given in figure 2.2, here the updated model and the optimal model coincide. The optimal model does not describe the true behavior of the system for reasons given in section 2.1.6.

The problem in (2.6) is often formulated as a constrained optimization problem, to take into account the range for which the parameter values are feasible. For example to limit the upper and lower bounds of the dimensions of a beam cross-section.

2.1.4. FEMU methods

In FEMU two methods are available, an overview of these methods is given below. One of these methods is used in this research.

FEMU's goal is to change the system matrices $\mathbf{K}, \mathbf{C}, \mathbf{M}$ of an prior constructed model in order to better match the observed behavior. Changing these matrices can be done in two ways: directly or iteratively[12].

Direct methods

Direct methods change the elements of the system matrices in one step to better match the experimental behavior. The updated system matrices can reproduce the measured data exactly. The measured data is contaminated by noise which is also replicated by the updated model. Using this method the solution is found in one step making it a computationally inexpensive method. However the change of the matrix elements is done without taking into account the shape functions of the elements, resulting in the lost of essential system properties like positive-definiteness and structural connectivity. As a consequence the physical meaning of the model is lost. Also no physical explanation can be found for the changes in the model, as a result it is not known what was faulty in the original model. The models found by using this method are called *representational*.

Iterative methods

In iterative methods system matrices are a function of some parameters, the response of the system is thus also a function of these parameters. These parameters can be the material properties (Poisson's ratio, Young's modulus, density, etc.) or the dimensions of the modeled system. These parameters are linked to the entries of the system matrices by the shape functions of each FE-element. As a result the physical meaning of the model remains when a parameter is changed. Also a changing parameter has a direct physical interpretation, this means that an updated model will provide insight into what was faulty in the original model. The models found by using this method are called *knowledge-based* models. One of the difficulties of this method is the selection of the parameters and to what extend the physical meaning that can be attributed to the updated parameters, this depends on the richness of information present in the measurement data.

2.1.5. Sensitivity based FEMU

Sensitivity based FEMU is an iterative method that is used in this research to validate the structural model, in this section the different elements needed in this method will be explained. Also the uses and limitations of the method will be discussed.

Sensitivity based FEMU aims to minimize the difference between measured and the predicted behavior, by changing a set of parameters that influence the behavior of the analytical model. At it's core is the solution of an optimization problem, a number of steps have to be taken to set up this problem correctly in order to find a physically meaningful solution. This solution must then be checked by comparing the model against measurements not used in the updating procedure, if the comparison is good the model is validated. An overview of the steps is given here is given in figure 2.3, showing the work flow of the sensitivity based FEMU. The steps in figure 2.3 are now explained shortly, a more detailed explanation of these steps can be found in the remainder of this chapter.

1. First the need for a better FE-model is identified and what behavior of the structure should be better modeled by the FE-model. If the need for FE-model updating is there the FEMU procedure can start.

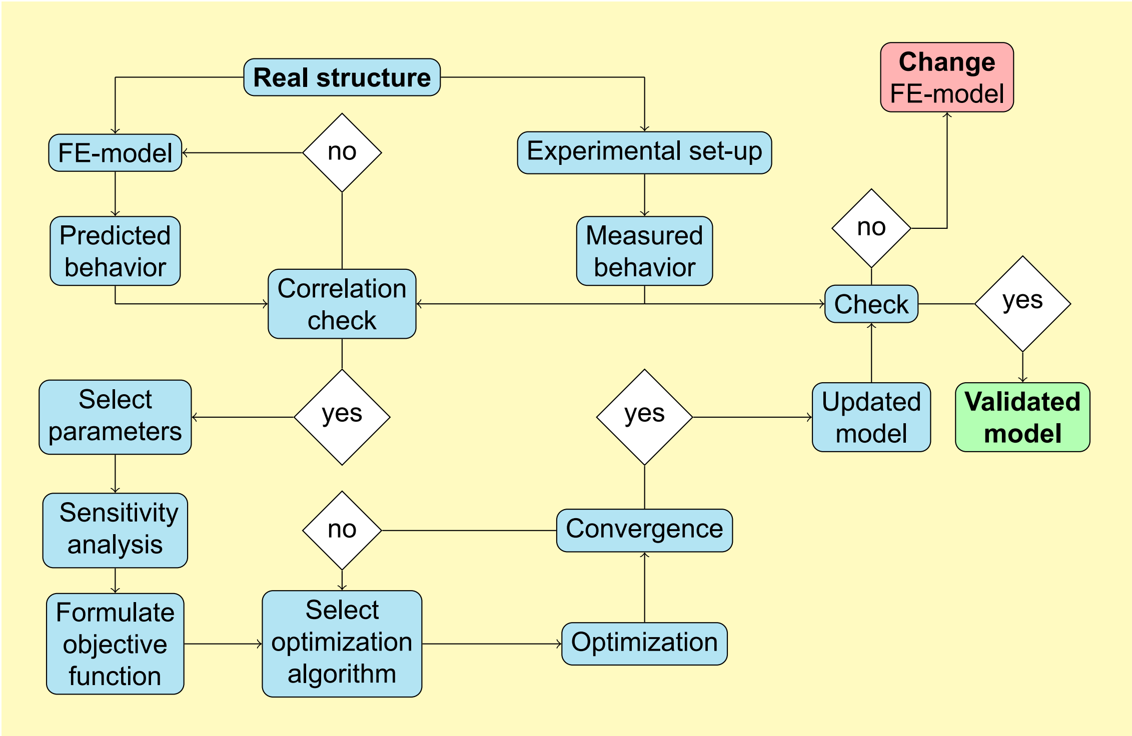

Figure 2.3: Overview showing the basic steps of the sensitivity based FEMU method.

2. Construct an initial FE-model of the structure using best practices, for ships an example of these practices can be found in [14]. This requires drawings, pictures, etc. of the structure to model it correctly. Also the behavior that needs to be captured by the model should be taken into account. The initial FE-model provides the predicted behavior.

3. A measurement setup needs to be devised, the measurement setup should be able to capture the behavior that is of interest from step 1. The experimental set-up provides the measured behavior.

4. Check for correlation between the predicted and measured behavior. If there is correlation proceed, other wise adapt the FE-model. This makes sure that S_3 and S_2 overlap.

5. Parameters are selected, these parameters can change the behavior of the FE-model. The parameters are subjected to a sensitivity study, where non-sensitive parameters are neglected. The parameterization defines S_3.

6. An objective function is formulated defining the optimization problem.

7. An optimization algorithm is selected to solve the optimization problem, if the algorithm converges an updated model is found. Otherwise select a different optimization algorithm.

8. An updated model is not necessarily a validated model. The updated model is tuned to the behavior present in the measurement data used in the updating procedure. Whether the updated model correlates well with behavior not present in the updating measurement data remains to be seen. To go from an updated model to a validated model, the predicted behavior of the updated model is compared with the measured behavior from data not used in the updating procedure. If these two behaviors correlate and the predicted behavior of the updated model is correlates better than the predicted behavior of the initial model, the updated model is a validated model. If the updated model does not correlate better, the initial model should be changed. This can be done in two ways: change the parameters of the initial model or construct an entirely new initial model. FEMU is then applied to the changed initial model.

2.1.6. FE-model errors

Adjusting the parameters of a model can lead to a better model but this is only the case when the parameters have the ability to influence the differences between the predicted and observed behavior. Other aspects of the model may be erroneous, which may not be affected by parameter changes. The different error types in an FE model are given below following the description given by Mottershead[19]:

Idealization errors These are errors that arise from the assumptions made in modeling the characteristics of a structure, and they arise from:

- *Simplification of the structure.* For example a stiffened plate is modeled by using plate elements with an effective plate thickness which represents the stiffeners. Such an assumption is accurate depending on the loading and boundary conditions.
- *Modeling of the mass.* For example when the system with a distributed mass is modeled with too little lumped masses or when the an eccentricity in the lumped masses is not taken into account.
- *Element formulation.* For example when an element is used that neglects a certain deformations, like a Euler-Bernoulli beam element that neglect transverse shear deformation.
- *Mesh connectivity.* The elements are not connected, or to the wrong node.
- *Boundary condition modeling.* For example when a assumed rigid connection is actually flexible.
- *Joint modeling.* For example when the misalignment of structural elements is neglected in the model.
- *Assumptions on the loading.*
- *Geometric shape assumptions.*
- *Linear modeling.* Using a linear model whereas the behavior of the structure is non-linear for the conditions that are studied.

Discretization errors These are errors that arise form the use of numerical methods, FEA is a numerical method and these errors are thus inherently present in the methods.

- *Too coarse model.* For example when the element size is too great to properly model the eigen-frequencies in modal analysis.
- *Truncation* For example when too little modes are taken into account in a modal description of the dynamic response.

Model parameter errors. These are errors in the parameters used in the FE model, these can come from incorrect measurements/estimates of quantities like:

- *Material properties.* Like the E-modulus, Poisson's ratio or mass density.
- *Dimensions of the structural elements.* Like the dimensions of the cross-section of a beam element.
- *Stiffnesses of springs.*

Due to these errors there is a difference between the predictions of the model $\mathbf{G}(\boldsymbol{\theta}_M)$ and the true behavior $\mathbf{d}$ of the system. This difference is quantified by the modeling error $\boldsymbol{\eta}_G$ in (2.8).

$$\boldsymbol{\eta}_G = \mathbf{d} - \mathbf{G}(\boldsymbol{\theta}) \tag{2.7}$$

It is useful to split up the model error $\boldsymbol{\eta}_G$ in two parts (2.8).

$$\boldsymbol{\eta}_G = \boldsymbol{\eta}_{er} + \boldsymbol{\eta}_\theta \tag{2.8}$$

1. $\boldsymbol{\eta}_{er}$, describes the discretization & modeling errors. This error term is hard to quantify for a model, it can be minimized by making sure the model is modeling the relevant physical phenomena with sufficient accuracy and to check the errors in the code properly. This term is not influenced by the FEMU method used in this research. For convenience called the modeling error from now.

2. $\boldsymbol{\eta}_{\theta}$, solely describes the model parameter error. It is this term that can be influenced by the parameter settings, and FEMU will try to minimize the residual by changing this term. This term will be called the parameter error from now.

The presence of the modeling error $\boldsymbol{\eta}_{er}$ implies that the true behavior of the system cannot be found using FEMU, and that the model class S_3 does not contain the one model that describes the true behavior of the system[10].

2.1.7. Experimental data

The experimental data in FEMU is obtained via measurements. Two types of measurement regimes can be distinguished.

1. Static, measurements are time-independent. Typical measured quantities are displacement and strains at certain positions of the structure.

2. Dynamic, measurements vary in time. Typical measured quantities include accelerations, strains at certain positions of the system.

The experimental data from dynamic measurements is time-dependent. Comparing the experimental behavior and the measured behavior in the time-domain is difficult since it requires exact knowledge of the input to the system at each time instance. This may be possible for a controlled laboratory experiment, but in many cases the input to the system is unknown for full-scale operational structures. And as a result it is impossible to replicate the measured behavior exactly in time using the model. An alternative way of characterizing dynamic structural systems is used. Instead of looking at the configuration of the system at each time instance dynamic systems are characterized by derived parameters like: natural frequencies, mode shapes, frequency-response-functions. These can be found using modal analysis. Modal parameters can also be determined for the FE-model, hence a comparison with the experimental data is possible. So before the experimental data from a dynamic experiment is used - in most cases - it is first transformed to a derived parameter.

Errors in the experimental data

FEMU makes use of experimental data, this data is inherently contaminated with random measurement noise and/or systematic error/bias caused by faults in the measurement devices. The raw signals coming from the measurement devices are processed, this signal processing can also lead to the introduction of errors[10]. The measurement error $\boldsymbol{\eta}_m$ is the sum of these errors, and it quantifies the difference between the measured behavior $\mathbf{d}_m$ of the structure and the true behavior of the structure $\mathbf{d}$, see (2.9).

$$\boldsymbol{\eta}_m = \mathbf{d}_m - \mathbf{d} \tag{2.9}$$

The experimental data used for FEMU should represent the actual behavior of the system [13]. The measurement error $\boldsymbol{\eta}_m$ should not reach levels which obscure the true behavior or introduce non-physical 'measurement' behavior.

2.1.8. Combining data and model errors

To quantify the total error the measurement and model error need to be combined. (2.9) and (2.8) can be rearranged and to find (2.10). From these equations it is clear that the true behavior of the system is given by the model predictions minus the model errors $\boldsymbol{\eta}_{\theta}$ & $\boldsymbol{\eta}_{er}$ on the one hand, and the measurements corrected for by the measurement error $\boldsymbol{\eta}_m$ on the other hand. An overview of the error is given in figure 2.4.

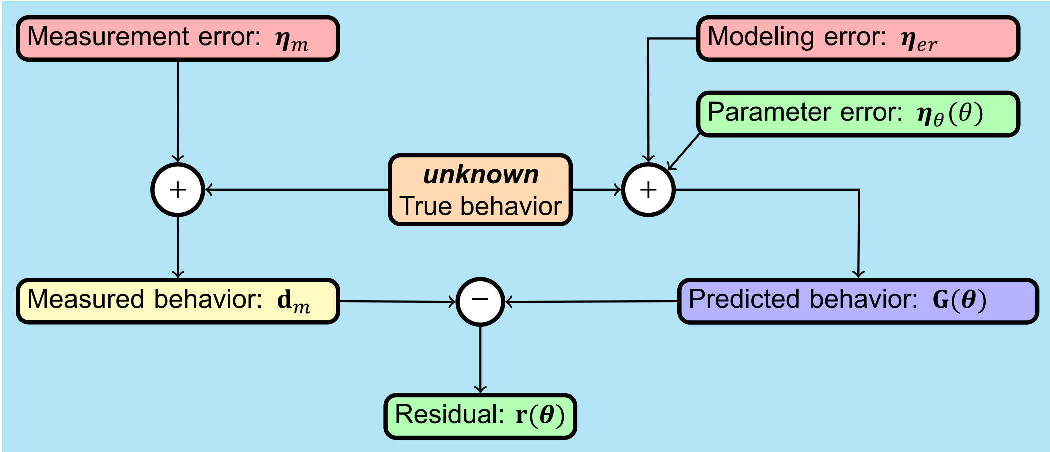

Figure 2.4: Overview of the relation between the true behavior, measured behavior and the predicted behavior.

$$\begin{aligned} \mathbf{d} &= \mathbf{d}_m - \boldsymbol{\eta}_m \\ \mathbf{d} &= \mathbf{G}(\boldsymbol{\theta}) + \boldsymbol{\eta}_\theta - \boldsymbol{\eta}_{er} \end{aligned} \tag{2.10}$$

By combining the equation in (2.10) the residual $\mathbf{r}(\boldsymbol{\theta})$ can be found. It is this residual that is minimized in FEMU.

$$\mathbf{d}_m - \boldsymbol{\eta}_m = \mathbf{G}(\boldsymbol{\theta}) + \boldsymbol{\eta}_\theta + \boldsymbol{\eta}_{er} \tag{2.11}$$

$$\mathbf{d}_m - \mathbf{G}(\boldsymbol{\theta}) = \boldsymbol{\eta}_\theta + \boldsymbol{\eta}_{er} + \boldsymbol{\eta}_m = \mathbf{r}(\boldsymbol{\theta}) \tag{2.12}$$

The residual $\mathbf{r}(\boldsymbol{\theta})$ is defined as the difference between the measured behavior and the predicted behavior. From equation (2.12) it is apparent that the residual is equal to the sum of three errors. However, only one of these errors - $\boldsymbol{\eta}_\theta$ - is changed in FEMU. If the measurement error $\boldsymbol{\eta}_m$ and the modeling error $\boldsymbol{\eta}_{er}$ are not small then the minimizing the residual $\mathbf{r}(\boldsymbol{\theta})$ will result in a model $\mathbf{G}(\boldsymbol{\theta})$ that is updated to errors, and a poorly updated model be found.

2.1.9. Quantification of errors

FEMU results may be susceptible to errors, see appendix A.2 for a mathematical explanation. Properly taking the effects of these errors into account is necessary, these errors are uncertain. And to take these uncertain quantities into account a move from a deterministic description to a stochastic description is needed. In deterministic FEMU a model is assumed to be updated when the error between the measured and predicted behavior is minimized, the updated parameters are found without confidence intervals. Stochastic FEMU takes into account uncertainties in the model data and/or uncertainties in the FE-model, the updated parameters will have confidence intervals. The probabilistic methods model uncertainties using statistical methods and assign probability density functions (PDF's) to uncertain quantities. These PDF's then propagate to the outcomes of model, quantifying their uncertainties. Often there is not enough information available about the uncertain quantities to assign a representative and truthful PDF's to the parameter[10], for example a quantity may be known to have a value within a certain bounds but how it's distributed is unknown. The selection of the PDF's may thus be seen as arbitrary and to overcome this problem non-probabilistic stochastic FEMU methods have been developed. The non-probabilistic and probabilistic approach can be combined, these methods are called mixed or hybrid.

In this research the errors and their uncertainties are quantified as follows. For the modeling error only the parameterization error is assumed to be significant. The measurements are assumed to be unbiased and they are also assigned a variance to quantify the confidence in them. The resulting updated parameters have a mean value and a variance.

2.1.10. Parameters

The way a model is parameterized determines what changes are possible to the predicted behavior. As a consequence parameters should be chosen so that by altering the parameters the phenomena that were mis-modeled or not represented in the initial model are corrected. The number of parameters that can be updated meaningfully is determined by the amount of information contained in the measurements. To avoid problems of ill-conditioning - discussed later - the number of parameter should be kept small. Selection of the parameters is a critical step in FEMU, as it determines the accuracy of the resulting model [13].

There are basically two ways of selecting parameters [13]. These are linked to the different methods of FEMU. For direct methods all entries in the system matrices can change, and as a result no parameters can be selected in this method. For iterative methods parameters can be selected, different strategies for parameterization are explained below.

Substructure methods

In this method the parameters are linked to a single element or a group of elements and the system matrices are altered by summing a scaled matrix to the system matrices. For the stiffness matrix $\mathbf{K}$ this is shown in (2.13), where $\boldsymbol{\theta}_j$ is the parameter, N is the number of parameters and $\mathbf{K}_j$ the matrix representing number of elements, or the substructure.

$$\mathbf{K} = \mathbf{K}_0 + \sum_{j=1}^{N} \boldsymbol{\theta}_j \mathbf{K}_j \tag{2.13}$$

The parameters in this method can be defined in two ways, the initial value can either be 0 or 1. Setting the initial value to 1 results in a normalization of the parameter values, this is useful in the sensitivity based FEMU method due to the better conditioning of the sensitivity matrix. The resulting matrices should be independent of the choice of initial values.

Physical parameters

The parameters are directly linked to physical quantities of the model, like geometric or material properties. These parameters can be linked to a single element or a group of elements. The relationship between a parameter and the stiffness matrix is - in general - non-linear. Using this method a physical interpretation of the updated parameters is immediately apparent. However, the only errors that can be corrected are those connected to the values of the physical parameters.

Allowable finite element families

Another way of parametrization is by choosing parameters that allow for a change in the structure of the element matrices. This is done by changing the eigenvalues and eigenvectors of individual elements. An issue with this method is the loss of physical insight into changes of the model.

Selecting parameters

After deciding on a parameterization method the next step is to select the the type and the number of parameters to be used. In this research the model is parametrized with physical parameters, mainly because there is a direct physical interpretation of the parameter changes. And the following discussion has only been checked for validity for such parameters.

First it's convenient to define what is meant by a parameter $\boldsymbol{\theta}$. In this case a parameters is a *physical quantity*, like a plate thickness, connected to a *set of elements*. A large number of parameters can be defined in this way for a FE-model, every element-physical quantity combination can be used as a parameter. However using a large number of parameters leads to a complex and time consuming updating procedure, which is most likely marred by issues as: ill-conditioning, under-determination and getting stuck in local minima. These problems can be reduced or avoided by[12]:

1. Choosing physical relevant parameters that sufficiently affect the residual, ie. they are sensitive.

2. Avoiding over-parametrization along the structure, and avoiding nearly linearly dependent columns of the sensitivity matrix. This can be done by not defining the parameters element wise but over a group of elements or substructures. Another option to define the element properties along a substructure by using a function which is characterized by only a few parameters.

It is thus important to reduce the number of parameters as much as possible. And in general the number of parameters should not be larger than the number of measurements[12]. To select parameters the insight of the analyst can be used. Another option is to use a method for error-localization, the regions in which a FE-model is erroneous are used for the parameter selection. An example of such a method is the force balance method [9].

After an initial set of parameters has been chosen, some parameters may have the same effect on the residual. This can be tested by checking the angles between the columns of the sensitivity matrix. If the angle between two columns is small the two parameters should be merged into one parameter to avoid ill-conditioning[19], note that this is only possible if the physical quantity connected to the different parameters is the same.

In this research the parameters are chosen using insight of the analyst/researcher.

2.1.11. Sensitivity Analysis

Sensitivity analysis studies how a parameter of a model influences the response of the model. In model updating it can be used to: identify sensitive areas in the model, provide insight for parameter selection, selection of the responses, and in sensitivity based model updating methods. In this section the formulation of sensitivities which are used in this research are discussed.

The basic formulation of a sensitivity is given in (2.14), it is the derivative of the response R_j w.r.t. to a parameter θ_i. What a parameter is in this context is explained in more detail in 2.1.10.

$$S_{ij} = \frac{\partial R_j}{\partial \theta_i} \tag{2.14}$$

The sensitivities can either be calculated analytically or numerically. Analytical methods have the advantage of being computationally more efficient compared to numerical methods. Analytical methods require a dedicated implementation to determine the derivatives of the matrices, this results in (2.15). Numerical methods may be more expensive computationally but they have the advantage of being generic, the sensitivity equation (2.14) is evaluated using finite differences as in (2.16).

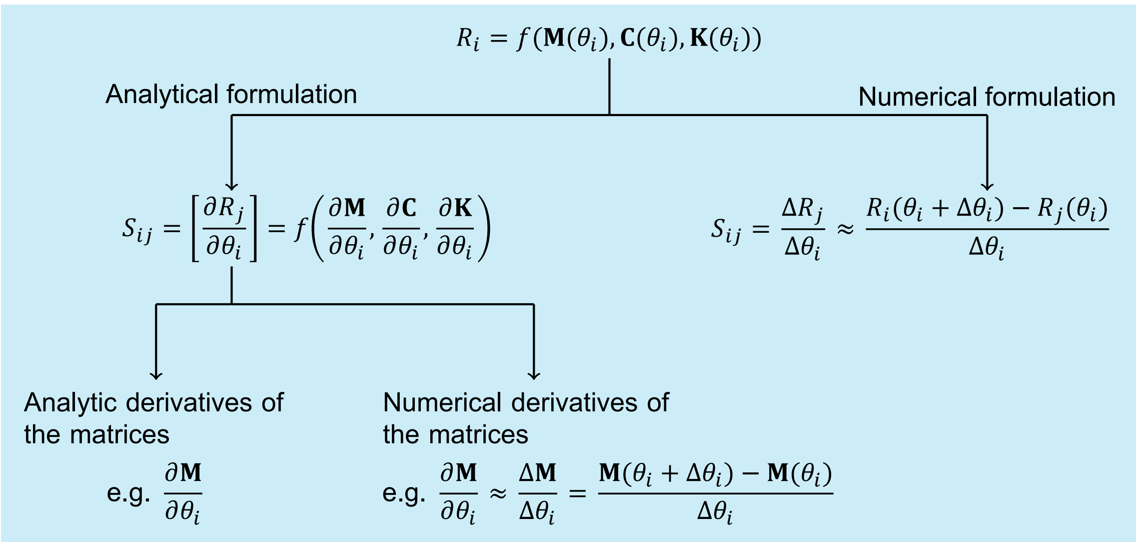

Figure 2.5: Different ways of determining sensitivities, adapted from [22].

$$S_{ij} = \left[\frac{\partial R_j}{\partial \theta_i}\right] = f\left(\frac{\partial \mathbf{M}}{\partial \theta_i}, \frac{\partial \mathbf{C}}{\partial \theta_i}, \frac{\partial \mathbf{K}}{\partial \theta_i}\right) \tag{2.15}$$

$$S_{ij} \approx \frac{\Delta R_j}{\Delta \theta_i} \approx \frac{R_i(\theta_j + \Delta\theta_j) - R_i(\theta_j)}{\Delta \theta_j} \tag{2.16}$$

Numerical sensitivity

The numerical sensitivity is defined by (2.16), as the finite difference derivative of a response w.r.t. a system parameter. Calculating the sensitivity this way is general and straightforward to implement. However the computational cost become large quickly with an increase of parameters and DOF's. Since for each response-parameter combination, the problem has to be solved.

Normalization of the sensitivity

In FEMU the sensitivities appear in the sensitivity matrix $\mathbf{S}$ when solving the linearized objective function, see (2.37). The objective of FEMU is to find an updated model whose parameters only differ slightly from the initial model. Because of this the sensitivities are normalized as in equation (2.17), where $\theta_{0,i}$ is the the initial setting of parameter i and $R_{0,j}$ is the measured value of the response j. Also normalization of the sensitivities will result in a better conditioned sensitivity matrix $\mathbf{S}$ [12].

$$S_{ij,norm} = \frac{\partial R_j}{\partial \theta_i} \frac{\theta_{0,i}}{R_{0,j}} \tag{2.17}$$

When the sensitivity matrix is normalized the least square problem in equation 2.38 becomes.

$$\frac{\epsilon_j}{R_{0,j}} = \frac{z_j}{R_{0,j}} - \frac{\partial R_j}{\partial \theta_i} \frac{\theta_{0,i}}{R_{0,j}} \frac{\delta \theta_i}{\theta_{0,i}} \tag{2.18}$$

2.1.12. Strain sensitivities

The static displacement is measured using strain gauges, this means that the sensitivities of the strains are needed. The strain sensitivity is found by differentiating (2.19) w.r.t. a parameter.

$$\boldsymbol{\epsilon} = \mathbf{Bu} \tag{2.19}$$

This results in equation (2.20), from which it is apparent that the strain sensitivity depends on:

- The shape functions of the strains $\mathbf{B}$ and its derivative.
- The nodal displacements $\mathbf{u}$ and its derivative.

At first glance the non-zero shape-function derivative may seem peculiar, however the shape-function of the finite element used in this analysis are not independent of the stiffness. However the shape-function derivative can be zero in case the parameter element set does not include the element where the strain is measured.

$$\frac{\partial \boldsymbol{\epsilon}}{\partial \theta_i} = \frac{\partial \mathbf{B}}{\partial \theta_i}\mathbf{u} + \mathbf{B}\frac{\partial \mathbf{u}}{\partial \theta_i} \tag{2.20}$$

2.1.13. Analytical formulation of undamped eigenvalue and eigenvector sensitivities

An undamped structural eigenvalue problem, as given in (2.54), is solved to find the natural frequencies and the corresponding mode shapes of a system. This equation can be derived to a parameter to find the sensitivities of the eigenvalues and the eigenvectors. The derivation w.r.t. θ_i yields equation (2.21). From this equation the expressions for the sensitivities of the eigenvalues and eigenvectors will be derived in this section, this derivation is in line with the derivation of Nelson [20].

$$\left[\mathbf{K} - \omega_j^2\mathbf{M}\right]\frac{\partial \boldsymbol{\phi}_j}{\partial \theta_i} + \left[\frac{\partial \mathbf{K}}{\partial \theta_i} - \omega_j^2\frac{\partial \mathbf{M}}{\partial \theta_i} - \frac{\partial \omega_j^2}{\partial \theta_i}\mathbf{M}\right]\boldsymbol{\phi}_j = 0 \tag{2.21}$$

Equation (2.21) can be written as (2.22). Where $\mathbf{Z}(\omega_j)$ represents the dynamic stiffness given in equation (2.24) and $\mathbf{B}(\omega_j)$ is given by equation (2.23).

$$\mathbf{Z}(\omega_j)\frac{\partial \boldsymbol{\phi}_j}{\partial \theta_i} = \mathbf{B}(\omega_j) \tag{2.22}$$

with

$$\mathbf{B}(\omega_j) = -\left[\frac{\partial \mathbf{K}}{\partial \theta_i} - \omega_j^2\frac{\partial \mathbf{M}}{\partial \theta_i} - \frac{\partial \omega_j^2}{\partial \theta_i}\mathbf{M}\right]\boldsymbol{\phi}_j \tag{2.23}$$

and

$$\mathbf{Z}(\omega_j) = \left[\mathbf{K} - \omega_j^2\mathbf{M}\right] \tag{2.24}$$

The dynamic stiffness $\mathbf{Z}(\omega_j)$ is singular at each eigen-frequency ω_j, see (2.24), the result is that (2.22) does not necessarily have a solution. The null-space of the dynamic stiffness is spanned by $\boldsymbol{\phi}_j$. And using theorems from linear algebra [18] it is know that the equation $\mathbf{Zq} = \mathbf{B}$ only has a solution when B is orthogonal to the null-space of $\mathbf{Z}$, see (2.25). Equation (2.25) defines the sensitivities of the eigen-frequencies and these can be found as in (2.26).

$$\boldsymbol{\phi}_j^T\mathbf{B}(\omega_j) = 0 \tag{2.25}$$

$$\frac{\partial \omega_j^2}{\partial \theta_i} = \boldsymbol{\phi}_j^T\left[\frac{\partial \mathbf{K}}{\partial \theta_i} - \omega_j^2\frac{\partial \mathbf{M}}{\partial \theta_i}\right]\boldsymbol{\phi}_j \tag{2.26}$$

The solution of the mode shape sensitivity is more involved. A solution of a linear system is given by the sum of a particular solution $\mathbf{p}$ and a homogeneous solution $\alpha\mathbf{v}_h$ as in (2.27) [18].

$$\mathbf{Ax} = \mathbf{b} \quad with \quad \mathbf{x} = \mathbf{p} + \alpha\mathbf{v}_h \tag{2.27}$$

Applying this to (2.22) - which defines the mode shape derivative - leads to solution in the form of 2.28. The homogeneous solution of (2.22) are the vectors spanning null-space of $\mathbf{Z}(\omega_j)$ which in this case is the eigenvector $\boldsymbol{\phi}_j$.

$$\frac{\partial \boldsymbol{\phi}_j}{\partial \theta_i} = \boldsymbol{\psi}_j + \alpha_j\boldsymbol{\phi}_j \tag{2.28}$$

A particular solution $\boldsymbol{\psi}_j$ of (2.22) can be found by using the approach of Nelson[20]. He assumes that one component of the particular solution is set to 0, now a row and a column can be removed from $\mathbf{Z}(\omega_j)$. The system of equations is now non-singular and a solution can be found. The arbitrarily zeroing of a component of $\boldsymbol{\psi}_j$ is corrected for by the the homogeneous solution. The zeroed element in $\boldsymbol{\psi}_j$ is the element for which $|\boldsymbol{\phi}_j|$ is maximum. For each eigenvector derivative the reduced system (2.29) needs to be solved.

$$\begin{bmatrix} \left[\mathbf{K} - \omega_j^2\mathbf{M}\right]_{11} & 0 & \left[\mathbf{K} - \omega_j^2\mathbf{M}\right]_{13} \\ 0 & 1 & 0 \\ \left[\mathbf{K} - \omega_j^2\mathbf{M}\right]_{31} & 0 & \left[\mathbf{K} - \omega_j^2\mathbf{M}\right]_{33} \end{bmatrix} \begin{Bmatrix} \psi_{1..k-1} \\ \psi_k \\ \psi_{k+1..n} \end{Bmatrix} = \begin{Bmatrix} \mathbf{B}(\omega_j)_{1..k-1} \\ 0 \\ \mathbf{B}(\omega_j)_{k+1..n} \end{Bmatrix} \tag{2.29}$$

The coefficient α_j can be found from realizing that the mode shapes are mass normalized, differentiating the condition for mass-normalization (2.59) w.r.t. a parameter and substituting the mode shape derivative (2.28) into (2.30). In this research the mass is assumed to be constant w.r.t. a parameter θ_i.

$$\frac{\partial}{\partial\theta_i}\left[\boldsymbol{\phi}_k^T\mathbf{M}\boldsymbol{\phi}_\mathbf{j}\right] = 2\boldsymbol{\phi}_j^T\mathbf{M}\frac{\partial\boldsymbol{\phi}_j}{\partial\theta_i} + \boldsymbol{\phi}_j^T\frac{\partial\mathbf{M}}{\partial\theta_i}\boldsymbol{\phi}_j = 0 \tag{2.30}$$

This leads to the expression (2.31), which determines α_j.

$$2\boldsymbol{\phi}_j^T\mathbf{M}[\boldsymbol{\psi}_j + \alpha_j\boldsymbol{\phi}_j] = \boldsymbol{\phi}_j^T\mathbf{M}\boldsymbol{\psi}_j + \alpha_j = 0 \tag{2.31}$$

This concludes the eigenvector and eigenvalue derivative of a undamped system. This analysis is suitable for systems with distinct eigenvalues and eigenvectors. Techniques to find sensitivities for systems with repeated eigenvalues are available, see for example [21]. In this research the above formulations of the sensitivities suffices, since the eigenvalues and eigenvectors of the studied system are distinct.

Approximations of the Eigenvector derivative.

Determining eigenvector sensitivities using Nelson's method - as discussed in section 2.1.13 - can become computationally expensive for systems with a large number of DOF's. Approximate formulations of eigenvector sensitivities are available. A class of methods that approximates the properties of dynamical systems are projection methods[2]. Projection methods rely on the assumption that an accurate description of a dynamical system can be found in a subspace that is spanned by the columns of a projection matrix $\mathbf{T}$. That is, the matrices that describe the system can be transformed to a smaller subspace while retaining the most important properties of the system matrices/system behavior needed in an analysis. Projection methods reduce the DOF's of a model and lead to a reduction in computational cost, while giving in on accuracy. In iterative model updating system matrices change as the parameters change, to reduce computational costs further a transformation matrix that is constant for a certain parameter setting range is desirable, since the calculating a transformation matrix is computationally expensive. Such a transformation matrix can be found as is explained in [1]. A well known projection method is the projection of the system on a truncated modal basis. Fox and Kapoor[11] used a truncated modal basis to find an approximate expression for the eigenvector derivative, see equation (2.32). A comparison between the eigenvector derivatives using this method and Nelson's method is below given in section 3.5.3.

$$\frac{\partial\boldsymbol{\phi}_j}{\partial\theta_i} = \sum_{k=1}^{n_{modes}} a_{jk}\boldsymbol{\phi}_k \quad with \quad a_{jk} = \begin{cases} \dfrac{\boldsymbol{\phi}_k^T\left[\dfrac{\partial\mathbf{K}}{\partial\theta_i} - \omega_j^2\dfrac{\partial\mathbf{M}}{\partial\theta_i}\right]\boldsymbol{\phi}_j}{\omega_j^2 - \omega_k^2} & \text{for} \quad j \neq k \\ -\dfrac{1}{2}\boldsymbol{\phi}_j^T\dfrac{\partial\mathbf{M}}{\partial\theta_i}\boldsymbol{\phi}_j & \text{for} \quad j = k \end{cases} \tag{2.32}$$

Analytical MAC derivative

The Modal Assurance Criterion(MAC) derivative is derived here, the MAC value is defined in equation (2.34). Differentiating this equation w.r.t. a parameter gives (2.33), in this equation $\boldsymbol{\phi}_i$ is the predicted mode shape and $\boldsymbol{\phi}_j$ is the measured model shape. The measured mode shape is independent of any parameter change, as a result its derivatives are not present in (2.33).

$$\frac{\partial MAC_{ij}}{\partial\theta_k} = \frac{\boldsymbol{\phi}_j^H\left[\dfrac{\partial\boldsymbol{\phi}_i}{\partial\theta_k}\boldsymbol{\phi}_i^H + \boldsymbol{\phi}_i\dfrac{\partial\boldsymbol{\phi}_i^H}{\partial\theta_k}\right]\boldsymbol{\phi}_j\boldsymbol{\phi}_i^H\boldsymbol{\phi}_i - \boldsymbol{\phi}_j^H\boldsymbol{\phi}_i\boldsymbol{\phi}_i^H\boldsymbol{\phi}_j\left[\dfrac{\partial\boldsymbol{\phi}_i^H}{\partial\theta_k}\boldsymbol{\phi}_i + \boldsymbol{\phi}_i^H\dfrac{\partial\boldsymbol{\phi}_i^H}{\partial\theta_k}\right]}{\left[\boldsymbol{\phi}_i^H\boldsymbol{\phi}_i\right]^2\boldsymbol{\phi}_j^H\boldsymbol{\phi}_j} \tag{2.33}$$

2.1.14. Objective function

At the core of sensitivity based FEMU is an objective function which defines a residual that is to be minimized. In the formulation of the residual several quantities can be used depending on the analysis. The quantities used in this research are discussed in this section.

Strain measurements

For the static deformation the difference between the measured strains and the predicted strains is in the objective function.

Modal Assurance Criterion

The modal assurance criterion (MAC) is a technique to asses the correlation between two mode-shapes. The MAC can be calculated using (2.34), and requires only the knowledge of the mode-shapes for which the correlation is to be determined. The MAC will give a value between 1 and 0, where 1 indicates perfect correlation and 0 no correlation. In FEMU it is used to pair measured and predicted mode-shapes, and to distinguish mode shapes that are close in natural frequency. It can also be used in the objective function where a MAC value of 1 is the objective. By itself it is not such a good updating objective since the MAC value of modes that are similar do not change much. However when it is combined with another objective like the eigenvalue it is useful because it will make sure that the modes whose frequencies are compared will be the same modes.

$$MAC_{ij} = \frac{\boldsymbol{\phi}_i^H \boldsymbol{\phi}_j \boldsymbol{\phi}_j^H \boldsymbol{\phi}_i}{\boldsymbol{\phi}_i^H \boldsymbol{\phi}_i \boldsymbol{\phi}_j^H \boldsymbol{\phi}_j} \tag{2.34}$$

Natural frequencies

Natural frequencies can be used as in the objective function, they describe the global behavior of a system. When comparing natural frequencies one must make sure that the frequencies belong to the same mode shape. In other words the frequencies and mode shapes must be paired before a comparison is made. Natural frequencies can be determined for the FE-model as explained in section 2.2.4.

2.1.15. Updating procedure

In this section the solution of the optimization problem in sensitivity based FEMU is discussed. As follows from the discussion of model classes in section 2.1.3 FEMU results in an optimization problem (2.6). In sensitivity based FEMU a set of parameters $\boldsymbol{\theta}_M^*$ is sought that minimizes the residual $\mathbf{r}(\boldsymbol{\theta})$; the difference between the difference between predicted behavior $\mathbf{y}(\boldsymbol{\theta})$ and measured behavior data $\mathbf{d}_m$. The residual is given by equation (2.1.15), in general this is a non-linear function of the parameters.

$$\mathbf{r}(\boldsymbol{\theta}) = \mathbf{d}_m - \mathbf{y}(\boldsymbol{\theta}) \tag{2.35}$$

The optimization problem is given by (2.6). In sensitivity based FEMU this problem is solved using the Gauss-Newton method, this method iteratively linearizes the equations and finds a least squares solution at each iteration step until convergence is obtained, see A.1 for a derivation. Linearizion of the residual using the first order Taylor expansion at $\boldsymbol{\theta}_i$, a certain parameter setting, leads to 2.37 where $\mathbf{S}|_{\boldsymbol{\theta}_i}$ is the sensitivity matrix at $\boldsymbol{\theta}_i$ and $\mathbf{z}(\boldsymbol{\theta}_\mathbf{i})$ the linearized residual at $\boldsymbol{\theta}_\mathbf{i}$.

$$\mathbf{r}(\boldsymbol{\theta}) = \mathbf{d} - \mathbf{y}(\boldsymbol{\theta}) \approx \mathbf{d} - \mathbf{y}(\boldsymbol{\theta}_\mathbf{i}) - \mathbf{S}|_{\boldsymbol{\theta}_i}\delta\boldsymbol{\theta} \tag{2.36}$$

$$\mathbf{z}(\boldsymbol{\theta}_\mathbf{i}) = \mathbf{d} - \mathbf{y}(\boldsymbol{\theta}_\mathbf{i}) = \mathbf{S}|_{\boldsymbol{\theta}_i}\delta\boldsymbol{\theta} \tag{2.37}$$

The problem in (2.37) has the form of a fundamental problem studied in linear algebra, see discussion in A.2. An approximate solution can be found using the least-square method, the several formulations used in this research are given here.

Standard least-squares
The standard least square solution leads to the objective function given in .

$$J(\delta\boldsymbol{\theta}) = \epsilon^T\epsilon \quad with \quad \epsilon = \mathbf{z}(\boldsymbol{\theta}_i) - \mathbf{S}|_{\boldsymbol{\theta}_i}\delta\boldsymbol{\theta} \tag{2.38}$$

Weighted least-squares
A weighting matrix $\mathbf{W}_{\epsilon\epsilon}$ can be used to weight the terms of the residual, in order to take into account differences in measurement confidences, this leads to the weighted least square method. The weighting matrix is a diagonal matrix with the weights on the diagonal. These weights are usually the reciprocal of the variance of the respective measurement. Applied to FEMU this leads to the following objective function.

$$J(\delta\boldsymbol{\theta}) = \epsilon^T\mathbf{W}_{\epsilon\epsilon}\epsilon \tag{2.39}$$

Ill-posed least-squares
When the FEMU problem is ill-posed extra information can be added to regularize the problem, see A.2.1. Applying regularization to leads to the following objective function. (2.1.15).

$$J(\delta\boldsymbol{\theta}) = \epsilon^T\mathbf{W}_{\epsilon\epsilon}\epsilon + \lambda^2\delta\boldsymbol{\theta}^T\mathbf{W}_{\theta\theta}\delta\boldsymbol{\theta} \tag{2.40}$$

The regularization term here adds weight to changes in the parameter value $\delta\boldsymbol{\theta}$, thereby it will make sure that the parameters will stay closer to their original estimate than when no regularization is used. The matrix $\mathbf{W}_{\theta\theta}$ is a diagonal matrix with the inverse of variance of the initial parameter estimates, the effect of $\mathbf{W}_{\theta\theta}$ is that the uncertain parameter estimates will change more than parameters which are less uncertain. The parameter λ controls the balance between the measurement residual and the regularization term.

Finding $\delta\boldsymbol{\theta}$
To find a step $\delta\boldsymbol{\theta}$, the objective function $J(\delta\boldsymbol{\theta})$ needs to be minimized. A condition for a minimum is that the derivative is equal to zero, hence the objective function is derived w.r.t. $\delta\boldsymbol{\theta}$ and equated to zero, see (2.41). From this equation the the iteration step $\delta\boldsymbol{\theta}$ can be found.

$$\frac{\partial[J(\delta\boldsymbol{\theta})]}{\partial[\delta\boldsymbol{\theta}]} = 0 \tag{2.41}$$

In each iteration the $\delta\boldsymbol{\theta}$ is added to the parameters setting $\boldsymbol{\theta}_i$, convergence is reached after the change in parameters $\delta\boldsymbol{\theta}$ is smaller than a certain threshold. The pseudo-inverse provides general way to solve (2.37) and in practice the pseudo-inverse is used to solve (2.37) directly as in equation (2.42). If the condition number of the pseudo-inverse is too large regularization is used as in (2.40), when derived as in (2.41) the step size is found as in equation (2.43).

$$\delta\boldsymbol{\theta}_i = \mathbf{S}|^+_{\boldsymbol{\theta}_i}\mathbf{z}(\boldsymbol{\theta}_i) \tag{2.42}$$

$$\delta\boldsymbol{\theta}_i = (\mathbf{S}|^T_{\boldsymbol{\theta}_i}\mathbf{W}_{\epsilon\epsilon}\mathbf{S}|_{\boldsymbol{\theta}_i} + \lambda^2\mathbf{W}_{\theta\theta})^{-1}\mathbf{S}|^T_{\boldsymbol{\theta}_i}\mathbf{W}_{\epsilon\epsilon}\mathbf{z}(\boldsymbol{\theta}_i) \tag{2.43}$$

Equations (2.42) and (2.43) have been implemented in `MatLab` to iteratively solve the non-linear least square problem. Two algorithms are available to solve the optimization problem, see figure 2.3.

2.1.16. Poor results in FEMU

Because FEMU is an inverse method it is difficult to point out what the causes are of a poorly updated model[17]. The poor results may be caused by: the selection of parameters, the objective function, the measurement data, an incorrect model, or a combination of these. In figure 2.6 two different errors are illustrated, in figure 2.6a the formulation of the initial model does not correlate with the data and as a result there is no parameter setting that can make the model move to the optimal model. In figure 2.6b a poor choice of an objective function is shown, the updated model does not correlate with the experimental data.

When the updated model is not satisfactory, the FEMU process should be executed repeatedly with different parameters and/or objective function. The quality of the measurement data should be assessed and the model should be verified for correlation. A systematic method to overcome the problems in model updating has been proposed by Kim and Park[17]. They proposed a multi-objective optimization procedure together with a parameter selection procedure and successfully applied the method.

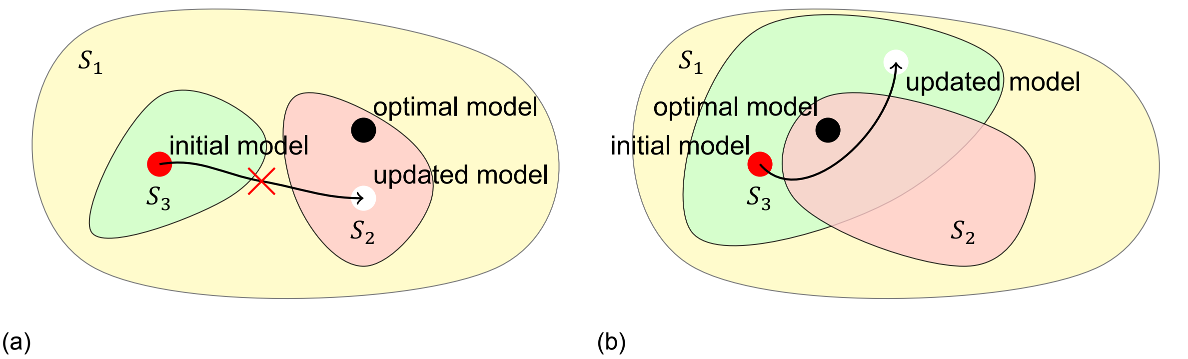

Figure 2.6: Illustrations of problems encountered in FEMU. Bad parameter selection (a), and erroneous definition of the objective function (b).

2.2. Structural analysis

In this section the relevant theory of structural analysis is discussed. In this research the beam structural element is used. The beam structural element is the main topic of this section. Departing from fundamental a fundamental description of structures/solids and some assumptions the beam element is formulated. The reasons for choosing this model are discussed. Two formulations of the beam element are explained. Then the basics of the finite element method are discussed.

2.2.1. Solid mechanics

Solid mechanics is the branch of science that describes the deformations of solid bodies. The theory is based on two main assumptions[5]:

1. The physical world is idealized by a 3-dimensional Euclidean space, this is a vector space in which points are described by a set of 3 real numbers, $\mathbf{x} = (x, y, z)$. The metric of the Euclidean space describes the distance between two points and is given by, $||\mathbf{x}_1 - \mathbf{x}_2||$. In this space it is assumed that Newtons laws of motion hold.

2. A body is idealized as a continuum that it is infinitely divisible.

These assumptions hold for the description of macro behavior of bodies. Solid mechanics uses three sets of equations to find a mathematical description of a body, these are:

1. **Kinematic equations**: describe how a body moves and deforms, and prescribe a relation between the displacement field and the strains in the body. There are restrictions on the displacement field: it has to be a continuous one-to-one mapping and the volume of the body before and after the deformations must be greater than zero.

2. **Constitutive equations**: describe how stresses and strains are related, they depend on the material that is modeled and on the magnitude of the deformations.

3. **Equilibrium equations**: describe the force equilibrium of the body at each point.

By combining these equations a set of partial differential equations is found that accurately describes the behavior of solid bodies in three dimensions. These equations are also called the governing equations. The governing equations are complex and solutions for these equations can be found only for simple geometries. The governing equations can be simplified by introducing additional assumptions, these assumptions follow from observations of a deforming body. For example it is known that a steel wire deforms only in one direction when a - not too great - force is applied at its ends. With this information the deformation can be assumed to occur in only 1-dimension simplifying the the equations considerably.

2.2.2. Beams

The simplifications that can be made for the behavior of the body of interest in this research are explained here.

Why beams?

In this research the global deformations of a ship are of interest. Because of hydro-mechanical considerations most ships are slender bodies, for which one dimension is much greater than the other two dimensions. The global deformations of slender bodies can be accurately modeled by the beam model. This approach has been successfully applied in the past and is still used to determine some of scantling rules of classification societies. The ship considered in this research is unconventionally shaped, it is not slender as can be seen from the cover image and figure C.1, which shows the basic structure of the ship save the deck-house. A 1-dimensional beam model can thus not accurately describe the behavior of this structure, it is assumed that a collection of interconnected 1-dimensional beams in a plane provides a sufficiently accurate description of the ship's global behavior for the purposes of this research.

Assumptions of the beam model

A beam is a structural element that can describe the transverse bending and shearing deformation of a slender body. Also the axial and torsional behavior can be included in the model. The following assumptions are made for the beam model:

- It has a neutral-line which coincides with the centroid of the cross-section. The neutral line is stress free when pure bending is applied to the beam.
- It has a cross-section that is rigid and oriented perpendicular to the neutral line when the beam is undeformed.

These assumptions lead to a kinematic description of the beam which is fully determined by the orientation of the cross-sections and the position of the point with respect to the neutral line. The position of a point on the neutral line is described by three translations, and the orientation of the cross-sectional plane is described by three rotations. The beam model thus reduces the three dimensional kinematic description of a slender body to a 1-dimensional description with 6 degrees of freedom at each point on the neutral line. An additional assumption can be made related to the orientation of the cross-section with respect to the neutral line. If the cross-section is assumed to remain perpendicular the neutral line at all times, the deformation of a beam is fully described by the neutral line. This assumption leads to the Euler-Bernoulli beam model, which neglects shear deformation. In the Timoshenko beam model the last assumption is not made and shear deformation is taken into account, although in a simplified form. Because shear deformation is taken into account a Timoshenko beam is more flexible than an Euler-Bernoulli beam of equal dimensions. What beam model is appropriate depends on whether or not shear deformations can be neglected, this depends on the ratio between the shear deformation and bending deformations. For a uniform cantilever beam of length L with a force F at the end the ratio between the shear and bending deformation is given by (2.44), for a beam with a rectangular cross-section. In (2.44) I is the moment of inertia of the cross-section, A the area of the cross-section, b the width and h the height, k_s the shear coefficient, E Youngs-modulus and G the shear modulus.

$$\frac{\delta_{shear}}{\delta_{bending}} = \frac{\left(\frac{FLk_s}{AG}\right)}{\left(\frac{FL^3}{3EI}\right)} = c\left(\frac{bh^3}{bhL^2}\right) = c\left(\frac{h}{L}\right)^2 \tag{2.44}$$

From (2.44) it is clear that the ratio between shear and bending deformation is determined by the the ratio between the beam height and the length of the beam. Whether or not shear should be taken into account depends on this value. For beams that are stubby - similar height and length - and also for slender beams that vibrate at high frequency, shear effect should be taken into account.

Kinematic relations

The assumptions for the Timoshenko beam lead to the following kinematic relations describing the possible configurations of a beam (2.45), for a derivation see [16]. In (2.45) v_i is the translation of a point in the beam, u_i is the displacement of the neutral line, ϕ_i the rotation of the cross-section.

$$\begin{aligned} v_x(x,y,z) &= u_x - \phi_z y + \phi_y z \\ v_y(x,y,z) &= u_y - \phi_x z \\ v_z(x,y,z) &= u_z + \phi_x y \end{aligned} \tag{2.45}$$

By assuming small deformations linear relations between the strain and displacement field can be used. The strains for the beam are then given by 2.46, with the curvature about the x-axis κ_x assumed constant in x. In this equation ϵ_{xx} is the total strain in x-direction and γ_{xy} and γ_{xy} are the shear strains in xy and xz direction respectively.

$$\begin{aligned} \epsilon_{xx} &= \frac{\partial v_x}{\partial x} &&= \frac{\partial u_x}{\partial x} - \frac{\partial \phi_z}{\partial x} y + \frac{\partial \phi_y}{\partial x} z \\ \gamma_{xy} &= \frac{\partial v_y}{\partial x} + \frac{\partial v_x}{\partial y} &&= \frac{\partial u_y}{\partial x} - \frac{\partial \phi_x}{\partial x} z - \phi_z \\ \gamma_{xz} &= \frac{\partial v_x}{\partial z} + \frac{\partial v_z}{\partial x} &&= \frac{\partial u_z}{\partial x} + \frac{\partial \phi_x}{\partial x} y + \phi_y \end{aligned} \tag{2.46}$$

The derivatives of the displacements and the rotations of the neutral line are given by (2.47) where ϵ_x is the axial strain, γ_y and γ_z the average shear deformations in y and z direction respectively, ϕ_z and ϕ_y the rotation of the cross-section about the z and y axis respectively, κ_y and κ_z are the curvature about the y and z axis respectively.

$$\begin{aligned} \frac{\partial u_x}{\partial x} &= \epsilon_x \,, & \frac{\partial \phi_x}{\partial x} &= \kappa_x \\ \frac{\partial u_y}{\partial y} &= \gamma_y + \phi_z \,, & \frac{\partial \phi_y}{\partial y} &= \kappa_y \\ \frac{\partial u_z}{\partial z} &= \gamma_z - \phi_y \,, & \frac{\partial \phi_z}{\partial z} &= \kappa_z \end{aligned} \tag{2.47}$$

By using (2.47) and assuming a homogeneous, isotropic and linear elastic material the relations between the stresses and the strains is given by (2.48), where E is Youngs modulus and G is the shear modulus.

$$\begin{aligned} \sigma_{xx} &= E(\epsilon_x - \kappa_z y + \kappa_y z) \\ \tau_{xy} &= G\left(\gamma_y - \kappa_x z\right) \\ \tau_{xz} &= G\left(\gamma_z + \kappa_x y\right) \end{aligned} \tag{2.48}$$

The forces and moments for at each point on the neutral line can be derived by integrating the stresses in (2.48) in doing this the cross-sectional properties of the beam like moment of inertia, area and polar inertia moment follow. By inserting these force and moment relations in the equilibrium equations a set of differential equations is found that describe the deformations of an Timoshenko beam, see [16] for the entire derivation. Solving these equations is possible for a single beam, but becomes cumbersome for multiple connected beams. To circumvent this issue the Finite element method is used.

2.2.3. Finite element method

As mentioned solving the governing equations analytically is difficult and in most cases not possible, to overcome this an approximate solution is sought. The most popular method for this in structural mechanics is the finite element method. FEM is a numerical method that finds approximate solutions by splitting up the solution domain into sub-domains. On each sub-domain the solutions is described by simple functions, like 2^{nd} order polynomials. In doing so approximate solutions can be found on bodies with complex geometries. FEM has become the go-to tool in structural analysis over the past decades, however the results of an FE model must always be looked at with care. The numerical method can be marred with errors and non-physical behavior. For an elaborate discussion on FE method see [8], some properties of the of the Timoshenko beam element are explained next.

Shape functions

The shape function describe the displacement field inside the domain of an element. It is common to assume a n^{th} polynomial as a shape function. In case of the Timoshenko beam element several shape functions are possible, in this research the following shape functions are used:

- 1^{st} order or linear polynomials for the displacement in x-direction and rotation about the x axis
- 2^{nd} order or quadratic polynomials for rotations about the y and z axis .
- 3^{rd} order or cubic polynomials for the displacement in y and z direction.

These shape functions are of the same order as the solutions of the differential equations that describe the behavior of the Timoshenko beam. This means that the FE formulation and the analytical formulation should give the same result.

Matrices

Using the shape functions the stiffness matrix $\mathbf{K}$ of the beam element can be found by using equation (2.49), where $\mathbf{B}$ is the matrix with the shape function derivatives and $\mathbf{E}$ is the constitutive matrix. The stiffness matrix $\mathbf{K}$ is a function of the geometry and material properties of the beam.

$$\mathbf{K} = \int_0^l \mathbf{B}^T \mathbf{E} \mathbf{B} dx \tag{2.49}$$

The consistent mass matrix $\mathbf{M}$ of the beam element is found by using (2.50), where ρ is the density and $\mathbf{N}$ is the matrix with the shape functions. This formulation results in a fully populated mass matrix. A computationally more efficient way to represent the mass of a beam element is by mass lumping. This results in a mass matrix with diagonal elements, several mass lumping techniques are available. In this research the consistent mass matrix is used.

$$\mathbf{M} = \int_0^l \rho \mathbf{N}^T \mathbf{N} dx \tag{2.50}$$

The mass and stiffness matrices are given in the local element coordinates. The assembly of the system matrix requires the elements to be transformed to global coordinates. A translation does not effect the element matrices, only when elements are rotated element matrices need to be transformed. This is done by a matrix transformations as given in equation (2.51). If the element coordinate system is aligned with the global coordinate system $\mathbf{T}$ will be the identity matrix.

$$\mathbf{K}_{global} = \mathbf{T}^T \mathbf{K}_{local} \mathbf{T} \tag{2.51}$$

With the mass and the stiffness matrix in the global coordinates the system matrices can be assembled by using the nodal connectivity as dictated by the mesh. The assembled matrices are then used to formulate matrix equations. Solving matrix equation is a bookkeeping exercise, and the linear algebra software `MatLab` is used to solve the matrix equations.

2.2.4. Dynamics in FEM

In this section the solution of finite element formulation of an undamped structure is explained.

A FE formulation of an undamped structure results in a system of n second order differential equations, these equations may be coupled. The equations can be represented in matrix form as in (2.52), in which $\mathbf{M}$ and $\mathbf{K}$ are nxn matrices representing the assembled mass and the stiffness matrices respectively. The force in time is represented by $\mathbf{f}(t)$ an $nx1$ vector. The displacements and the accelerations of each DOF are given by $\ddot{\mathbf{x}}(t)$ and $\mathbf{x}(t)$ respectively, both $nx1$ vectors.

$$\mathbf{M}\ddot{\mathbf{x}} + \mathbf{K}\mathbf{x} = \mathbf{f}(t) \tag{2.52}$$

To solve this system of equations the homogeneous part is considered first, leaving out the forcing term in equation (2.52). An assumption on the response of the system is made, namely that the response $\mathbf{x}(t)$ is harmonic. Using this assumption the response can be written as a product of a constant spatial function and a harmonic temporal function, see (2.53). The spatial function is the mode-shape of the system, for each mode shape there is a natural frequency of which determines the frequency of the harmonic function.

$$\mathbf{x}(t) = \mathbf{x}(\omega)e^{i\omega t} \tag{2.53}$$

Substituting (2.53) into (2.53) yields (2.54), this is the structural eigenvalue problem. With ϕ_j and λ_j representing the j-th eigenvectors and eigenvalues. Each eigenvalue and eigenvector pair physically represents a vibration mode with a natural frequency and a mode shape. Where the natural frequency ω is equal to the square root of the eigenvalue λ, and the mode shape is the eigenvector.

$$\mathbf{K}\boldsymbol{\phi}_j = \lambda_j \mathbf{M}\boldsymbol{\phi}_j \quad with \quad j = 1...n \tag{2.54}$$

The solution of the undamped eigenvalue problem gives mode shapes that are orthogonal to the mass, left multiplying the structural eigenvalue problem (2.54) with the transpose of the mode shapes gives (2.55).

$$\boldsymbol{\phi}_k^T \mathbf{K}\boldsymbol{\phi}_j = \lambda_j \boldsymbol{\phi}_k^T \mathbf{M}\boldsymbol{\phi}_j \tag{2.55}$$

Interchanging the subscripts of the and transposing this equation and using the fact that the $\mathbf{K}$ and $\mathbf{M}$ are symmetric gives (2.56).

$$\boldsymbol{\phi}_k^T \mathbf{K}\boldsymbol{\phi}_j = \lambda_k \boldsymbol{\phi}_k^T \mathbf{M}\boldsymbol{\phi}_j \tag{2.56}$$

Subtracting (2.55) from (2.56) for distinct eigenvalues gives (2.58) where m_j is the generalized mass of mode j.

$$\lambda_k \boldsymbol{\phi}_k^T \mathbf{M}\boldsymbol{\phi}_j = 0 \quad for \quad j \neq k \tag{2.57}$$

$$\lambda_k \boldsymbol{\phi}_k^T \mathbf{M}\boldsymbol{\phi}_j = m_j \quad for \quad j = k \tag{2.58}$$

The generalized mass can be used to normalize the eigenvectors. Normalization is possible because a scaled eigenvector is also an eigenvector. The result of normalizing with respect to the generalized mass results in (2.59), where the masses are set to unity.

$$\boldsymbol{\Phi}^T \mathbf{M}\boldsymbol{\Phi} = \mathbf{I} \quad with \quad \boldsymbol{\Phi} = [\boldsymbol{\phi}_1, ..., \boldsymbol{\phi}_n] \tag{2.59}$$

The mass normalization substituted in (2.55) leads to (2.60) where $\boldsymbol{\Lambda} = diag(\lambda_j)$.

$$\boldsymbol{\Phi}^T \mathbf{K}\boldsymbol{\Phi} = \boldsymbol{\Lambda} \tag{2.60}$$

The eigenvectors resulting from this normalization are generally called normal modes. The normalization of the modes is used in the derivation of the sensitivities.

"The ability to simplify means to eliminate the unnecessary so that the necessary may speak."

Hans Hofmann

3 Cantilever beam

In this chapter the test case is presented. First the reasons for using a test case are discussed. Then the properties of the test case are explained. The results of different formulations of the beam element are compared. Different concepts needed in FEMU - which were discussed in chapter 2 - are elucidated using the test case. Each analysis is introduced, after which the results of the analysis are presented and then discussed. In the last part of this chapter the cantilever beam is used in a simulated updating procedure, and to finish the most important results are summarized.

3.1. Why a test case?

In this section the question posed in the title of this section is answered. The reasons for first using the cantilever beam as a test case are threefold: error detection, code verification and to gain insight into the concepts in FEMU. When studying a simple problem, coding errors can be detected more easily. The behavior of a cantilever beam has been studied extensively and is well understood therefore non-physical behavior can be detected more easily. If the results of the test case can be explained physically and when different formulations match, the analyst can assume that the code is verified or at least have more confidence in the results. Lastly using a simple test case provides a good way to familiarize the author and reader with the concepts involved in FEMU; like the sensitivities of natural frequencies and mode shapes.

3.2. Beam geometry and properties

In this section the geometry and the properties of the test case are discussed. For the test case a cantilever beam has been chosen. The geometry of the test case is depicted in figure 3.1a, and the FE-mesh of the beam is depicted in 3.1b. It consists of 30 elements each - 1 meter in length - and 31 nodes, there are 2 DOF per node: a rotation about the y-axis and a translation in z-direction. The other DOF's are constrained in this test case. In figure 3.1b the colored areas depict the parameters used in the optimization problem. The parameters have been chosen this way because the number of parameters is a small enough to keep the sensitivity matrix small but big enough for multiple solutions to be possible. The parameter properties have been chosen to be the beam height h and width b, this is done to show the difference in sensitivity between the beam width and height. The cantilever beam uses the same type of cross-section as the ship model, see figure 4.4. The dimensions of the cross-section and other properties are given in table 3.1. The mass of the beam depends on the cross-sectional dimensions. Several characteristics of the beam are investigated, like mode shapes and natural frequencies. Two formulations for the beam finite elements are used Euler-Bernoulli(EB) and Timoshenko(TIM). For the Euler-Bernoulli formulation an analytical(AN) solution is also used as a comparison.

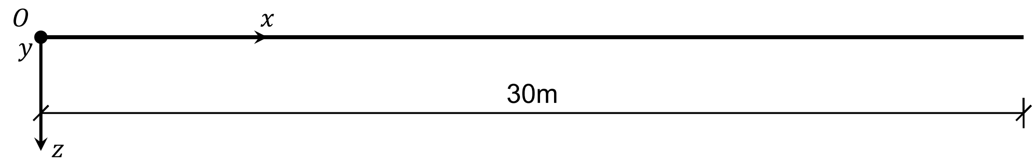

(a) Geometry and axis in this problem, y-axis is pointing out of plane towards the reader.

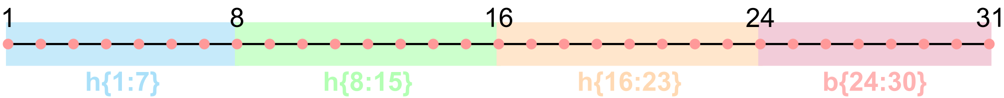

(b) The mesh of the beam used as a test case, and the parameters used in the optimization problem shown in colors.

Figure 3.1: The geometry and the parameters used to test the beam.

Table 3.1: The cross-sectional dimensions and material properties used in the cantilever beam analysis.

property	value	unit
h	1	m
b	1.5	m
t_{fl}	$5.00e-03$	m
t_{web}	$5.00e-03$	m
E	$2.10e11$	Pa
ρ	$7.85e03$	$kg \cdot m^{-3}$
G	$8.08e10$	Pa
ν	0.3	-

3.3. Beam deflection

In this section the results for the static beam deflection of three formulations and two load cases are presented and discussed.

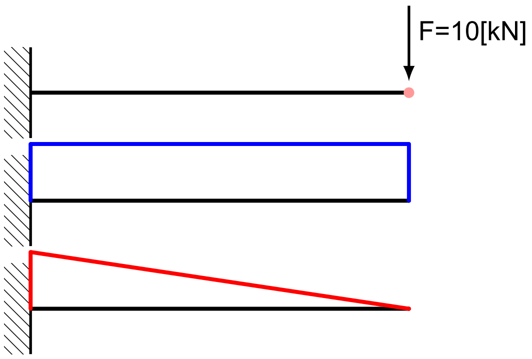

(a) Load case 1

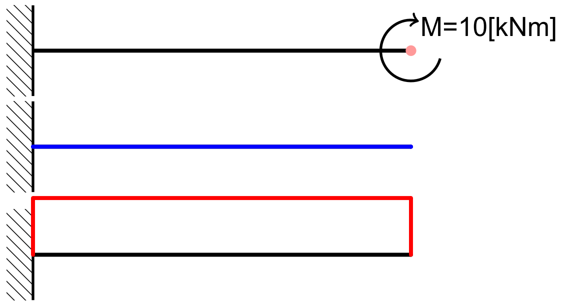

(b) Load case 2

Figure 3.2: Load cases of the cantilever test problem. Internal shear forces (in blue) and bending moments (in red) along the beam are shown qualitatively.

Table 3.2: Comparison of the tip-deflection between solution found using analytic(AN), Euler-Bernoulli(EB) beam and Timoshenko (TIM) beam.

Load case	AN [mm]	EB [mm]	TIM [mm]	difference EB-TIM[-]
1	94.79	94.79	94.88	-0.09%
2	4.74	4.74	4.74	0.00%

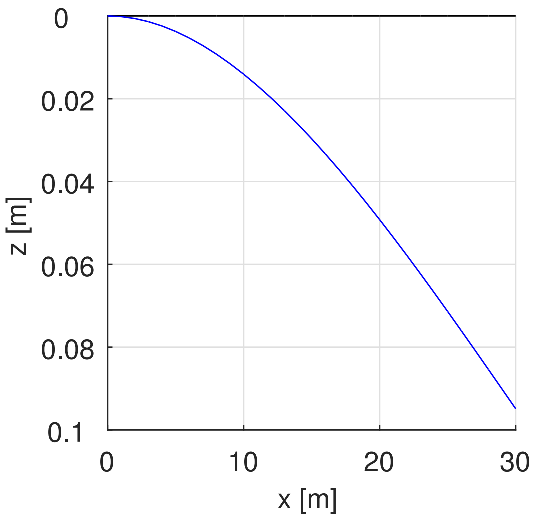

(a) LC 1

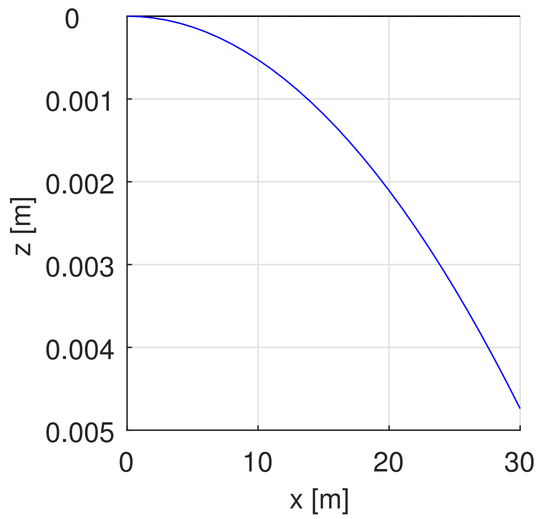

(b) LC 2

Figure 3.3: Response of the Timoshenko beam for the two LC's, only the response of the Timoshenko beam is shown because nearly coincide for LC1 and coincide for LC2.

Results

The deflection of the beam tip for the Euler-Bernoulli beam and the Timoshenko beam is shown in table 3.2. Also for an Euler-Bernoulli beam the analytical deflection is given, to verify the numerical results. For Load Case(LC) 1 the analytical and numerical results are the same for the Euler-Bernoulli beam but differ for Timoshenko beam, its deflection is slightly larger. The deflection of the Timoshenko beam is depicted in figure 3.3 for both LC's. For LC1 in figure 3.3a near the end of the beam there is little curvature. For LC 2 there is curvature along the entire length of the beam and it decreases moving away from the fixed support.In appendix B the static deflection calculated using the implementation of the Timoshenko beam element in this thesis is compared that of the same element using ANSYS.

Discussion

The tip deflection of the Timoshenko beam is greater for LC 1. This can be explained by the inclusion of shear deformation, making the Timoshenko beam more flexible. The difference is small because the governing deformation mode is bending for LC 1. For LC 2 the results are the same for the three formulations, in this LC no shear force is present hence there is no shear deformation. For LC 1 the curvature near the end is very small and it is greatest at the support, this is what is expected because the curvature is proportional to the bending moment and the curvature shows the same trend as the bending moment in figure 3.2a. For LC2 the bending moment is constant along the beam. Beam theory predicts a constant curvature for a constant bending moment, however the curvature near the support is clearly greater than near the tip in figure 3.3b. In Euler-Bernoulli and Timoshenko beam theory the curvature is approximated by the second derivative, the curve in figure 3.3b is a quadratic polynomial and thus has constant curvature in the beam theory approximation.

3.4. Natural frequency of vibration

In this section the natural frequencies of vibration of the cantilever beam are found using three formulations: analytic, Euler-Bernoulli and Timoshenko. A comparison between the three is made. The methods explained in section 2.2.4 have been used to determine the natural frequencies and the mode shapes.

Table 3.3: Natural frequency comparison of the first four flexible modes of an Euler-Bernoulli beam.

Mode	Analytic [Hz]	Numerical [Hz]	relative difference [-]
1	1.31	1.31	0.04 %
2	8.19	8.16	0.30 %
3	22.92	22.76	0.70 %
4	44.92	44.34	1.28 %

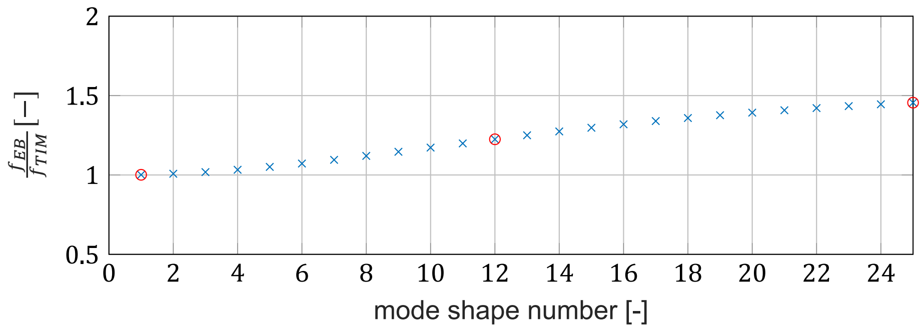

Figure 3.4: Natural frequency comparison between the Euler-Bernoulli beams formulation, $k_s \rightarrow \infty$, and the Timoshenko beam, relative values. Red circles indicate mode shapes plotted in figure 3.5.

Results

In table 3.3 the natural frequencies found using the FE method and analytic are compared, the relative difference is calculated as in appendix F.1. For the first four modes the natural frequencies are shown, the difference is small. And increases as the mode shape number increases. The mode shapes depicted in figure 3.5 are in line with the - well-known - analytical mode shapes. In figure 3.4 the ratio between the natural frequencies of an Euler-Bernoulli beam and a Timoshenko beam is shown for the first 25 modes. For the first mode the ratio between the frequencies is 1. As the mode number increases the ratio increases, for the higher modes the natural frequency of the Timoshenko beam is increasingly lower than that of the Euler-Bernoulli beam. If a line were drawn through the point the derivative of this curve goes from 0 to a maximum value around mode 12, after which the derivate decreases.

Discussion

The changing ratio between the natural frequency of the mode shapes of an Euler-Bernoulli and a Timoshenko beam can be explained by looking at the mode shapes in figure 3.5. For the 1^{st} flexible mode shape the mode shapes of the two formulations coincide, this mode shape is dominated by bending deformation which is modeled in the same manner for Timoshenko and Euler-Bernoulli beams, thus the stiffness k is almost the same and also the mass m is moving in the same way for this mode, there is little rotation of the cross-sections. Hence we expect the same natural frequency $\omega_n = \sqrt{k/m}$, this is also what is shown in figure 3.4. For mode 12 and and 25 the mode shapes are different, these mode shapes have considerable shear deformation. The disparity between the Timoshenko and Euler-Bernoulli beam is most pronounced at the fixed end where the more flexible Timoshenko beam deforms more, whereas at the free end the mode shapes almost coincide. The 'wavelength' of the mode shapes of the Timoshenko beam is thus slightly larger than that of the Euler-Bernoulli beam. At first this seems odd, a bigger 'wavelength' would mean a stiffer beam, however the mode shape is determined by a combination of stiffness *and* mass. In the Timoshenko beam more mass is moving due to the inclusion of shear deformation. The greater modal mass explains the larger 'wavelength'. For the higher modes the stiffness k of the Timoshenko beam is increasingly smaller compared to the Euler-Bernoulli beam, also the modal mass is increasingly bigger for the Timoshenko beam because the rotational inertia of the shear deformation is taken into account. With more mass and less stiffness, the basic formula, $\omega_n = \sqrt{k/m}$, thus predicts a lower natural frequency for the higher modes, which shown observed in figure 3.4.

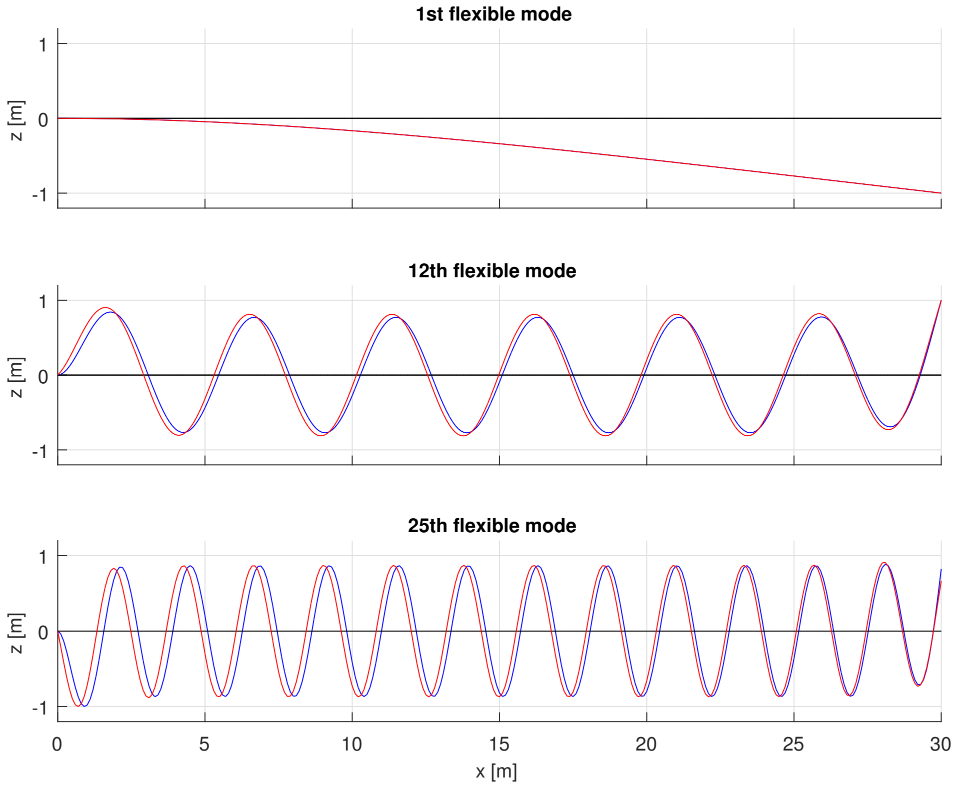

Figure 3.5: Mode shape comparison between the Euler-Bernoulli(blue) beam, and the TIM(red).

3.5. Sensitivities

In this section the sensitivities of the cantilever beam are presented. First for the static displacement and then for the natural frequencies and mode shapes. The results will provide insight into the concept of a sensitivity and what the sensitivities of different quantities look like. The sensitivities here are calculated using the semi-analytical approach explained in section 2.1.11. The sensitivities were also determined fully numerically and the results were found to be the same or very close, less than a permille difference in most cases, indicating the proper implementation of the semi-analytical approach in `MatLab`. Normalization of the sensitivities is done in line with equation 2.17.

3.5.1. Static displacement sensitivity

The results for the static displacement sensitivity of the tip displacement of the cantilever beam are given here, as well as a short discussion of the results.

Table 3.4: Normalized sensitivities of the static tip displacement for LC 1 and four parameters, determined in different ways.

parameter	AN [-]	EB [-]	TIM [-]	relative difference %
h {all}	2.1925	2.1925	2.1912	0.06%
b {all}	0.8212	0.8212	0.8206	0.07%
t_{fl} {all}	0.8075	0.8075	0.8069	0.07%
t_{web} {all}	0.1788	0.1788	0.1794	-0.33%

Results

In figure 3.6 the sensitivity of the static displacement of the tip is shown for the beam in figure 3.1a and LC1 as in figure 3.2a. Both the absolute 3.6a and the normalized sensitivities 3.6b are shown. The parameters used are the h the height, b width, t_{fl} flange thickness and t_{web} web thickness for all elements. The figure 3.6a depicting the absolute sensitivity shows that

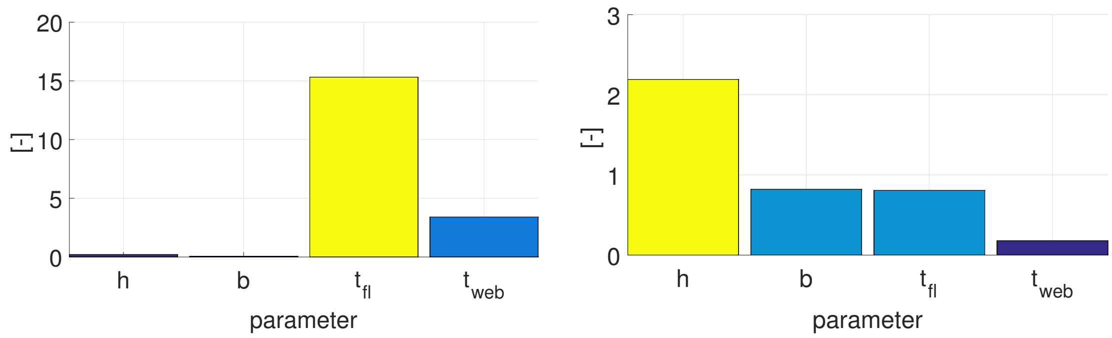

(a) Absolute sensitivity.

(b) Normalized sensitivity

Figure 3.6: Sensitivity of the static tip displacement of an Euler-Bernoulli beam for LC1, both the absolute (a) and the normalized (b) sensitivity are shown.

t_{fl} is most sensitive parameter, and t_{web} is about one fifth as sensitive as t_{fl}. The parameters h and b show a small absolute sensitivity compared to t_{fl}, h is somewhat more sensitive than b. The normalized sensitivity in figure 3.6b shows that h is the most sensitive parameter, b and t_{fl} are about a third as sensitive and t_{web} the least sensitive.

A comparison between the normalized sensitivity of static response of the tip is shown in table 3.4, for three formulations: Analytic, Euler-Bernoulli and Timoshenko. The relative difference between the Euler-Bernoulli and Timoshenko beam are shown in the last column, see appendix F.1 for the definition of the relative difference. The sensitivities for analytical and Euler-Bernoulli are the same. The Timoshenko beam is less sensitive for h, b and t_{fl} and more sensitive for t_{web}. The differences in sensitivity are small between Euler-Bernoulli and Timoshenko beams.

In figure 3.7 and 3.8 the normalized sensitivity of the tip displacement are shown for LC1 and LC2 respectively. For the parameters defined as follows: for each element four properties can be changed for 30 elements this results in 120 parameters and their sensitivities. The sensitivities are shown for the Euler-Bernoulli beam and Timoshenko beam in (a) and (b) respectively. In (c) the sensitivity of Euler-Bernoulli beam is divided by the sensitivity of the Timoshenko beam. For both LC1 and LC2 the sensitivity of the elements is greatest at the support and decreases going closer to the tip, this is true for all parameters and both the Timoshenko and Euler-Bernoulli beam. The ratios between the sensitivity of the different properties is like those found for the tip displacement in figure 3.6b. The ratio between the sensitivities for LC1 shows that the Timoshenko beam is more sensitive if parameters close to the tip are used, t_{web} shows the biggest difference in sensitivity.

Discussion

The results in figure 3.6 can be explained as follows. The displacement of the tip is governed by the bending stiffness of the beam, the bending stiffness is proportional to the moment of inertia of the cross-section. Absolute the t_{fl} and t_{web} are the most sensitive because their magnitude is smaller by a factor 200 compared to b and h in this analysis. An absolute change in a parameter will have a relatively big effect on t_{fl} and t_{web} and as a result these parameter have the greatest absolute sensitivity. The flange thickness is more sensitive than t_{web} because t_{fl} is more effective in increasing the moment of inertia as it increases the area that is further from the neutral axis, the same reasoning is true for h and b. The normalized sensitivity looks at a relative changes and now the h is the most sensitive parameter. In FEMU the values of the parameters should only change slightly and to minimize conditioning problems in the sensitivity matrix the normalized sensitivity should be used[12].

In table 3.4 the analytical and the Euler-Bernoulli beam have the same sensitivity this is because they use the same formulation to determine the displacement. The difference between the Euler-Bernoulli and Timoshenko beams is small, and is caused by the shear deformation. The bending deformation is the same for the Euler-Bernoulli and Timoshenko beams, and shear deformation is only taken into account by a Timoshenko beam. The amount of

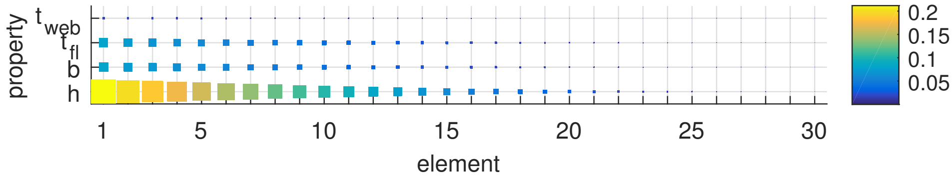

(a) Timoshenko beam normalised tip sensitivity.

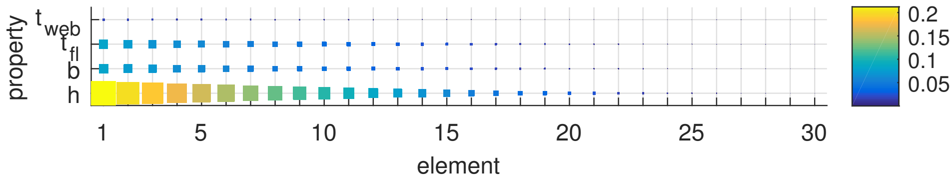

(b) Euler-Bernoulli beam normalised tip sensitivity.

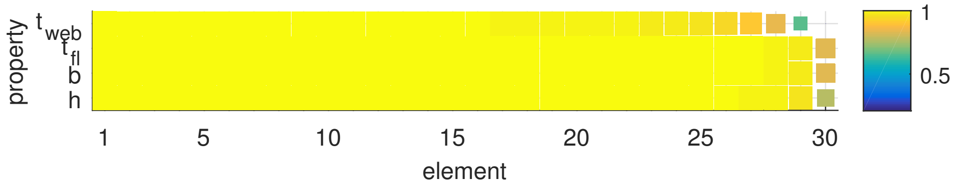

(c) Euler-Bernoulli normalised tip sensitivity divided by Timoshenko normalised tip sensitivity.

Figure 3.7: Normalized sensitivity of the tip response for load case 1 for each individual element parameter combination. The area of the squares is proportional to the value of the sensitivity.

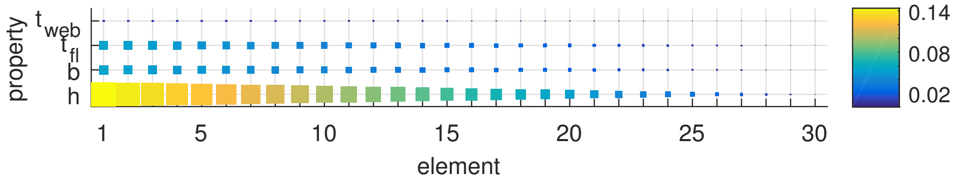

(a) Timoshenko beam normalised tip sensitivity.

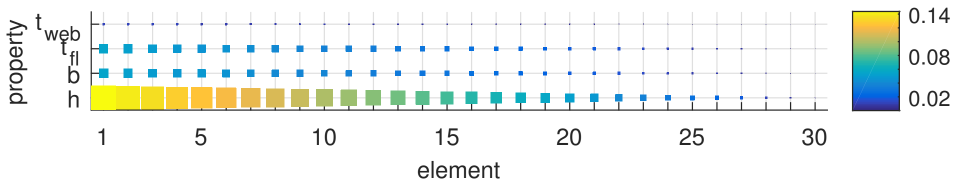

(b) Euler-Bernoulli beam normalised tip sensitivity.

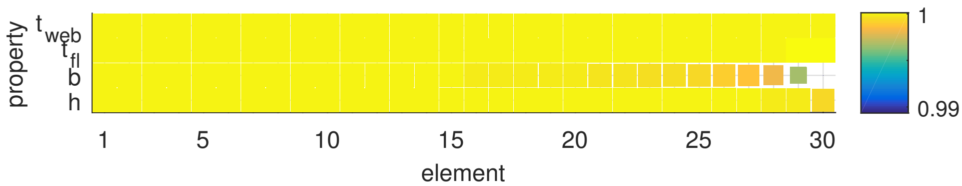

(c) Euler-Bernoulli beam normalised tip sensitivity divided by Timoshenko beam normalised tip sensitivity.

Figure 3.8: Normalized sensitivity of the tip response for load case 2 for each individual element parameter combination. The area of the squares is proportional to the value of the sensitivity.

shear deformation is determined by the ϕ in equation (3.1), if $\phi = 0$ there is no shear deformation. Equation (3.1) shows that ϕ is proportional to the moment of inertia I divided by the effective shear area A_{shear}. This explains the relative differences seen in table 3.2. The web thickness, t_{web}, is more sensitive for the Timoshenko beam because it relatively increases the A_{shear} compared to I and thereby reduces the shear stiffness of the beam and increases ϕ. Changing h,b and t_{fl} results in a relatively smaller shear area and thus increases the shear stiffness, resulting in a smaller sensitivity.

$$\phi = \frac{12EIk_s}{AGL^2} \propto \frac{I}{A_{shear}} \quad with \quad k_s = \frac{A}{A_{shear}} \tag{3.1}$$

In figure 3.7 and 3.8 the decrease in sensitivity for the parameters moving away from the support can be explained by the bending moment along the beam. The bending moment dictates the tip response and it is greatest close to the support and decreases linearly to zero at the tip. For LC1 there is a constant shear force along the beam. The shear deformation is small compared to the bending deformation close to the support, because there the bending moment is much greater than the shear force. Closer to the support the ratio between the shear force and the bending moment becomes smaller and shear deformation becomes relatively more important. The parameter that changes the shear response most is t_{web} for the same reasons as explained in the previous paragraphs, this is also what is seen in 3.7c. For LC2 the sensitivities are the same because there is no shear force, and bending deformation is taken into account in the same way for both the Euler-Bernoulli and Timoshenko beam. For LC2 in figure 3.8c there seems to be a difference in sensitivity but the differences are very small, hence the assumption that sensitivities for LC2 are the same for the Euler-Bernoulli and the Timoshenko beam is reasonable.

3.5.2. Natural frequency sensitivity

In this section the natural frequency sensitivities for the cantilever beam are presented for both the Euler-Bernoulli and the Timoshenko beam. And the differences between the sensitivities for the two beam formulations are discussed.

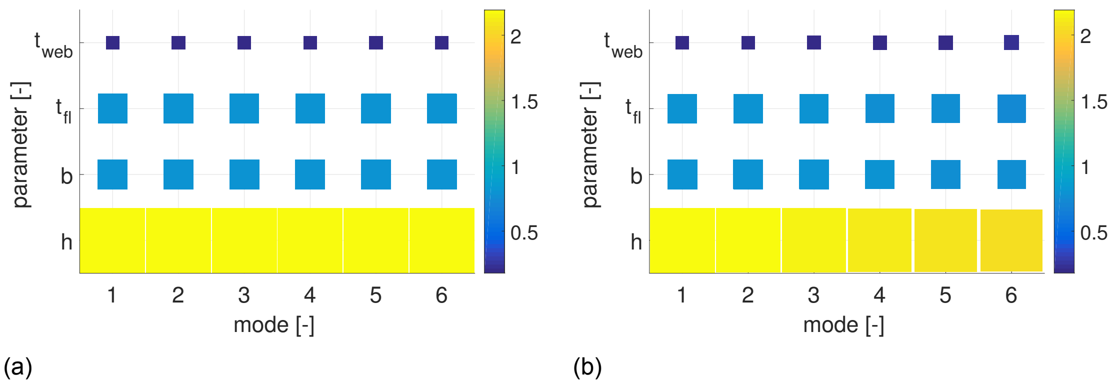

Figure 3.9: Sensitivity of the natural frequency of the cantilever beam using the Euler-Bernoulli beam (a) and Timoshenko beam (b).

Table 3.5: Sensitivities of the first 6 natural frequencies of the Euler-Bernoulli beam divided by the Timoshenko beam, for different parameters

	mode					
parameter	1	2	3	4	5	6
h\{all\}	1.01	1.01	1.02	1.03	1.04	1.06
b\{all\}	1.01	1.01	1.02	1.03	1.05	1.07
t_{fl}\{all\}	1.00	1.01	1.02	1.03	1.05	1.07
t_{web}\{all\}	0.99	0.97	0.93	0.88	0.82	0.77

Results

In figure 3.9 the sensitivities of the natural frequencies are shown for the two beam formulations. In in table 3.5 a quantitative comparison of the differences between the Euler-Bernoulli and Timoshenko beam formulation is shown, the natural frequency sensitivity of the Euler-Bernoulli beam is divided by that of the Timoshenko beam. For the first mode the differences are small and they increase as the mode shape number increases. The Euler-Bernoulli beam is more sensitive for the parameters h, b and t_{fl} and less sensitive for t_{web} compared to the Timoshenko beam. For the sensitivity of each parameter is constant in function of the mode shapes shown here.

Discussion

Explaining the difference in sensitivity between the Euler-Bernoulli and Timoshenko beam is more involved for the natural frequency than for the static response. Because the natural frequency is determined by the mass and the stiffness participating in each mode shape, also called the modal mass and stiffness. For the lower modes the difference in sensitivity is almost the same, for this mode the taking shear into account does not change the ratio between the stiffness and the mass significantly. The effect of shear is more pronounced in higher modes, hence the higher modes will show a bigger difference in sensitivity. The sensitivity of t_{web} becomes smaller because this increases ϕ, reducing the modal stiffness and increasing the modal mass. For the other parameters the sensitivity becomes bigger because of the reduction of ϕ, increasing the modal stiffness and reducing the modal mass.

3.5.3. Mode shape sensitivity

In this section the mode shape sensitivities - or derivatives - are given for the cantilever beam. These are more complicated concepts, according to the author. For a clearer understanding of the mode shape derivative and how it is connected to a parameter the first mode shape of the cantilever shown in a function of several parameters, also the natural frequency of vibration is shown. Then the mode shape derivative is depicted for different parameters and different ways of determining the mode shape derivative, namely numerical, Nelson and Fox Kapoor, see section 2.1.11 for a description of these methods.

Mode shape derivative explained

To elucidate the concept of a mode shape derivative the first flexible mode shape of the cantilever beam is shown in function of different parameters, in figures 3.10 to 3.13. The parameter property value is normalized and varies from 0.5 to 1.5; the reference mode shape has property value 1. The absolute change in mode shape compared to the reference mode is shown on the left, the colors of the surface indicate the normalized relative difference in mode shape compared to the reference mode shape. In the figure on the right the mode shapes at several parameter settings are indicated by the white lines on the surface, the coloring of the surface indicates the normalized relative change in mode shape compared to the reference mode shape. The absolute change in mode shape is small in for most parameters, looking carefully at the mode shapes in figure 3.12 shows the change mode shape. Taking the directional derivative of the surface at a point and in the direction of the property change gives the mode shape derivative of that point defined by a property value and a x-coordinate. A mode shape derivate then found by taking the directional derivate at each x-coordinate, and it has the same mathematical form as a mode shape. Figure 3.10 shows the mode shape in function of $h\{all\}$, if all element properties are changed at the same time the mode shape does not change. Figure 3.11 shows the mode shape in function of $h\{1\}$, this has a significant influence on the mode shape, the same is true for $h\{10:20\}$ shown in 3.12. The mode shape in function of $h\{30\}$ does change but this change is small.

The natural frequencies of the first mode shape are shown in figure 3.14. In this figure the biggest change in natural frequency is observed in the parameter $h\{all\}$. The parameter $h\{30\}$ has negligible influence on the natural frequency, the parameters $h\{10:20\}$ and $h\{1\}$ have some influence.The natural frequency is determined by $\omega_n = \sqrt{k/m}$, in this case these are the modal masses and stiffnesses. The parameter that has the biggest influence on the modal stiffness divided by the modal mass and will thus change the natural frequency the most. Indeed the parameter that changes the all elements is the most sensitive.

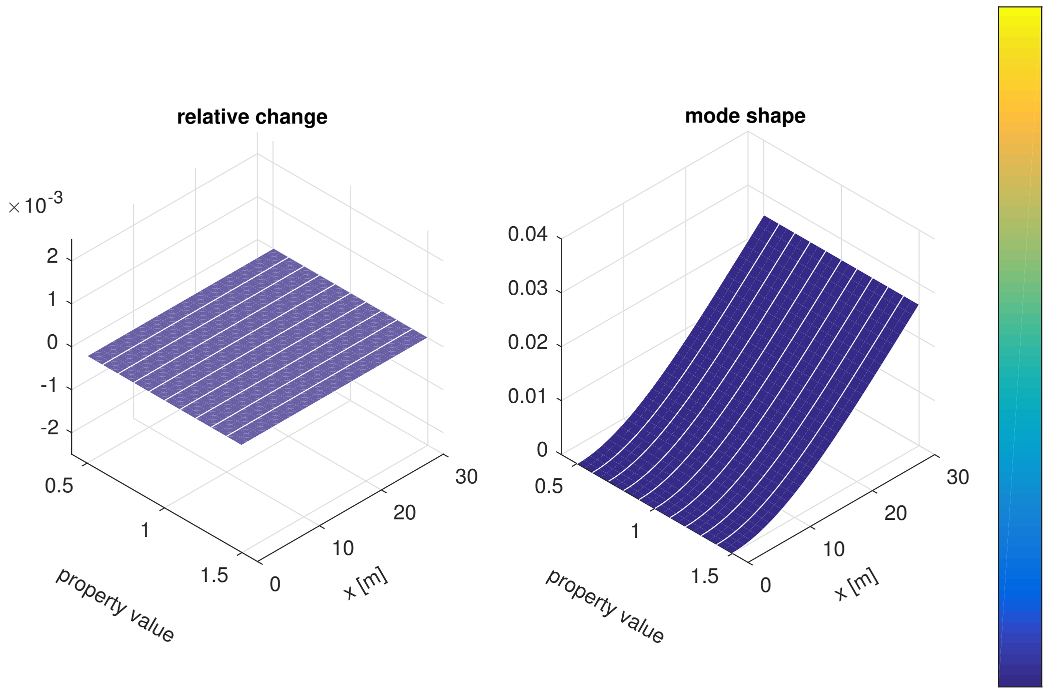

Figure 3.10: Mode shape in function of parameter $h\{all\}$, relative change in the left figure and the mode shape on the right. The white lines are the mode shapes at a certain property value.

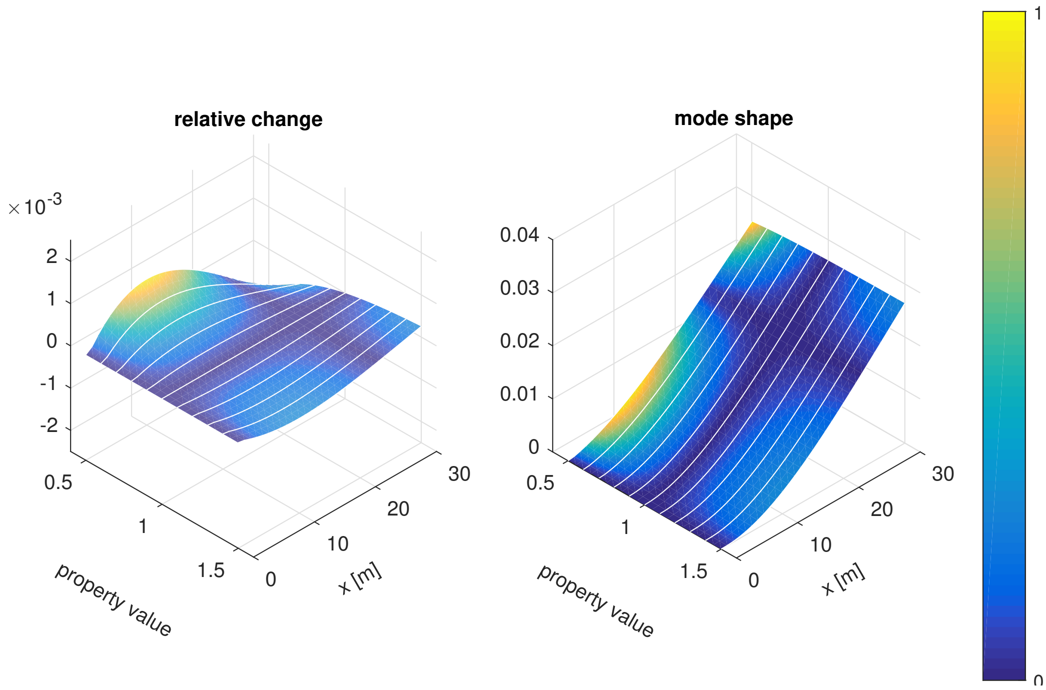

Figure 3.11: Mode shape in function of parameter $h\{1\}$, relative change in the left figure and the mode shape on the right. The white lines are the mode shapes at a certain property value.

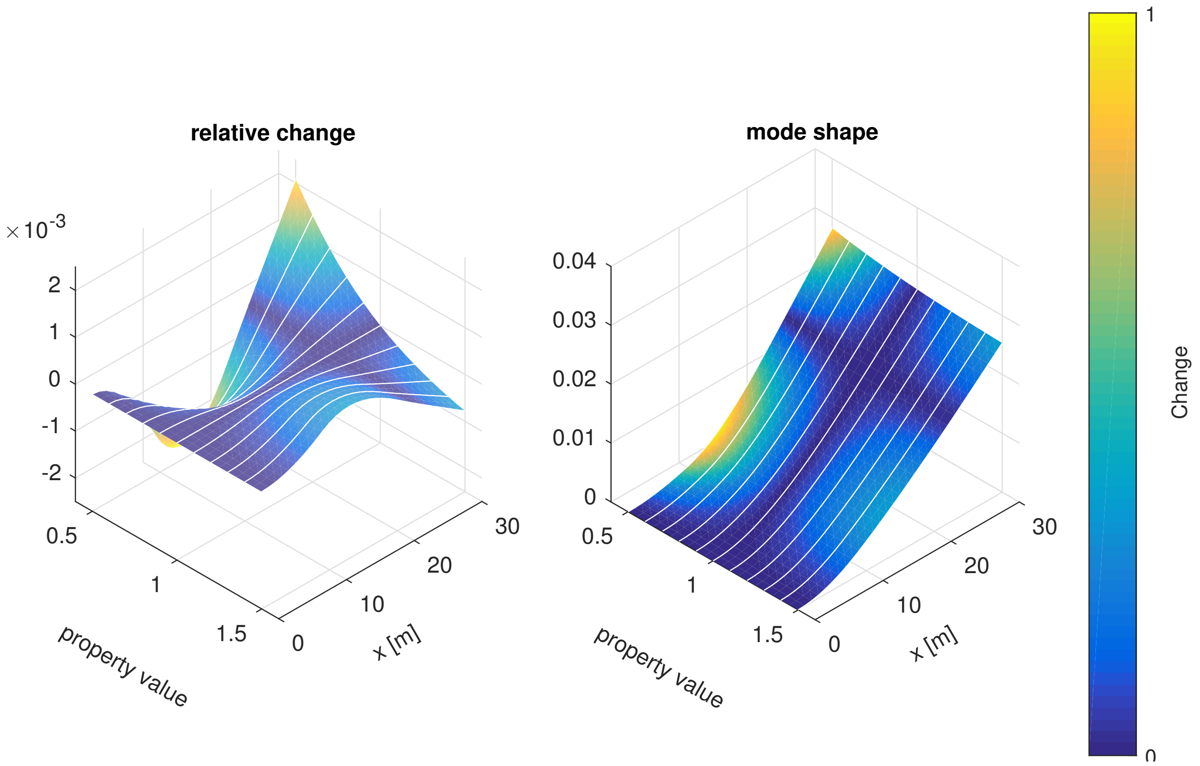

Figure 3.12: Mode shape in function of parameter $h\{10:20\}$, relative change in the left figure and the mode shape on the right. The white lines are the mode shapes at a certain property value.

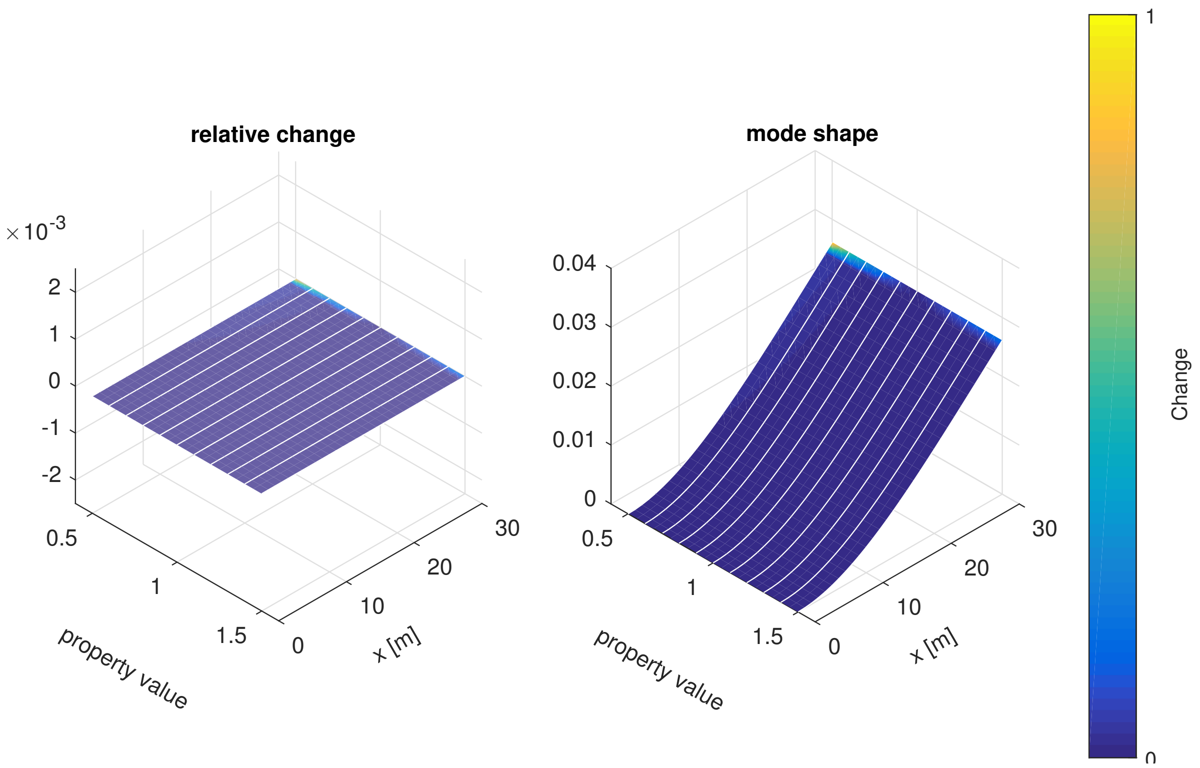

Figure 3.13: Mode shape in function of parameter $h\{30\}$, relative change in the left figure and the mode shape on the right. The white lines are the mode shapes at a certain property value.

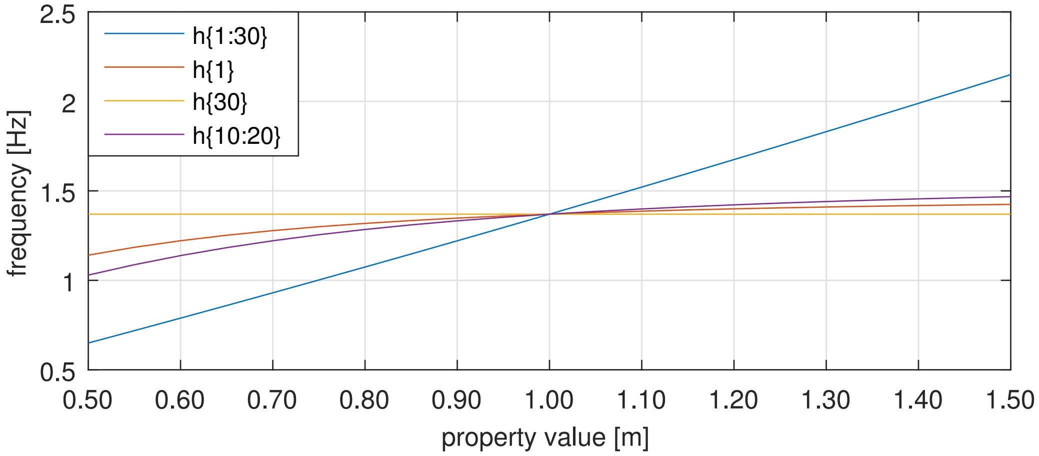

Figure 3.14: Natural frequency in function of 4 different parameters, notice the difference in variation between the parameters.

Next to the number of elements that are changed the position of the element matters. The position determines whether or not the elements connected to a parameter are deforming in a mode shape, this deformation then determines if the elements contribute significantly to the modal stiffness k. For the modal mass it matters whether or not the elements move for a particular mode shape. This explains the difference between the parameters $h\{1\}$ and $h\{30\}$, the element - at the beam tip - of latter parameters has negligible deformation compared to the element - at the support - of the former parameter. Parameter $h\{10:20\}$ both influences the modal mass and the modal stiffness, this parameter changes the natural frequency the 2^{nd} most. Depending on the number and position of elements connected to a parameter the sensitivity of the mode shape and the natural frequency changes. For some parameter choices the mode shape remains constant and only the natural frequency changes. When updating a model it thus essential to choose the right elements in a parameterization to correct for faulty mode shapes and natural frequencies. The mode shape change for parameter $h\{10:20\}$ and $h\{1\}$ - in figures 3.12 and 3.11 - look to have the same shape as the second mode shape. This has probably been the reason why Fox and Kapoor developed their method for determining mode shape derivatives, in which a truncated modal basis is used to approximate the mode shape derivative.

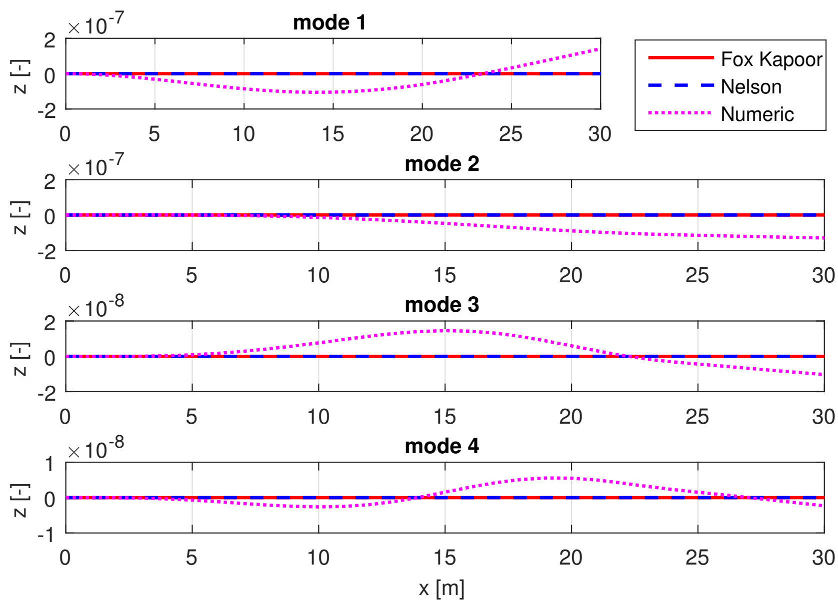

Figure 3.15: Sensitivity of the mode shape for the first four flexible modes of the cantilever beam for the parameter $h\{all\}$, determined using three different methods.

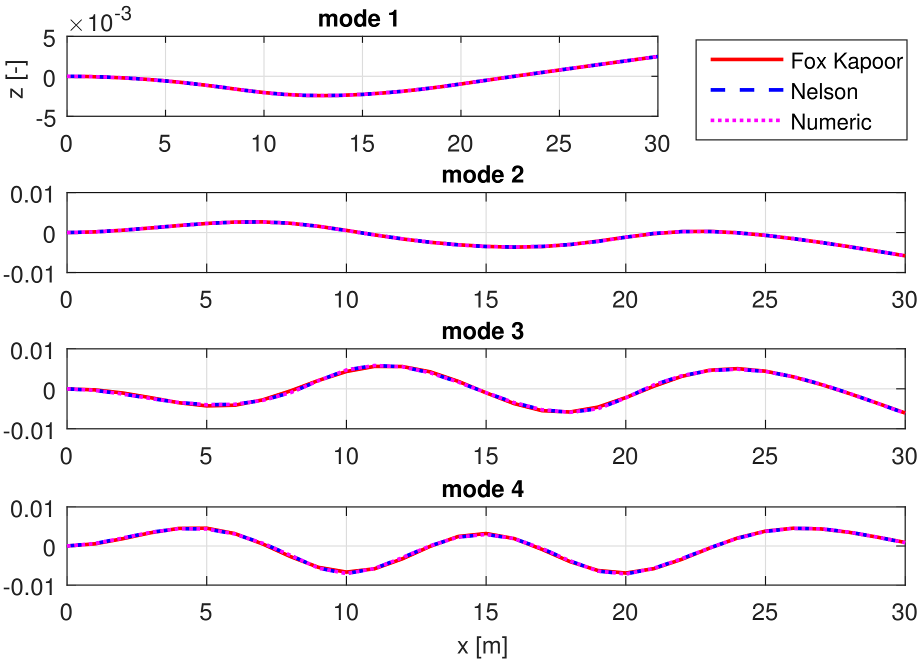

Figure 3.16: Sensitivity of the mode shape for the first four flexible modes of the cantilever beam for the parameter $h\{10:20\}$, determined using three different methods.

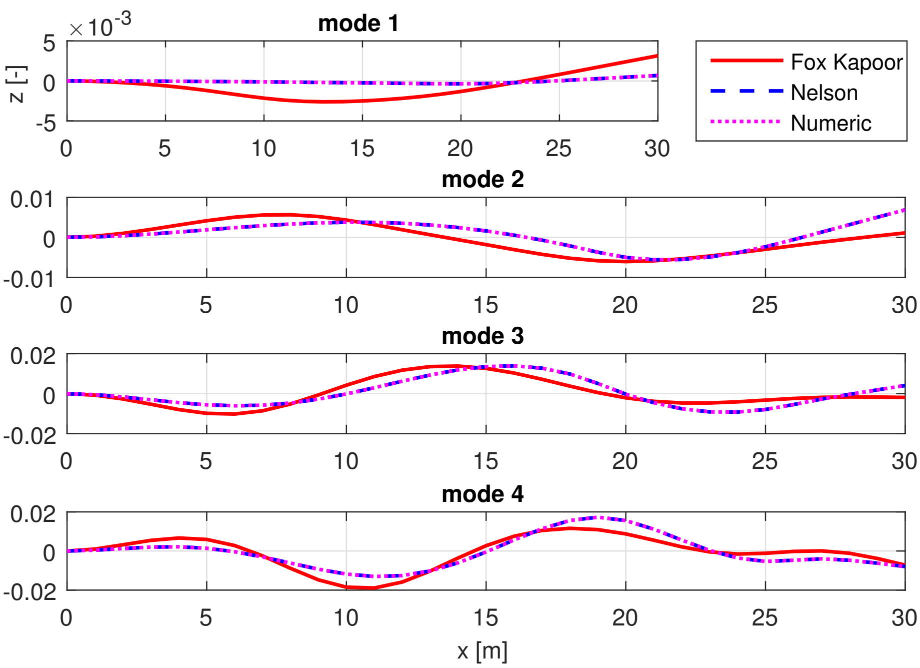

Figure 3.17: Sensitivity of the mode shape for the first four flexible modes of the cantilever beam for the parameter $h\{20:26\}$, determined using three different methods. 10 modes were used in the modal basis for Fox and Kapoor.

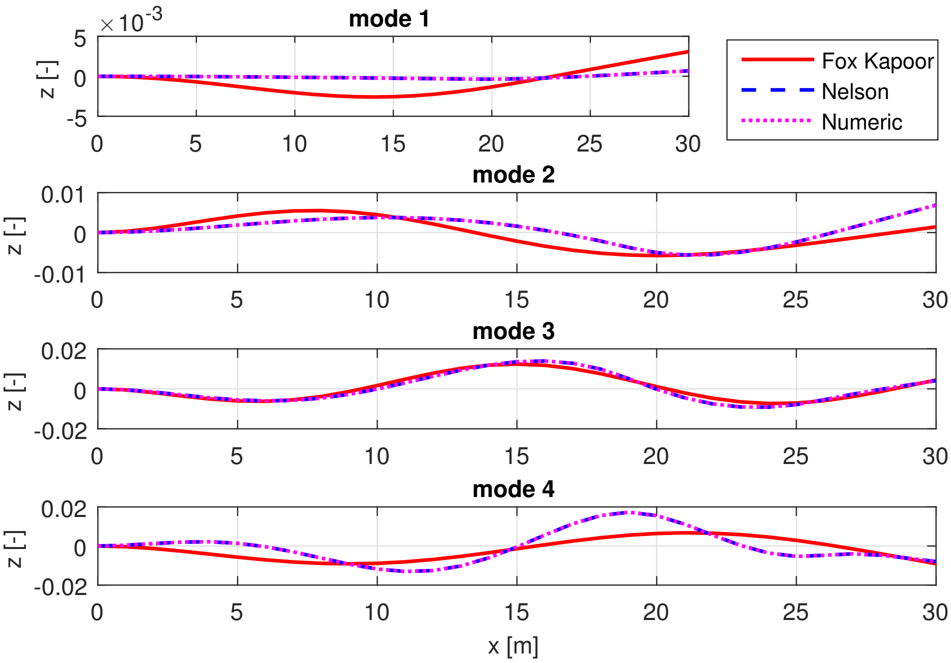

Figure 3.18: Sensitivity of the mode shape for the first four flexible modes of the cantilever beam for the parameter $h\{20:26\}$, determined using three different methods. 4 modes were used in the modal basis for Fox and Kapoor.

Results

The concept of a mode shape derivative has been explained in the previous paragraphs of this section. Now the mode shape derivative of different parameters and mode shapes - the first four flexible modes - are compared. For each mode shape derivative three ways of determining them are shown; Numeric, Nelson and Fox Kapoor. The parameters that have been used are $h\{all\}$, $h\{10:20\}$ and $h\{20:26\}$. Also the influence of the size of the modal basis in the method of Fox Kapoor is studied by varying the size of the modal basis. In figure 3.15 to 3.17 ten modes are used in the modal basis and in figure 3.17 four modes are used. In figure 3.15 the mode shape derivative is shown for the parameter $h\{all\}$. This derivative should be zero for all modes but the numeric solution shows a very small derivative, it is assumed that this is due to roundoff-errors in solving the eigenvalue problem. Nelson and Fox Kapoor show a mode shape derivative that is zero. In figure 3.16 the mode shape derivatives using the three methods coincide. In figure 3.17 and 3.18 the mode shape derivative is shown for the parameter $h\{20:26\}$ the difference between the figures is the number of modes used in the FK approximation, 10 vs 4 modes. In figure 3.17 10 modes are used in the modal basis to approximate the mode shape derivative, the mode shape derivatives determined using Fox and Kapoors method show a difference for all 4 mode shapes. If only 4 modes are used n the modal basis as in figure 3.18 the mode shape derivative of mode 3 determined using Fox Kapoor shows a smaller difference than when 10 modes are used in the modal basis. Mode 4 seems to be more at fault when 4 modes are used in the modal basis, and for mode 1 and 2 the mode shape derivatives determined using Fox and Kapoor do not change when 10 or 4 modes are used in the modal basis. By looking at the magnitude of the mode shape derivates in the figures, it can be seen that the mode shape have different magnitudes for different modes but the same parameter.

Discussion

The mode shape derivatives have been determined for the first four modes of the cantilever using three different methods. Three different parameters were used and for one parameter the modal basis used in Fox Kapoors method was varied. The results show that the results of the different methods depend on the choice of the parameter. The numerical and Nelsons method may be considered equivalent. The accuracy of the Fox and Kapoors method depends on the parameter choice, it was also shown that increasing the size of the modal basis does not necessarily lead to a better approximation. Fox Kapoors method uses a modal basis to approximate a mode shape, however the shape of a mode shape derivative is not necessarily well approximated by a linear combination of mode shapes in the modal basis. The numerical method and Nelsons method are the same for all mode shapes and parameters, save a numerical error for the first mode shape. Also for parameter $h\{all\}$ and $h\{10 : 20\}$ the methods give the same results for all the modes. This supports correct implementation of the different methods. In the rest of this research the Nelsons approach is used to determine the mode shape derivatives, because it is more accurate than Fox Kapoors method and computationally more efficient than the numerical method.

3.5.4. MAC value sensitivity

In this section the sensitivity of the MAC value for the cantilever beam is shown and discussed. The MAC value sensitivity has been determined using equation (2.33), in this equation the mode shape derivate appears.

Results

The values of the sensitivity matrix of the MAC are shown in 3.6 for the parameters: $h\{all\}$, $b\{all\}$,$t_{fl}\{all\}$ and $t_{web}\{all\}$. The parameters are not sensitive to the MAC value.

Table 3.6: MAC value sensitivity for the first 6 flexible modes.

	h	b	t_{fl}	t_{web}
1	1.96E-20	-1.47E-20	-2.51E-18	2.51E-18
2	7.25E-19	1.45E-19	3.71E-17	1.86E-17
3	5.19E-19	5.19E-19	0	1.33E-16
4	-3.60E-18	4.50E-19	-1.15E-16	0
5	-3.06E-18	0	0	0
6	-1.04E-17	-2.59E-18	6.63E-16	6.63E-16

Discussion

The very small sensitivity of the MAC value can be explained by the fact that changing all elements properties does not change the mode shape. And as a result the MAC value does not change, making the parameters insensitive.

3.6. FEMU of the cantilever beam

In this section the results of FEMU applied to the cantilever beam are presented. To this end virtual measurements were created using the parameter setting as shown in table 3.1. After the virtual measurement the parameter values were altered slightly, in a range of $\pm 20\%$. This way of altering is in line with what FEMU is meant for; tuning a model whose behavior correlates well with measured behavior. The altered model was then used in the updating procedure. Updating has been performed using two different types of data. One type is the displacement data from a static load case, and the other type is using the modal parameters of the beam. The influence of noise on measurements is investigated. For the static case the effect of a different number of measurements is investigated, in the case of four measurements the position of the measurement is varied. At its core FEMU is a optimization problem as presented in 2.1.15, the optimization methods have been implemented in `MatLab` by the author.

A note on simulated measurements

When simulated measurements are used the modeling error $\boldsymbol{\eta}_{er}$ is zero, because the measured behavior is found from the the same model that is updated only with different parameters. The true model exist in the model space S_3 when no noise is added to the virtual measurements, also the true behavior of the structure is equal to the measured behavior. In this case the parameter error $\boldsymbol{\eta}_{\theta}$ is equal to the residual, see equation (2.12). As a result the updated model should be equal to the true model. The parameter estimates should be the equal to the parameter values used to find the measured behavior. And serves as a way of verifying that the implemented updating algorithm works. In an actual FEMU procedure the updated model is never equal to the true behavior because of the ever-present modeling $\boldsymbol{\eta}_{er}$ and measurement $\boldsymbol{\eta}_m$ errors.

Table 3.7: The parameters used in the cantilever beam updating.

name	parameter
h1	$h\{1:7\}$
h2	$h\{8:14\}$
h3	$h\{15:23\}$
b	$h\{24:30\}$

Table 3.8: Sensor locations and condition number - at iteration step 1 - for the different analyses.

Analysis	sensor location	condition number
1	31	1.00E+00
3	12,18,31	1.03E+01
4-stable	5,18,20,31	6.66E+02
4-unstable	5,14,15,31	1.02E+15
4	5,12,24,31	2.42E+02
5	5,12,24,28,31	2.17E+02

3.6.1. Noiseless static data

The parameters used in the updating are shown in figure 3.1b and are repeated in table 3.7. The number of measurements and the position of the measurements has been varied, this can be seen in table 3.8, which also shows the condition number of the sensitivity matrix $\mathbf{S}$. The updating algorithm uses the pseudo-inverse to solve the least squares problem each iteration.

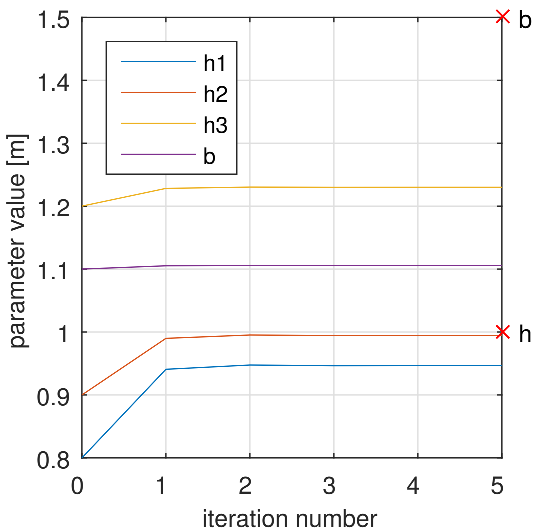

(a) 1 measurement

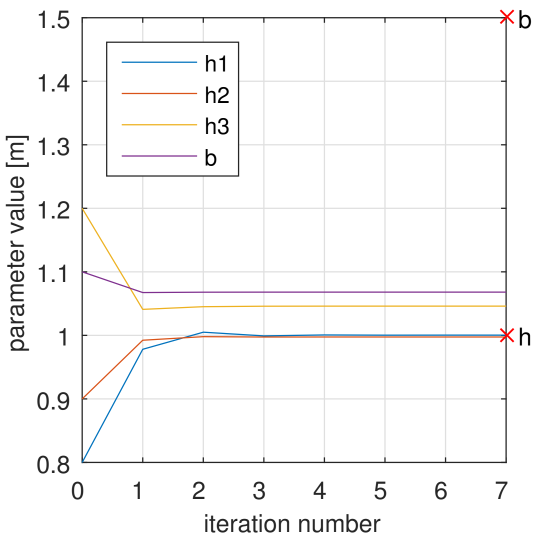

(b) 3 measurements

Figure 3.19: Updating a cantilever beam using 1 (a) or 3 (b) measurements. The values of the parameter at each iteration is shown in both cases convergence is reached after a small number of iterations.

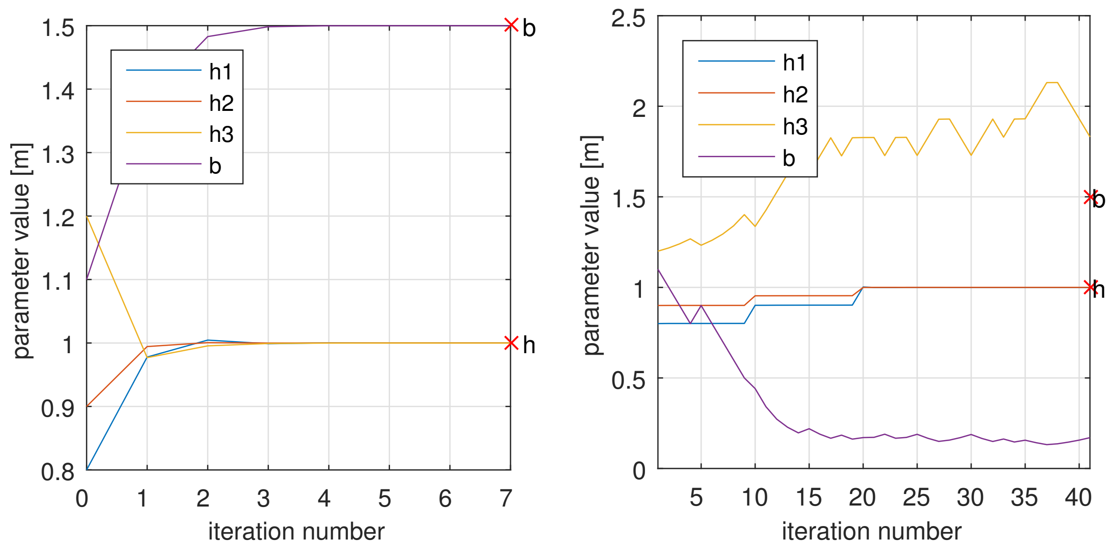

(a) 4 measurements, different areas

(b) 4 measurements, 2 in same area, unstable.

Figure 3.20: Updating of a cantilever beam using 4 measurements at different locations. The values of the parameter at each iteration is shown, (a) converges and (b) does not converge.

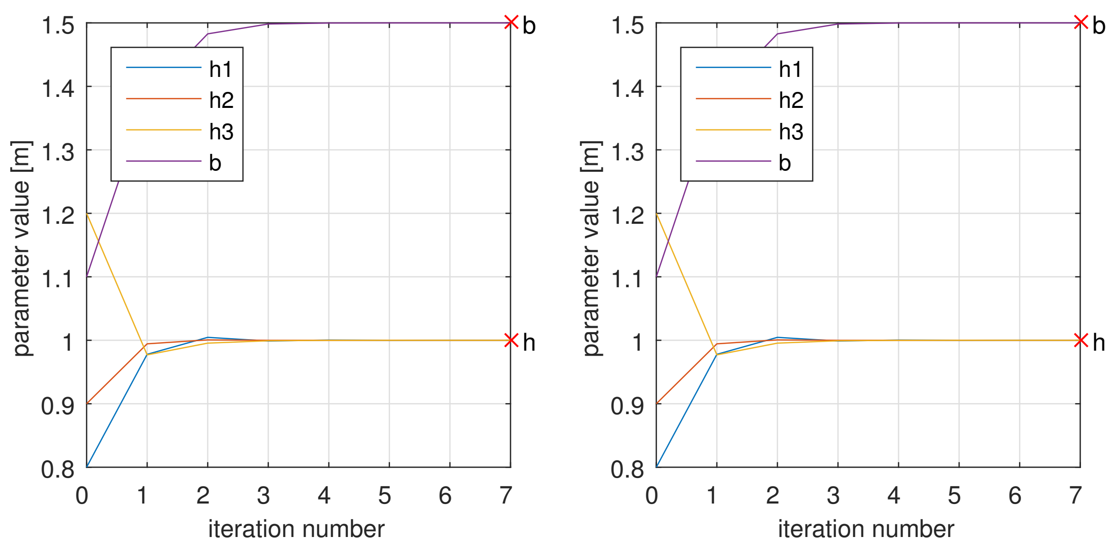

(a) 4 measurements, 2 in same area, stable.

(b) 5 measurements

Figure 3.21: Updating of a cantilever beam using a different number of measurements. The values of the parameter at each iteration is shown in both cases convergence is reached after a small number of iterations.

Table 3.9: Resulting parameter values for the different updating analyses.

		Analysis					
parameter	true value	1	3	4-stable	4-instable	4	5
h1	1.00	0.95	1.00	1.00	1.00	1.00	1.00
h2	1.00	0.99	1.00	1.00	1.00	1.00	1.00
h3	1.00	1.23	1.05	1.00	1.83	1.00	1.00
b	1.50	1.11	1.07	1.50	0.17	1.50	1.50

Table 3.10: The resulting parameter values after updating for different values of λ.

	λ^2		
parameter	0.01	0.05	0.1
h1	1.00	1.00	1.00
h2	1.00	1.00	1.00
h3	1.02	1.02	1.02
b	1.09	1.09	1.09

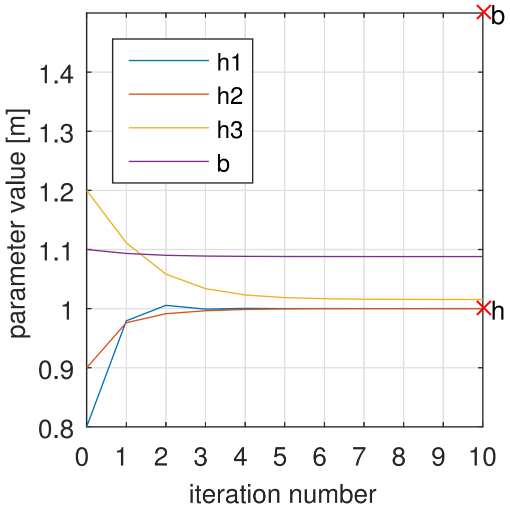

Figure 3.22: The updating the unstable case in figure 3.20b using regularization, with $\lambda^2 = 0.01$.

Results

The final values of the parameters after updating can be seen in table 3.9. The values during iterations can be seen in figures 3.19 to 3.21, these figures the true values of the parameters is indicated by the red crosses labeled b and h. All of the analyses converge save one, this is the analysis where the condition number of the sensitivity matrix is large. For this analysis the iteration step size was reduced in an attempt to find a converged solution, without the decreased step size the parameters would attain non-physical values quickly. After 40 iterations the solution still not converges and the algorithm was halted.

Discussion

From the analyses that converge the ones with an equal or greater number of parameters as measurements are able to recover the true value of the parameter. The under-determined analyses do converge but the solution is different form the true value. For the analyses where three measurements were used the values of h_1 and h_2 were found correctly. The algorithm finds a solution after a small number of iterations for all analyses save the unstable one, fast convergence is an indication of a well-posed updating procedure [12]. These were the noiseless measurements, and hence the variance is 0 for the updated parameter values.

Regularization

The unstable case with four measurements can be solved using a different algorithm, in this case the solution diverges because the condition number of the sensitivity matrix is very large. Using regularization a converging solution can be found, the results are shown in figure 3.22. The effect of the choice of the parameter λ is shown in table 3.10, the parameter values are the same for the different choices of λ. The difference that was found in a changing value for λ was the number of iterations needed to find a solution, this is in line with what Mottershead[19] found.

Table 3.11: Entries in the sensitivity matrix shown in 3.23.

1.75E+0	1.69E-9	9.71E-9	8.90E-9
1.45E+0	3.44E-1	1.09E-8	9.97E-9
1.08E+0	6.23E-1	1.76E-1	1.15E-8
9.63E-1	6.42E-1	2.95E-1	7.71E-3

3.6.2. Noisy static data

Adding noise is expected to cause problems when the sensitivity matrix has a large condition number. Noise is added to the measurements as defined in appendix F.2. To study the effect of noise on the updating procedure, analysis 4 was used because it has an equal number of measurements as parameters and should be able to recover the original parameter values in case of noiseless measurements.

Results

For different noise levels the resulting parameter values are shown in 3.12. As the noise level increases the true value of the parameters cannot be found and for a noise level of $1e-1$ no solution is found. The variance increases as the noise level increases, and the variance of the parameters closer to the support is greater. In figure 3.23 the sensitivity matrix for a noise level of $1e-5$ is shown, and its values in table 3.12. The parameter $h1$ is sensitive to all measurements and, $h2$ only to three, $h3$ only to two and b only to one. Parameter b is the least sensitive parameter both in terms of the number of parameters it influences and in the value of the sensitivity. In terms of updated values the least sensitive values change the most as the noise level increases.

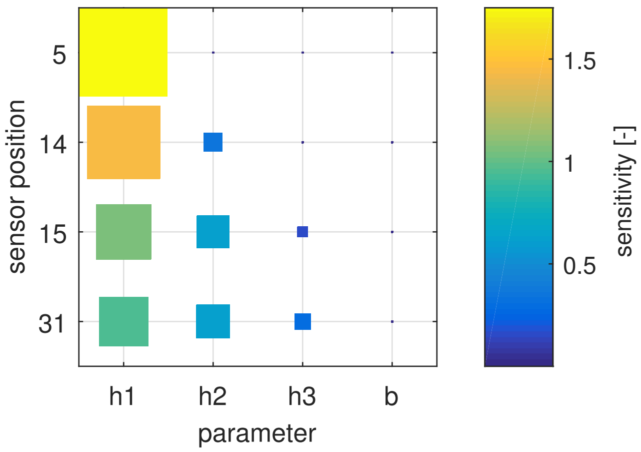

Figure 3.23: Sensitivity matrix for analysis 4 with $1e-5$ noise using static data, the size of the square is proportional to the sensitivity.

Table 3.12: Updating results with noise

	noise level				
parameter	1.00E-05	1.00E-04	1.00E-03	1.00E-02	1.00E-01
h1	1.00	1.00	1.00	1.00	4.78E+13
h2	1.00	1.00	1.00	0.99	2.50E+15
h3	1.00	1.00	1.01	1.14	-1.15E+15
b	1.50	1.46	1.18	0.25	-1.52E+12
variance					
h1	2.42E-10	2.42E-08	2.42E-06	2.44E-04	x
h2	3.06E-11	3.06E-09	3.08E-07	3.20E-05	x
h3	3.94E-12	3.91E-10	3.67E-08	1.73E-06	x
b	1.98E-15	2.14E-13	4.24E-11	1.88E-07	x

Discussion

The parameters that are less sensitive can change considerably during updating, and it is b that changes the most in the updating procedure when noise is added. Less sensitive parameters have to change more to accommodate the noise, choosing sensitive parameters is thus important for a realistic solution from FEMU. The noise changes the measured values, if the noise level is too big the measured behavior is distant from the real behavior and as a result updating the beam to such data will most likely result physically unrealistic parameter values. The algorithm using the pseudo-inverse does not converge for the high noise levels. Regularization could be used to alleviate convergence issues, however this will only solve the issue of convergence and will not help to find a physically realistic solution. Since the measured behavior - used to update the model to - is not representative of the true behavior because the measurement error η_m is too big.

3.6.3. Noiseless dynamic updating

In this section the results of the noiseless dynamic updating are presented and discussed. The parameters are the same as those in the static updating. The MAC value is determined by using the mode shape data from all DOF's, and contains the data of many measurements. For noiseless measurements the measurement error η_m is zero, the true behavior is measured.

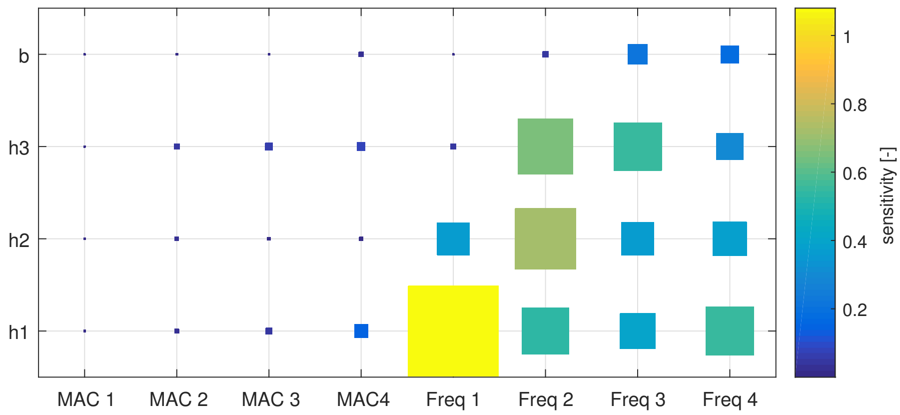

Figure 3.24: Sensitivity of the parameters at the start of the updating procedure using dynamic data, the size of the square is proportional to the sensitivity.

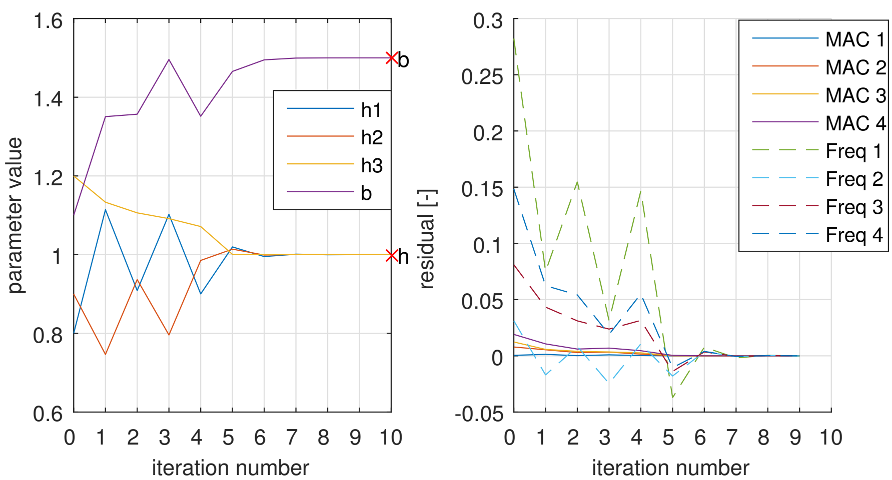

Figure 3.25: Dynamic updating parameter value on the left and residual on the right.

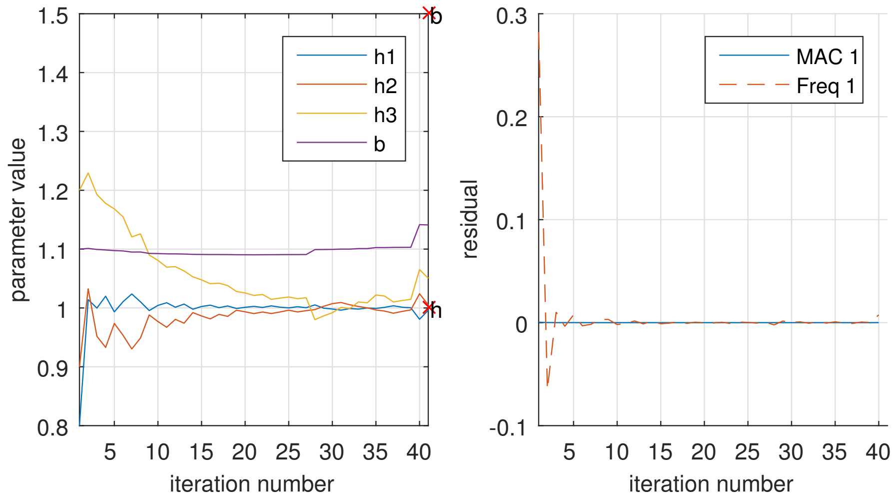

Figure 3.26: Dynamic updating parameter value on the left and residual on the right using 2 measurements.

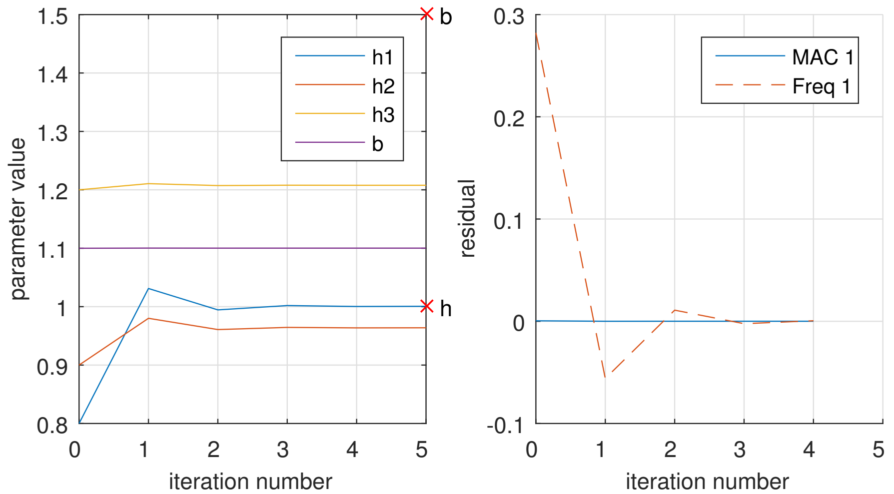

Figure 3.27: Dynamic updating parameter value on the left and residual on the right using 2 measurements and regularization.

Results

The sensitivities of the parameters can be seen in figure 3.24. There is a big difference in sensitivity between the MAC and frequency measurements. Overall the most sensitive parameter is $h1$. For different mode shapes different parameters are sensitive. In figure 3.25 the results of a dynamic updating procedure are shown. Here the residual is composed of the natural frequency and the MAC value for the first 4 modes. Convergence is reached after 10 iterations for this residual. In figure 3.26 the results of updating are shown when only two measurements are used, the solution does not converge although the residual is close to zero. The parameter values for h are close to the true values after 20 iterations but seem to diverge after 40 iterations. For parameter b the value is not close to the true value. Regularization is applied to this problem and the result can be seen in figure 3.27. The solution does converge in this case, only for parameter $h1$ the true parameter value is recovered. The value of parameter b does not change.

Discussion

A parameter in an area that will experience a lot of deformation for a mode shape will be sensitive. This explains why $h1$ is overall the most sensitive parameter, near the support there is deformation for each mode shape. The MAC values are not sensitive, because the MAC value is not sensitive to small changes in the mode shape. In the updating with only 2 measurements the correct value of $h1$ is found. For mode 1 parameter $h1$ is largely determines the mode shape because the elements connected to this parameter are the ones experiencing the most strain. Setting this parameter correctly is will reduce the residual, this is the reason why this parameter value is recovered correctly in figure 3.27. Using regularization the correct value for the most sensitive parameter was found.

3.6.4. Noisy dynamic updating

Noise is added to the measurements for the dynamic updating case with 8 measurements. The results can be seen in table 3.13 and 3.14, for the algorithm using the pseudo-inverse and regularization respectively. For both algorithms the solution gets closer to the true values as the noise level is reduced. Also the variance is reduced if the noise level is reduced. For a noise level greater than 1% the solution does not converge for the algorithm using the pseudo inverse. Using regularization a solution is found for a very high noise level of 10%. Noise seems to affect the dynamic updating procedure less than the static updating. One reasons for this could be the MAC value which is determined from measuring each DOF.

Table 3.13: Parameter values and variance after updating using the pseudoinverse, for different noise levels.

	noise		
parameter	1.00E-04	1.00E-03	1.00E-02
h1	1.00	1.00	0.03
h2	1.00	1.00	0.87
h3	1.00	1.00	1.21
b	1.50	1.50	2.38
variance			
h1	6.44E-09	6.43E-07	1.18E-05
h2	2.81E-09	2.82E-07	2.55E-04
h3	8.25E-09	8.27E-07	6.27E-06
b	1.63E-10	1.62E-08	1.86E-06

Table 3.14: Parameter values and variance after updating using regularization, for different noise levels.

	noise		
parameter	1.00E-03	1.00E-02	1.00E-01
h1	1.00	1.01	1.05
h2	1.00	0.99	0.96
h3	1.00	0.99	0.90
b	1.50	1.54	1.86
variance			
h1	6.49E-07	6.34E-05	5.38E-03
h2	2.91E-07	2.99E-05	3.40E-03
h3	8.33E-07	8.59E-05	1.23E-02
b	2.49E-08	2.39E-06	1.85E-04

3.7. Summary

In this section the a summary of the results in this chapter is presented.

For a simple cantilever beam the differences between two beam formulations - Euler-Bernoulli and Timoshenko - were investigated by looking at: the static response for two load cases and the dynamic/modal properties of the beam. The differences in the results were explained in every analysis. Then the sensitivities of the cantilever beam were investigated. The difference between the absolute and normalized sensitivity were explained. The static displacement sensitivity and natural frequency sensitivities were found for both beam formulations, a comparison has been made between the two formulations and differences were explained. The sensitivities were determined using different parameters to get a understanding of how a parameter choice affects the sensitivity. For the sensitivity of the natural frequency the first 6 flexible modes were used and it was shown that it is dependent on the mode number for the Timoshenko beam. For the Euler-Bernoulli beam the natural frequency sensitivity is independent of the mode number.

Then the mode shape derivate was explained by showing how a parameter value change affects the first flexible mode shape and natural frequency. This was done for several parameters and it was shown that different parameters affect the mode shape in a different way, and this difference can be explained by looking at: the mode shape, the parameter property and the location of elements connected to the parameter. The natural frequency of the first flexible mode shape was also shown in function of parameter values, using the same parameters as for the mode shapes. It was shown that a parameter that changes the mode shape not necessarily changes the natural frequency and vice-versa.

After explaining the mode shape derivative this quantity was shown for the first 4 flexible modes of the cantilever beam for three different parameters. The mode shape derivative has been determined using three methods, and differences between the results of these methods have been explained. The accuracy of Fox and Kapoor's method depends on the parameter choice and mode shape, using more mode shapes in the approximation does not necessarily lead to a better derivative. Nelson's method was found to be the most accurate and is used in the update algorithm. It was shown that the magnitude of the mode shape derivative can vary per mode while keeping the parameter constant. The

The cantilever beam was used in a FEMU procedure using simulated measurements for two types of data: static and dynamic. It was shown that the implemented algorithm is able to recover the original parameter values when proper measurement data is used. Adding noise to the measurements results in parameter estimates that deviate from the initial parameter values, the parameter estimates fit the model to a measured behavior that contains noise. If too much noise is added the parameter estimates are not realistic. Resulting in an updated model with a large parameter error $\boldsymbol{\eta}_{\theta}$, the predicted behavior of this model will be far from the true behavior. For an in ill-conditioned problem it was shown that a solution can be found when regularization is applied. Using regularization to alleviate convergence issues - of the pseudo-inverse algorithm - is appropriate only when the modeling error $\boldsymbol{\eta}_{er}$ and the measurement error $\boldsymbol{\eta}_{m}$ are small, that is difference between the measured and the predicted behavior is mainly due to the parameter error $\boldsymbol{\eta}_{\theta}$.

Essential concepts in FEMU were elucidated, and an intuition for FEMU was gained by the author. This intuition will be very useful when FEMU is used to update the beam model of the ship in the next chapter.

Finally a note on the results in this chapter: for the test case a selection had to be made concerning the parameters and their initial values, the measurement locations and positions. Changing these quantities will affect the results presented in this chapter but the observed phenomena should remain the same when these quantities are changed.

"With four parameters I can fit an elephant, and with five I can make him wiggle his trunk."

John von Neumann

4

Ships model

In this chapter FEMU of the beam model of the PS is discussed. In the first part of this chapter the properties of the beam model are discussed and the hydrostatic solution scheme is explained. Then model updating is applied to the beam model using simulated measurements for both the static and the dynamic case. For actual measurements only the static case is considered. Before the updating results are presented the correlation between the model and the measurements is shown, also the parameter choice is explained. In the last part a way to validate the updated models is presented and applied. And at the end of this chapter a summary is presented.

4.1. Structural model

In this section the properties of the simplified model of the ship are discussed. For clarity this model will be referred to as the beam model.

4.1.1. Model choice

In this section the model choice is discussed. Scientist and engineers use models to better understand physical phenomenon and to and make predictions concerning these phenomena. For such models is it desirable that physical phenomena that are relevant in the current study are captured in the model, and that leaves non-relevant phenomena are left out of the model. Applying this approach to the current research; the physical phenomenon that is relevant in this study is the global structural behavior of the PS. The model should thus be able to model this behavior correctly. Another requirement on the model is that it should be able to model the mass distribution and the buoyancy forces accurately.

For reasons explained in section 2.2.2 a finite element model using beam elements is used to model the behavior of the PS. The mesh of the finite element model should be detailed enough for the mass distribution to be modeled with sufficient accuracy. In this chapter the correlation between the beam model and the FEMAP model will be investigated.

4.1.2. Mesh

In this section the mesh of the beam model is presented. The mesh of the model is shown in figure 4.1. This mesh is chosen because the elements are located on the position of the transverse and longitudinal bulkheads. In this mesh all elements are Timoshenko beams except the element in between node 45 and 82, this is a bar element which represents a steel beam between the bows that is only subject to axial loads. Also the numbers of element is large enough to provide an sufficiently accurate description of the mass. The mass is considered to be known, and should be modeled accurately to make sure no additional model errors are introduced. Apart from the accurately modeling the mass the buoyancy forces also need to be modeled accurately using this mesh. The buoyancy forces are needed to find the static response of the beam model, and no error is assumed in the buoyancy forces.

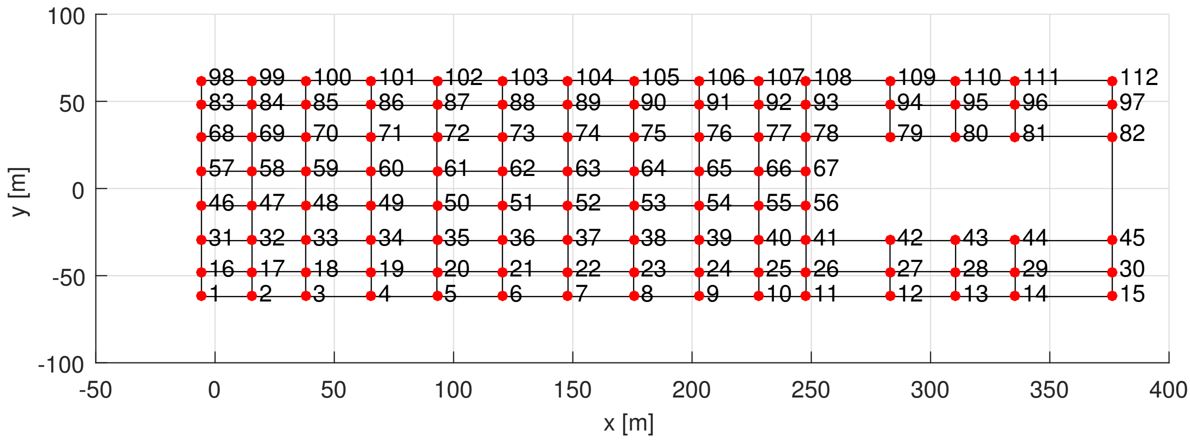

Figure 4.1: Mesh of the finite element model. The red dots represent the nodes, the numbers are the nodal numbers. The lines in between the nodes represent the elements.

Table 4.1: Main dimensions of the PS.

property	value
Length overall	$382[m]$
Breadth	$124[m]$
Slot length	$122[m]$
Slot width	$59[m]$
Depth	$30[m]$

The main dimensions of the PS are given in table 4.1, this information together with the locations of the bulkheads is needed to make the 2-dimensional mesh in shown in figure 4.1.

4.1.3. Properties of the elements

In this section the element properties of the beam model will be discussed. First the mass properties of the elements are discussed followed by the stiffness properties of the elements.

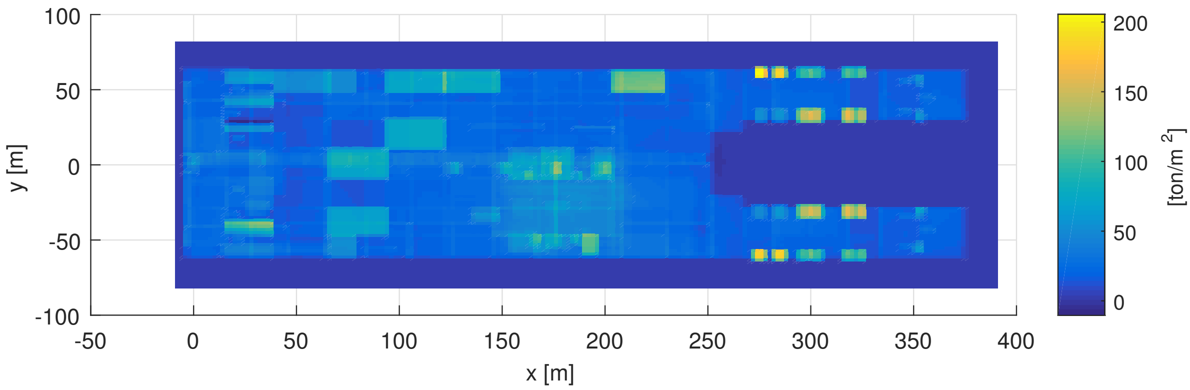

Figure 4.2: Mass distribution of the ship in x-y plane for a loading condition.

Element mass

The mass of the elements is found from the mass distribution of the ship, of which a detailed description is available in the Loading Conditioning Tool (LCT), see appendix **??** for an explanation. In the LCT the mass of the ship is split up in items and for each item two 1-dimensional mass distributions are available, one along the x-axis and one along the y-

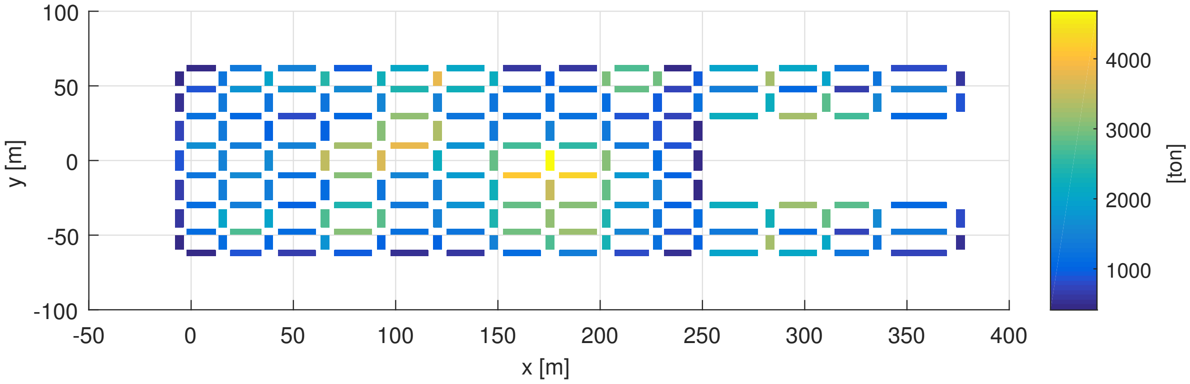

Figure 4.3: Mass of the elements for the same loading condition as in figure 4.2.

Table 4.2: Comparison of the coordinates of the COG, between model and LCT.

coordinate	model	LCT	difference
x[m]	163.42	163.14	0.28
y[m]	0.09	0.00	0.09
z[m]	0.00	17.42	17.42

axis[1]. Per mass-item these mass distributions are combined to find a mass distribution in the xy-plane. This mass distribution depends on the loading condition, an example of the total mass distribution is shown in figure 4.2. From the mass distribution several items of the ship can be identified, the mass of lifting beams are the small areas on the bow and also the deck-house can be identified. The thin lines on the model are caused by overlapping weights, these peaks will be smoothed when the mass is transferred to the elements. Also filled ballast tanks can be identified as the areas with a higher mass density.

The mass distribution in figure 4.2 is used to find the element masses, now it is explained how this was done. For each element an area is defined, the mass inside this area is summed and assigned to an element. The size of the area is the length of each element and half the width of the elements perpendicular to the element on each side. This works for elements in the interior mesh however elements along the edge only have elements perpendicular to them on one side. The area of the mass distribution is larger than the element mesh area, mass can be defined outside of the mesh area. The mass outside the mesh is taken into account by extending the area of influence of the elements on the boundary of the mesh. Three different cases for area extension can be found.

1. Elements along the boundary, excluding the elements inside the bow. For these elements the area of influence is extended to the edge of the mass distribution grid.
2. Elements longitudinal inside the bow area. The area of influence in extended to the center line, $y = 0$.
3. Elements transverse inside the bow area. The area of influence is not changed.

This means that all the mass inside the bows is transferred to the longitudinal elements along the bow. The mass distributed along the elements for the loading condition is given in figure 4.3.

As a check of the element masses found using the method described above, the Centre Of Gravity(COG) from the LCT and the elements masses are compared in table 4.2. The difference between the x and y showing that in the xy-plane the mass distribution is similar. The z-coordinate shows a big difference, the distribution is this direction has not been calculated for the elements, because the element are located in the xy-plane.

[1]In z-direction the center of gravity is given for each item. This informations is not needed for the model, since the beam elements are a 2 dimensional representation of the structure.

Table 4.3: Relative difference between inertia matrices from LCT and elements.

m_x	m_y	m_z	I_{xx}	I_{yy}	I_{zz}	I_{xy}	I_{xz}	I_{yz}
0.01%	0.01%	0.01%	-2.45%	1.24%	1.65%	7.93%	-100%	-100%

Another way to check the mass of the elements is by comparing the inertia matrix of the LCT and the elements, shown in 4.3. The linear inertial terms m_i show that there is is very small difference between those from the LCT and the beam model. Also for the rotational inertias I_{ii} there is and a small difference. The biggest difference is in the products of inertia related to the z direction I_{iz}, this is due to the concentration of the mass at $z = 0$ for the elements. The I_{xy} cross term also shows considerable difference.

The mass distribution is similar to that of the LCT which is considered to accurately model the real mass of the PS. This together with a fine enough mesh fulfills the requirement of an accurate mass description of the FE-model.

Element cross-section

The stiffness properties of a beam element are linked to the shape and size of its cross-section. The cross-section of the beam element could be chosen to be very detailed by modeling the looking at the structural components in of the PS, and use these to determine the cross-sectional properties. Another approach is to select a simple cross-section with similar cross-sectional properties as those the cross-sections of the PS. In this research a simple box-section has been chosen to model the cross-sectional shape of the element because of:

- Resembles coarsely the cross-section of the ship.
- Less cumbersome than using a detailed description, while the results may not be far of from the detailed description.
- Allows for updating of a simple parameter.

The element cross-section is depicted in figure 4.4, here the parameters are shown that define the dimensions of the cross-sections. These are: t_{fl} the flange thickness, t_{web} the web thickness, b the element width and h the element height.

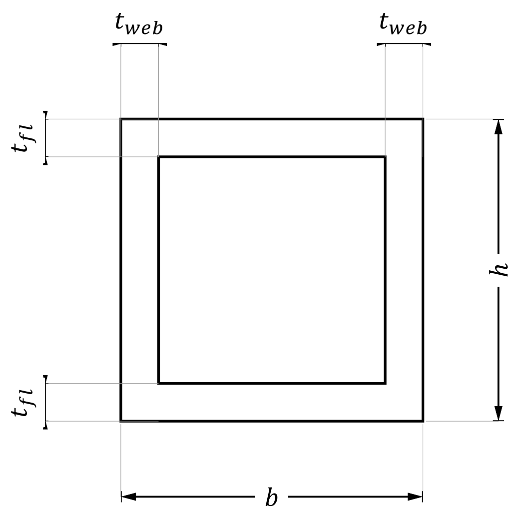

Figure 4.4: Cross-section and its dimensions used for the elements.

Element stiffness

The stiffness of the elements is determined by several properties, these are:

- Cross-sectional properties: Area, moment of inertia, shear factor.

- Material properties: Young's modulus and Poisson's ratio.
- Element length.

The material properties of the PS are assumed to be known accurately and constant throughout the ship, the properties needed are E, ν and G see table 3.1 for values used. The element length follows from the mesh of the beam model. The cross-sectional properties are the free variables that can influence the stiffness of each element. The cross-sectional properties are determined by the the dimensions of the cross-section given in figure 4.4. The element height h is given by the height of the ships cross-section at that point. The element width b follows from the mesh. The cross-sectional parameters that are "free" are the flange thickness t_{fl} and the web thickness t_{web}. For the initial model the web thickness is assumed to be constant throughout the beam model. The flange thickness can be different for each element, and it has been found by taking into account the actual deck and bottom thicknesses of the PS. Taking the the actual bottom and deck thicknesses results in a stiffness that is too small, because a number of stiffeners have not been taken into account. To make sure that a good initial estimate of the flange and web thicknesses is found, they have been manually tuned so that the natural frequency of the first 4 modes in figure 4.9 were close to the FEMAP model. The flange thickness for each element is given in figure 4.5, the constant web thickness is $32mm$. The wet modes have been used here because the initial plan was to use modal parameters extracted from measurement data, and it was deemed that for this the wet modes were more relevant for this, due to time constraints this planned research was not executed.

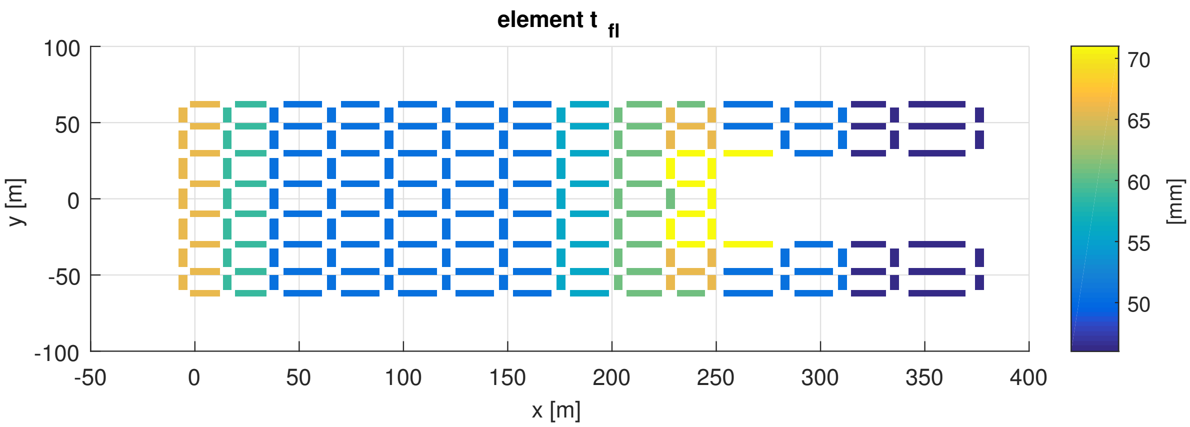

Figure 4.5: The flange thickness for each element.

The cross-sectional dimensions determine the values of the cross-sectional properties. The area A and moments of inertia I_y, I_z are trivial to calculate for the box cross-section. The shear factor is determined by formula (4.1), with A_{tot} the total area of the cross-section and A_{sh} the area that is effective in shear, in this case it is either the area of the flange or the web depending on the direction of the shear force.

$$k_s = \frac{A_{tot}}{A_{sh}} \tag{4.1}$$

The polar moment of inertia I_x is determined by summing the bending stiffnesses I_y and I_z. All the properties needed to determine the element stiffness matrix have been discussed.

4.2. Hydrostatic deflection and sensitivity

In this section the approximation for hydrostatic deflection is explained for the beam model, and also the sensitivity of the hydrostatic deflection is derived. These are needed in the updating procedure.

Hydrostatic deflection

The static load case is based on the PS floating freely in still water. In this condition the gravity forces, buoyancy forces and internal stressed are in equilibrium. For the beam model this is expressed by equation (4.2). In this equation the buoyancy force $\mathbf{f}_b$ is a non-linear function of displacement $\mathbf{x}$. The gravity force $\mathbf{f}_m$ is found by multiplying the mass matrix $\mathbf{M}_s$ with a vector $\mathbf{a}_z$ containing the acceleration of gravity g in z-direction - $9.81 m/s^2$ -as given in (4.3) and (4.4). Another term - $\mathbf{K}_c$ - is added to (4.2) to alleviate the the unrestrainedness of the system in the xy-plane. This term represents 3 soft springs in the xy-plane that make sure that the system is properly constrained and has a unique solution.

$$[\mathbf{K}_s + \mathbf{K}_c]\mathbf{x} + \mathbf{f}_b(\mathbf{x}) = \mathbf{f}_m \tag{4.2}$$

$$\mathbf{f}_m = \mathbf{M}_s \mathbf{a}_z \tag{4.3}$$

$$\begin{aligned} \mathbf{a}_z &= \{\mathbf{u}_z\, \mathbf{u}_z \dots \mathbf{u}_z\}^T \\ \mathbf{u}_z &= g\{0\,0\,1\,0\,0\,0\} \end{aligned} \tag{4.4}$$

To solve (4.2) the nonlinear term $\mathbf{f}_b$ is approximated as follows. Using the hull shape of the PS the displaced volume can be determined at any draft. The hull shape of the PS is known on a $2mx2m$. Using the weight of the PS the draft is found with zero trim and zero heel. At this draft $\mathbf{x}_\nabla$ a first order Taylor expansion is made for $\mathbf{f}_b$ as shown in (4.5), resulting in a linear hydrostatic spring stiffness $\mathbf{K}_h$. Substituting this expression into (4.2) leads to a linear equation for the hydrostatic displacement (4.7).

$$\mathbf{f}_b(\mathbf{x}) = \mathbf{f}_b(\mathbf{x}_\nabla) + \left.\frac{\partial \mathbf{f}_b}{\partial \mathbf{x}}\right|_{\mathbf{x}_\nabla} \mathbf{x} = \mathbf{f}_b(\mathbf{x}_\nabla) + \mathbf{K}_h \mathbf{x} \tag{4.5}$$

$$[\mathbf{K}_h + \mathbf{K}_s + \mathbf{K}_c]\mathbf{x} + \mathbf{f}_b = \mathbf{f}_m \tag{4.6}$$

$$\mathbf{x}_{tot} = \mathbf{x}_\nabla + \mathbf{x}_1 \tag{4.7}$$

Hydrostatic displacement sensitivity

The sensitivity of the hydrostatic displacement can be found by deriving equation (4.6) w.r.t. a parameter, shown in (4.8).

$$\frac{\partial}{\partial \theta_i}\big[[\mathbf{K}_h + \mathbf{K}_s + \mathbf{K}_c]\mathbf{x} + \mathbf{F}_b - \mathbf{F}_m\big] = 0 \tag{4.8}$$

All terms in (4.8) are independent of a stiffness parameter save the structural stiffness $\mathbf{K}_s$ and the displacement $\mathbf{x}$. Using this (4.8) can be written as (4.9), which gives the sensitivity of the static displacement of a parameter. To find this vector the matrix $\mathbf{C}$, $\frac{\partial \mathbf{K}_s}{\partial \theta_i}$ and vector $\mathbf{x}$ need to be known. All these quantities are known from the calculation of the hydrostatic deflection and the sensitivity of the structural stiffness.

$$\frac{\partial \mathbf{x}}{\partial \theta_i} = -\big[\underbrace{\mathbf{K}_h(\mathbf{x}_\nabla) + \mathbf{K}_s + \mathbf{K}_c}_{\mathbf{C}}\big]^{-1} \frac{\partial \mathbf{K}_s}{\partial \theta_i}\mathbf{x} = -[\mathbf{C}]^{-1}\frac{\partial \mathbf{K}_s}{\partial \theta_i}\mathbf{x} \tag{4.9}$$

4.3. FEMU of the beam model

In this section the results of the updating procedure applied to the FE model of the ship are presented. For simulated measurements updating is done using static and dynamic data. For the real measurements only static data was considered, due to time constraints the dynamic case using measurement data was not considered. The loading condition of the ship used is the one in which the ship is ballasted in such a way that the bending moment in the ship is minimal. This condition will be called the neutral loading condition.

The updating will be done in line with the work flow depicted in figure 2.3. The FE-model has been described in the previous sections. The experimental set-up is given in this research. Then the correlation between the predicted behavior and measured behavior is checked. After which the parameters are presented. The parameters are the same for every updating case. Then sensitivities of the parameters are checked, these are also different for each case because they depend on the parameter settings and what quantities are measured. After this the objective function is formulated and a optimization algorithm is selected to solve the optimization problem. After finding an updated model the behavior of this model was not compared with measured behavior not used in the updating. This step necessary to check whether an updated model is a valid model. In case of the simulated example this is not necessary since the true parameter values are known from the measurement, if the parameter estimates are the same as the true parameter values the updated model is considered to be validated. In case of updating to the actual measurements it was not possible to do the comparison for reasons explained below.

Normalization of the parameters

In the updating procedure the least square problem is normalized as in equation (2.18). Normalized parameter values are given in the result. A parameter contains a groups of elements for each element the property value may be different. For the normalization the average value of the parameter property has been taken. For the response the initial measured response has been used in the normalization.

Algorithms

The algorithms used to solve the non-linear least squares optimization problem in this chapter are discussed now, see section 2.1.15 for a derivation. These algorithms solve the non-linear problem iteratively using a linear approximation at each step. This results in a least square problem that is solved using the pseudo-inverse as in (2.42) and if no convergence was found regularization is used as in (2.43). In this chapter the values of the of the terms in equation (2.43) are the following: $\lambda^2 = 0.01$ and for $\mathbf{W}_{\theta\theta}$ the identity matrix is used. To calculate the variance of the updated parameter the expression (A.29) is used, using σ^2 as in (F.6). For $\mathbf{W}_{\epsilon\epsilon}$ a diagonal matrix is used with the reciprocal of the variance σ^2 on its diagonal.

4.3.1. Updating perquisites

In this section the results of several checks on the beam model are presented, these are needed before a model can be updated. The measured behavior is compared to the predicted behavior and checked for correlation. Parameters are selected and their sensitivities are checked. For the correlation the FEMAP model is assumed to represent the measured behavior. For the static behavior this assumption is backed by the comparison of strain measurements and the FEMAP model, see appendix D. The FEMAP model has more degrees of freedom than the beam model, and to make a comparison between the mode shapes using the MAC value the FEMAP mode shapes are condensed to the beam model mesh. To do this only the translations of the deck of the FEMAP model are used and these are transfered to the nodes. The transfer to the nodes is done by defining an area around the nodes of the beam model and average the displacements and translations of the FEMAP nodes inside this area.

Correlation static response

Before the model can be updated to the experimental data, the behavior of the beam model needs to correlate with measured behavior. For the measured behavior the FEMAP model is used. The LCT is used to create a loading condition which is used as input to both the FEMAP model and the beam model, this ensures that the mass distribution of the two models is the same. Then the hydrostatic response is determined for both models. In figure 4.6 the results of the comparison between the FEMAP model and the beam model is shown. Overall the two deformation look similar, the FEMAP shows a bigger deflection in the aft and the middle. And the beam model shows a bigger deflection for the two bows.

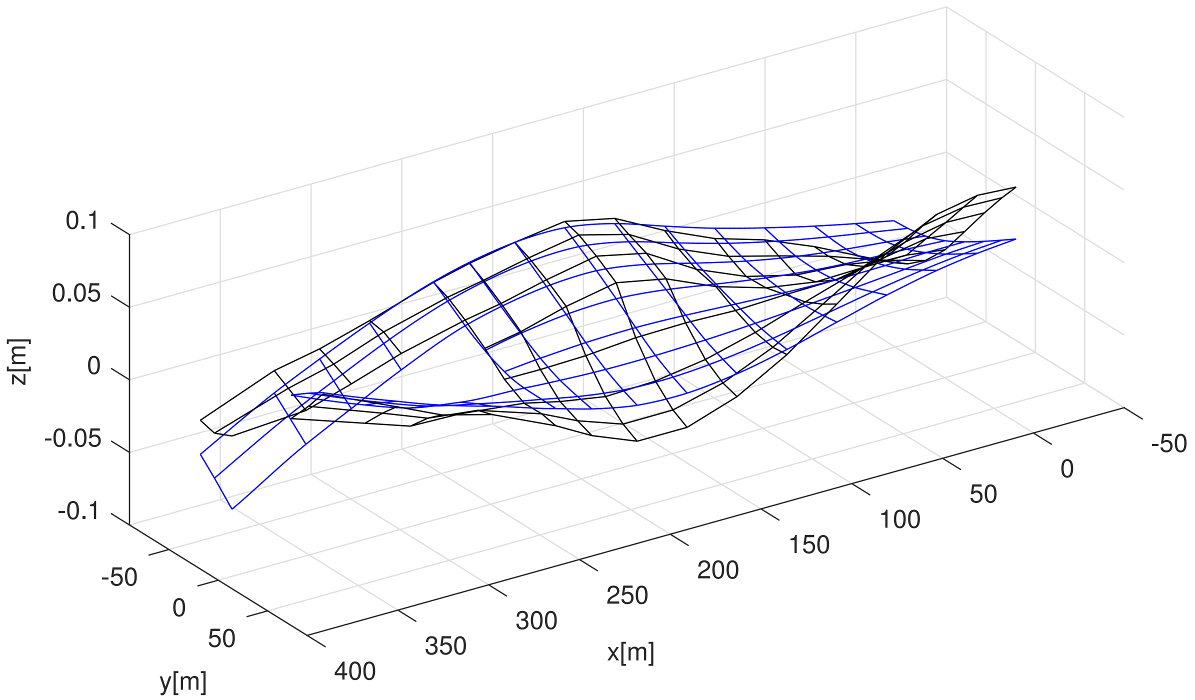

Figure 4.6: Comparison of the static deformation found from the model (blue) and FEMAP model (black), for a neutral load case.

Correlation of mode shapes

The correlation of the mode shapes is performed by calculating the MAC value between the modes of the beam model and the dry FEMAP model. The results can be seen in figure 4.8. For the dry model only the first 2 modes show a mac value close to 1 and thus a good correlation. The dry modes of the FEMAP model also include a number of modes that are more local. This explains why the only the first two modes correlate well. The natural frequencies of the wet modes have been used to find the initial web and flange thicknesses of the of elements, the natural frequencies of the first modes are similar for the beam model and the wet model. The wet modes are shown in 4.9. The wet modes shapes are comparable to mode 1, 2, 4 and 5 of the beam model shown in figure 4.7.

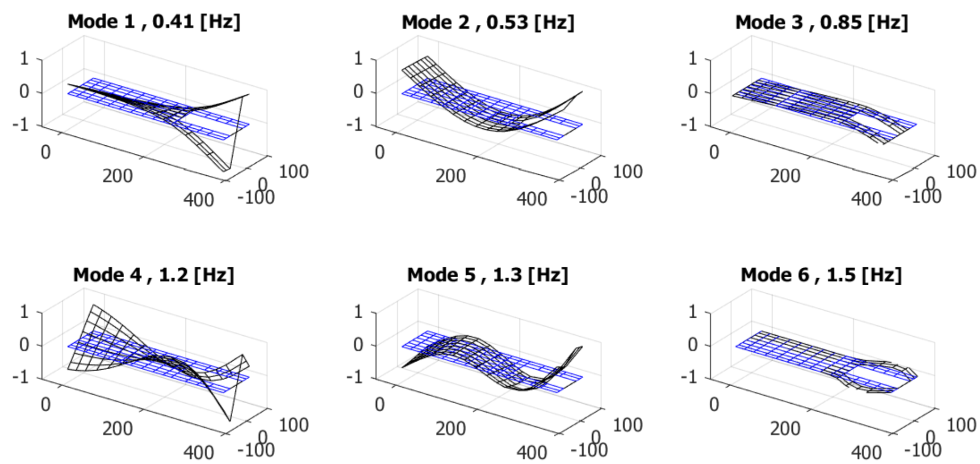

Figure 4.7: The first 6 flexible modes and natural frequencies of the beam model.

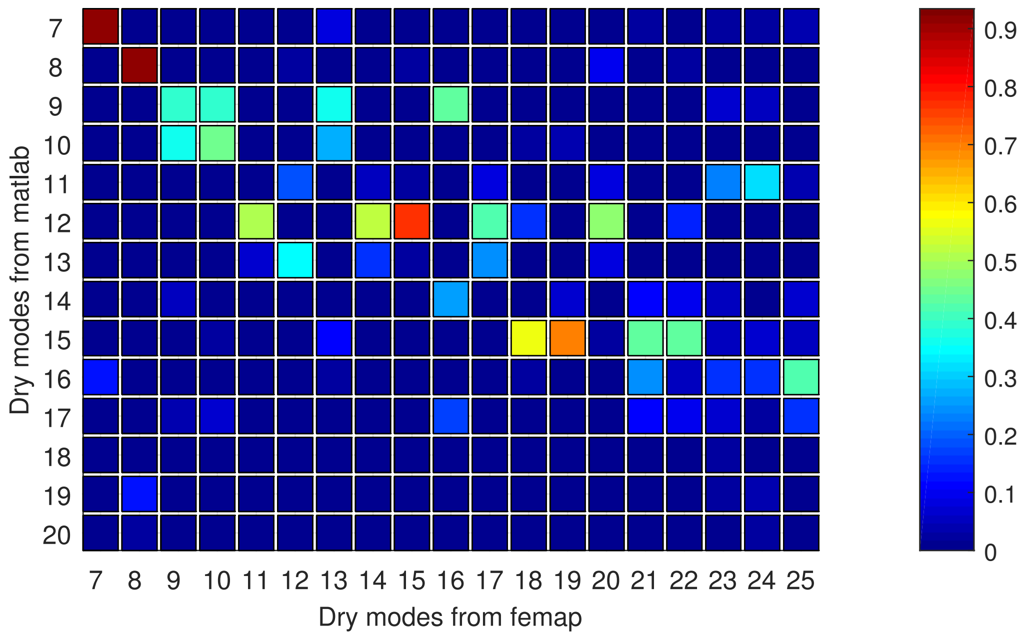

Figure 4.8: MAC values of the dry mode shapes from FEMAP and the beam model.

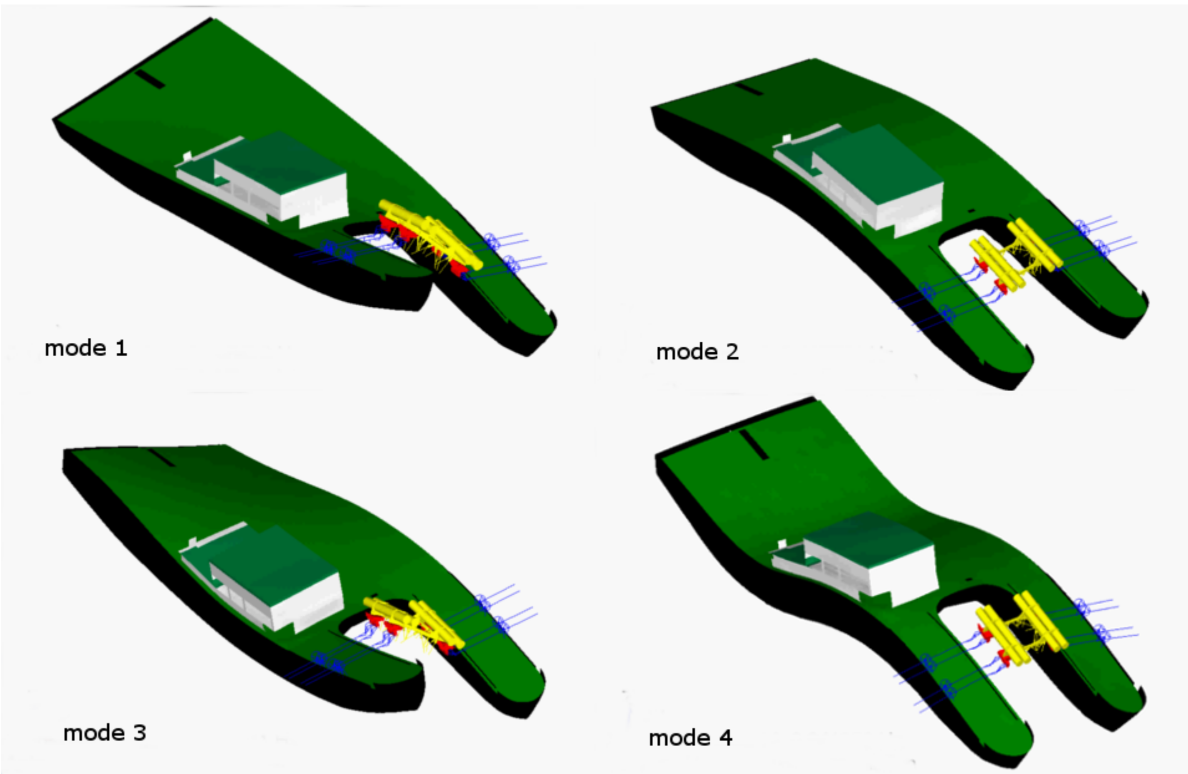

Figure 4.9: Wet modes of the ship determined using FEMAP where an approximation for the added mass is used.

Correlation conclusion

The overall static deformation of the beam model and the FEMAP model look similar, because of this it is assumed that the static behavior of the beam model correlates with the measured behavior. For the dynamic response the modal parameters were used to check the correlation. The dry modes-shapes showed a good correlation for only the first 2 modes, a qualitative comparison of the wet mode shapes shows a good correlation. Also the natural frequencies of the wet FEMAP model are similar to those of the beam model. Also for the dynamic behavior we assume a good correlation.

4.3.2. Parameter element groups

In this section the parameter choice is explained by looking at both the element groups and the properties used as a parameter. The assumptions used in the selecting the parameters are discussed as well as the consequences of these assumptions.

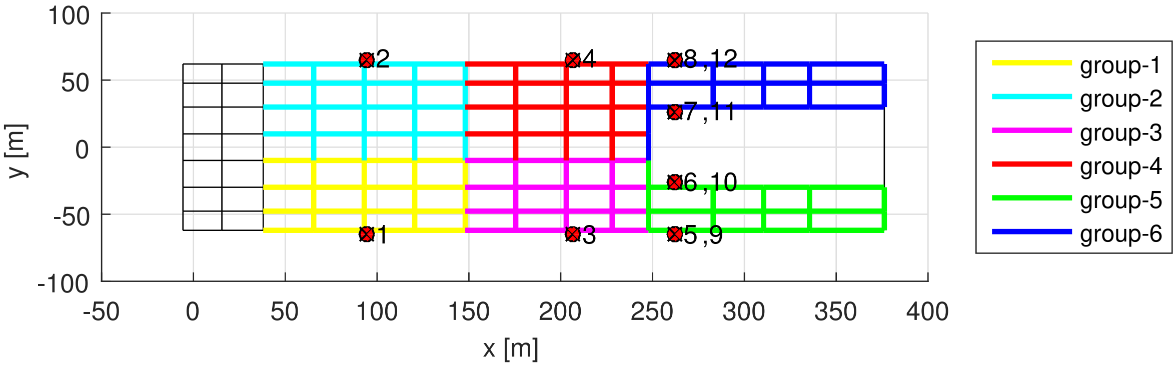

Figure 4.10: The element groups and the sensor locations.

Element groups

The parameter properties have to be linked to an element set. The number of parameters that can be updated using the available sensors is limited. The number of parameters should not exceed the number of measurements according to Mottershead[19]. A limited number of parameters also means that the number of element groups should be smaller than or equal to the number of sensors. Because of this the number of element groups has been limited to 6, the element groups are shown in figure 4.10. The element groups are defined in such a way that for the static updating each group contains at least one sensor, this is done to make sure that that the parameters are sensitive.

Table 4.4: Parameters used in the updating procedure of the ship model.

id	property	group
1	t_{flange}	1
2	t_{flange}	2
3	t_{flange}	3
4	t_{flange}	4
5	t_{flange}	5
6	t_{flange}	6
7	t_{web}	5
8	t_{web}	6

Properties

The parameters used in the updating of the beam model are shown in 4.4. In total there are 8 parameters, 6 parameters have the flange thickness as a property and 2 have the web thickness as a property. The choice for these parameters is based on engineering insight. The flange thickness is used in all parameter groups because it is the most effective in changing the bending stiffness. The web thickness is used as a parameter in the bows to correct for the shear stiffness, in the bows the shear stress is measured. The bending stiffness is governing for the normal strain measured by the long based strain gauges. The eight parameters are in theory sensitive to the measurements for the static case. For the dynamic case the natural frequencies and mode shapes are used as measurements, again in theory these quantities are also affected by the parameters that have been chosen. The sensitivity of the parameters is verified before updating, by checking the entries in the sensitivity matrix.

Assumptions

The parameterization - choice of property and element groups - in this research is based on engineering insight. Ideally the parameters and elements are chosen either by using a error finding method like the force balance method [9], and by careful study of the model assumptions and the difference between the predicted and observed behavior. Also only one parameter choice is used for the beam model of the ship. The assumptions is thus that by using the chosen set of parameters a valid conclusion can be drawn regarding the possibility of applying FEMU to the PS. This is quite an assumption when it is known that the results of FEMU are greatly dependent on the chosen parameters, see section 2.1.3 and section 2.1.10. However due to time constraints parameters were chosen using engineering insight and only a single parameterization was considered for the beam model.

4.4. Updating using simulated data.

In this section the updating results are presented when simulated measurements are used; first the results for the static case and then the results of the dynamic case. The simulated measurements are done in order to investigate whether or not the implemented algorithms work, and to investigate the effect of noise on the results. For the static case two different ways perturbing the initial model were tested.

4.4.1. Virtual measurements and perturbations

In this section the virtual measurement and perturbations are explained.The virtual measurement are created by using the parameter settings as they were found in section 4.1.3. The parameters are then perturbed in two ways. One way is by adding or removing plate thickness from the element group connected to a parameter, for all elements in a parameter group the element thickness is changed in a similar way. When updating the element properties are changed in the same way. This makes sure that the updating procedure is able to recover the original parameter values. A second way of perturbing the parameters was used,in addition to the other method, a random perturbation of the flange and web thickness is added to each element. The random perturbation is found by randomly drawing a plate thickness in mm from a uniform distribution with bounds $(-7, 7)$. This random perturbation of all elements results in a change in flange and web thickness that can not be recovered by updating. Introducing a modeling error $\boldsymbol{\eta}_{er}$. The true model can not be found in the model space S_3, making this a more realistic way to update the model.

4.4.2. Static updating

In this section the results of the static updating are presented and discussed. For the static updating 12 strain measurements are used in the residual. The loading condition used is a neutral one in which there is little bending. The parameters are those defined in table 4.4.

sensitivity

Before the updating starts the sensitivity of the parameters is checked, see figure 4.11. Parameter 6 and 8 are the most sensitive parameters for the strains sensors 11 and 12, they also show some sensitivity for sensors 7 and 8. These sensors are in the same area as the sensors and it makes sense that these measurement are sensitive to these parameters. Parameter 1 to 4 are most sensitive for the sensors in their areas, they also show some 'cross' sensitivity for sensor 1 to 4. This means that the stiffness in these areas affects the strain measurements in the other areas. Parameter 4 and 3 show some sensitivity for sensors 7, 8, 11 and 12. Parameter 5 and 7 are sensitive for sensors 6,7,9 and 10, these sensors are located in the same area as the parameters. Parameter 7 is also sensitive for sensor 4,5 and 6. Sensor 4 is next to the area of parameter 7 and it makes sense that a change in stiffness a neighboring area affects sensor 4. The sensitivity matrix does not to show any linearly dependent rows, the transpose of the sensitivity matrix is shown in figure 4.11 hence we look for linearly dependent rows. The least sensitive parameters are parameter 1 and 2, they show sensitivity only for sensor 1 and 2 respectively.

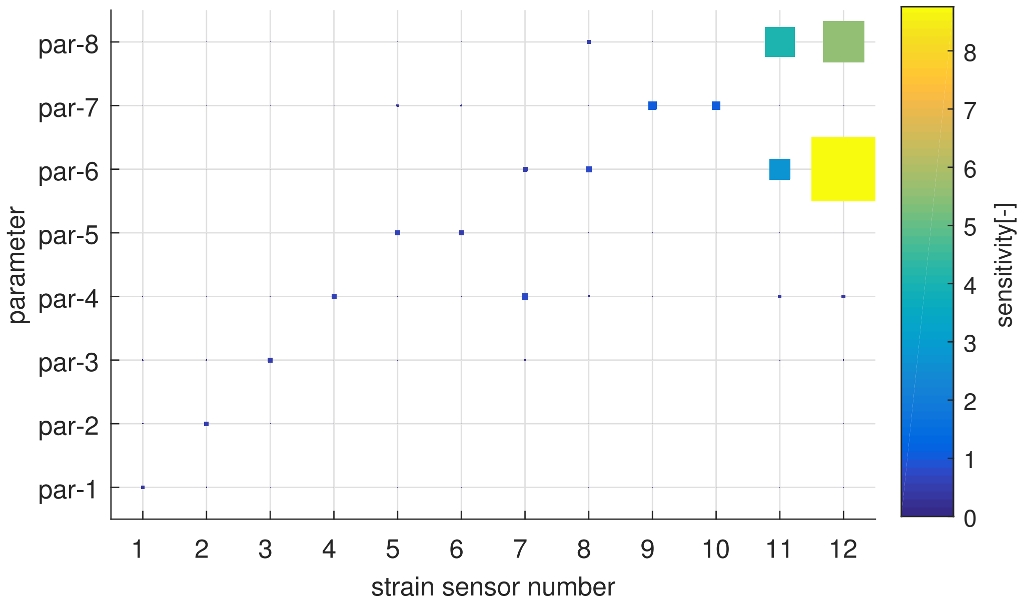

Figure 4.11: Normalized sensitivities for static updating, before updating. Size of the squares is proportional to the sensitivity.

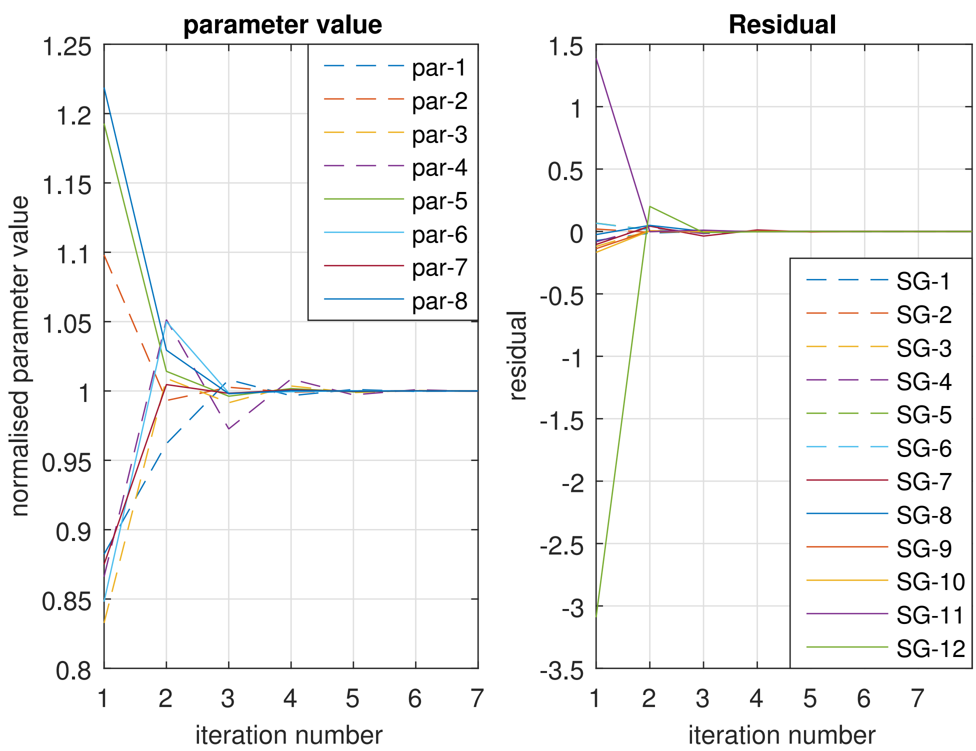

Figure 4.12: Static updating of the ship, normalized parameter value and residual at each iteration.

Results

The results of the updating procedure are given in figure 4.12, here the perturbation without the random change in plate thickness is used, a noise level of zero and the pseudo-inverse is used to solve the least squares problem each step. The parameters are recovered exactly after a small number of iterations. In table 4.5 the results for different noise levels is given. As the noise level is increased the mean parameter values deviate from the original values, also the variance increases as the noise increases. Parameters 8 does not seem to be affected by the noise level. In table 4.6 the results are given for the updating procedure where random perturbations to the plate thicknesses have been applied. The random perturbations should change the element properties so that the original parameters values are not recovered, this is only the case for parameter 1, 3 and 4. Comparing the results of the two ways of perturbing the model in table 4.5 and 4.6 shows that the results are similar.

Table 4.5: The results from static updating for different noise levels, using the pseudo-inverse.

	noise level				
parameter	0	1.00E-04	1.00E-03	1.00E-02	1.00E-01
1	1.00	1.00	0.99	0.93	0.52
2	1.00	1.00	1.01	1.08	1.69
3	1.00	1.00	1.00	1.01	1.12
4	1.00	1.00	1.00	0.99	0.89
5	1.00	1.00	1.00	1.01	1.06
6	1.00	1.00	1.00	1.01	1.05
7	1.00	1.00	1.00	0.99	0.94
8	1.00	1.00	1.00	1.00	1.00
	variance				
1	x	1.3E-08	1.3E-06	1.3E-04	1.5E-02
2	x	2.2E-09	2.2E-07	1.9E-05	9.2E-04
3	x	1.0E-08	1.0E-06	9.1E-05	3.5E-03
4	x	2.9E-08	2.9E-06	2.7E-04	1.8E-02
5	x	5.2E-09	5.2E-07	5.2E-05	4.7E-03
6	x	2.8E-09	2.8E-07	2.7E-05	2.4E-03
7	x	8.5E-09	8.5E-07	8.5E-05	8.6E-03
8	x	1.5E-08	1.5E-06	1.5E-04	1.4E-02

Table 4.6: The results from static updating for different noise levels, using the pseudo-inverse and random perturbations to the flange and web thickness. Updated parameter value divided by the original value.

	noise level				
parameter	0	1.00E-04	1.00E-03	1.00E-02	1.00E-01
1	1.05	0.93	0.94	0.90	0.62
2	1.00	1.05	1.03	1.03	1.29
3	0.99	1.02	1.01	1.03	1.12
4	1.02	0.99	1.00	1.00	0.91
5	1.00	1.00	1.00	1.00	1.06
6	1.00	1.00	1.00	1.00	1.05
7	1.00	1.00	1.00	1.00	0.94
8	1.00	1.00	1.00	1.00	1.00

Discussion

The parameter values are recovered exactly when the noise-level is zero and when no random perturbations are used, this is what is expected because in the residual the modeling error $\boldsymbol{\eta}_{er}$ and the measurement error $\boldsymbol{\eta}_m$ are zero. This indicates that the updating procedure works for the ships geometry for the static case. Parameter 1 and 2 are the least sensitive parameters, these parameters are most affected by noise. As the noise level increases all parameter values change save parameter 8. This is not what is expected. A reason for this may be implementation of the noise-level, the state of the random number generator was the same for each analysis, possibly the noise-level was small for sensor 12. The similarity of the results for the two ways of perturbing the model can be explained by the normalization of the parameter values, the values are averaged and the average of the normal distribution used to perturb the plate thicknesses is 0. The introduction of a modeling error $\boldsymbol{\eta}_{er}$ does not affect the parameter estimates - which are averaged - much. When looking at the individual plate thicknesses the results are different.

4.4.3. Dynamic updating

In this section the results of the dynamic updating are presented. For the dynamic updating the natural frequency and the MAC value of the first five modes are used in the residual. The parameters are the same as in the static updating procedure, see table 4.4. Here no random perturbation of the parameters is used and the effect of a modeling error $\boldsymbol{\eta}_{er}$ is not studied. The loading condition is the same as the one used in the static case. The optimization problem is solved using two approaches: the pseudo-inverse and regularization.

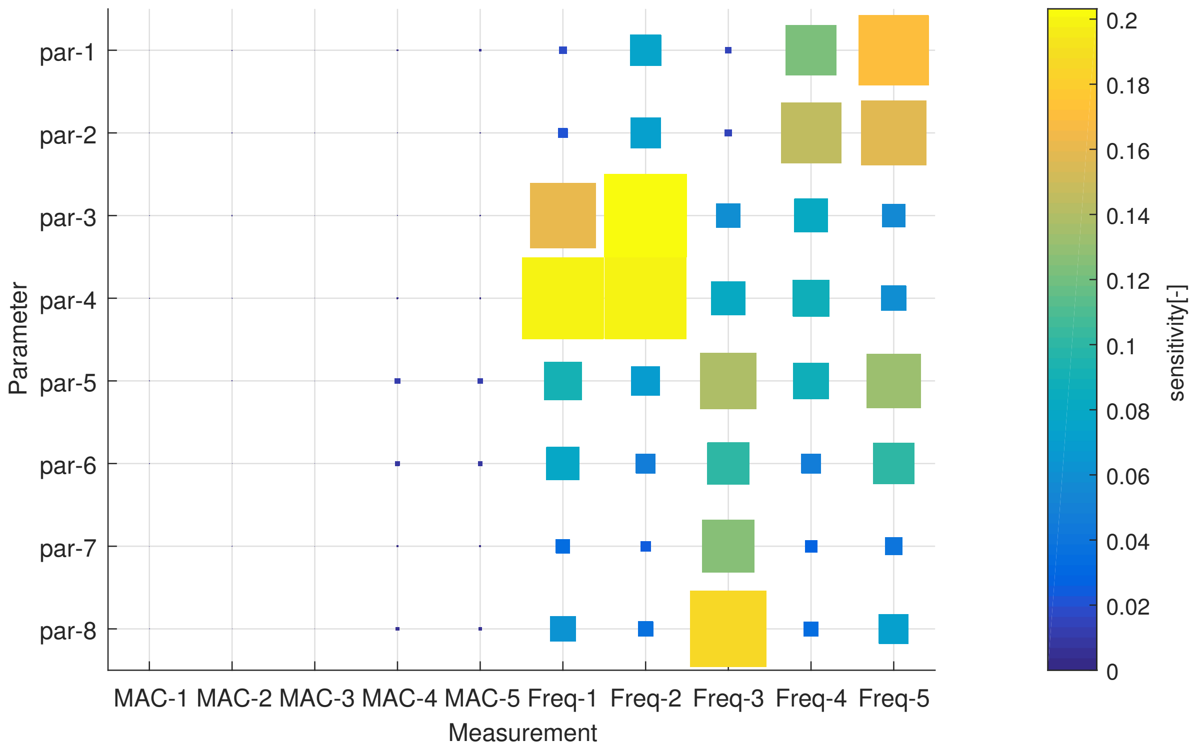

Figure 4.13: Normalized sensitivities of the parameters for the dynamic updating.Size of the squares is proportional to the sensitivity.

Sensitivities

First the sensitivities are checked to make sure the parameters are sensitive, see figure 4.13. In general the parameters are more sensitive to change the natural frequencies than the MAC values. Using the mode shapes in figure 4.7 the differences in sensitivity can be explained, by looking at which element groups experience significant strain in each mode. For example for the first mode the elements connected to parameter 1 and 2 do not strain considerably and are thus less sensitive than the other parameters. The sensitivity for the MAC values is bigger for mode 4 and 5 these modes strain considerably more elements than the other modes, and these mode shapes are more sensitive to change and as a result the MAC value. The MAC value is mainly used to make sure that the mode pairing is correct.

Results

For the current parameterization it was found that at least five mode shapes and natural frequencies were needed as measurements for the updating procedure to converge. In figure 4.14 the results of a updating procedure with a small noise level and using the pseudo-inverse are shown, the original parameter values are found. The residual for the natural frequency changes considerably while the MAC value residual is close to 0 at all times. In figure 4.16 the noise level is increased so that no converging solution is found, the residual is however close to zero. In figure 4.15 where regularization is used to find a solution to the non-converging problem in figure 4.16. A solution is found however the original parameter values are not recovered, but for parameter 1 to 4 better estimates are found than for parameter 5 to 8. The residual is close to zero.The results of the updating for two noise level is shown in 4.7, this is the greatest noise level for which the solution was still converging if the pseudo-inverse was used. The updated parameters are not effected much by the noise level.

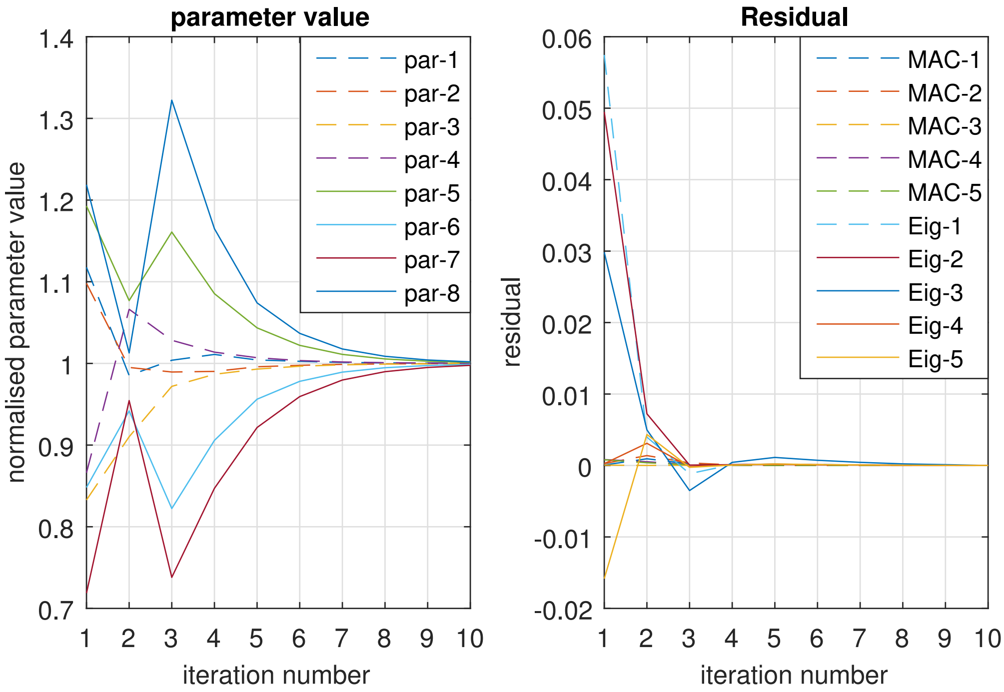

Figure 4.14: The parameter values and the residuals are shown at each iteration step. For updating using 5 modes, a noise level of $1e-9$ and the pseudo-inverse.

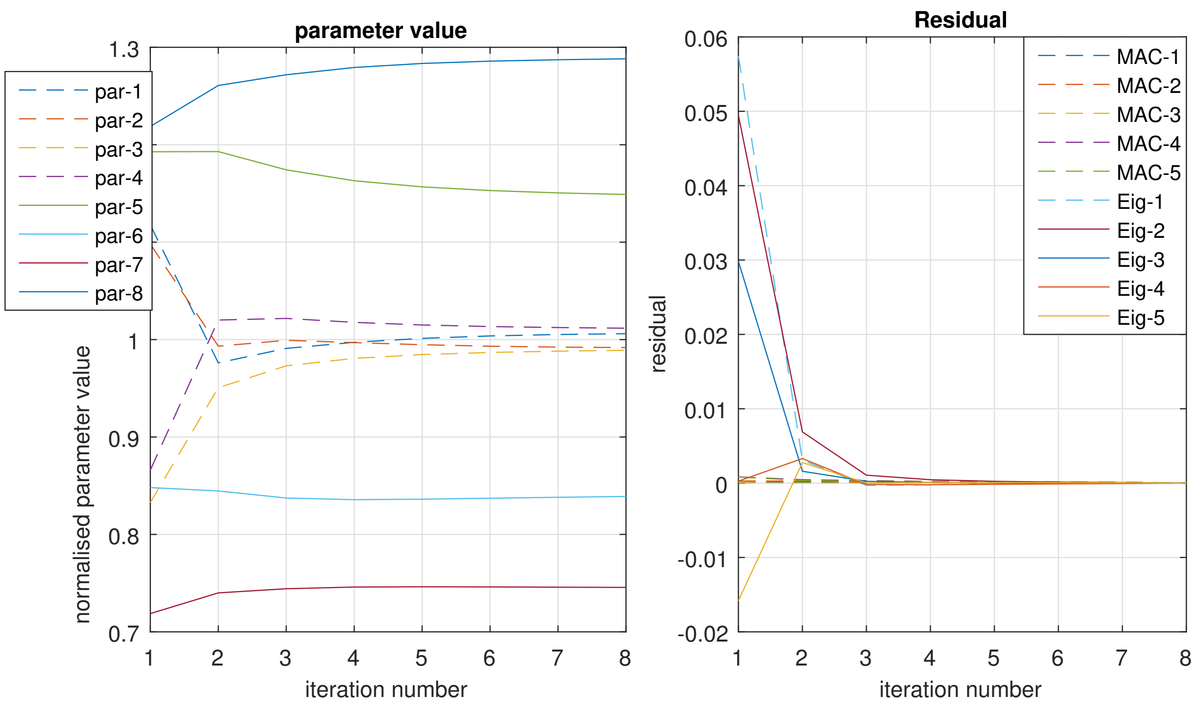

Figure 4.15: The parameter values and the residuals are shown at each iteration step. For updating using 5 modes, a noise level of $1e-5$ and regularization.

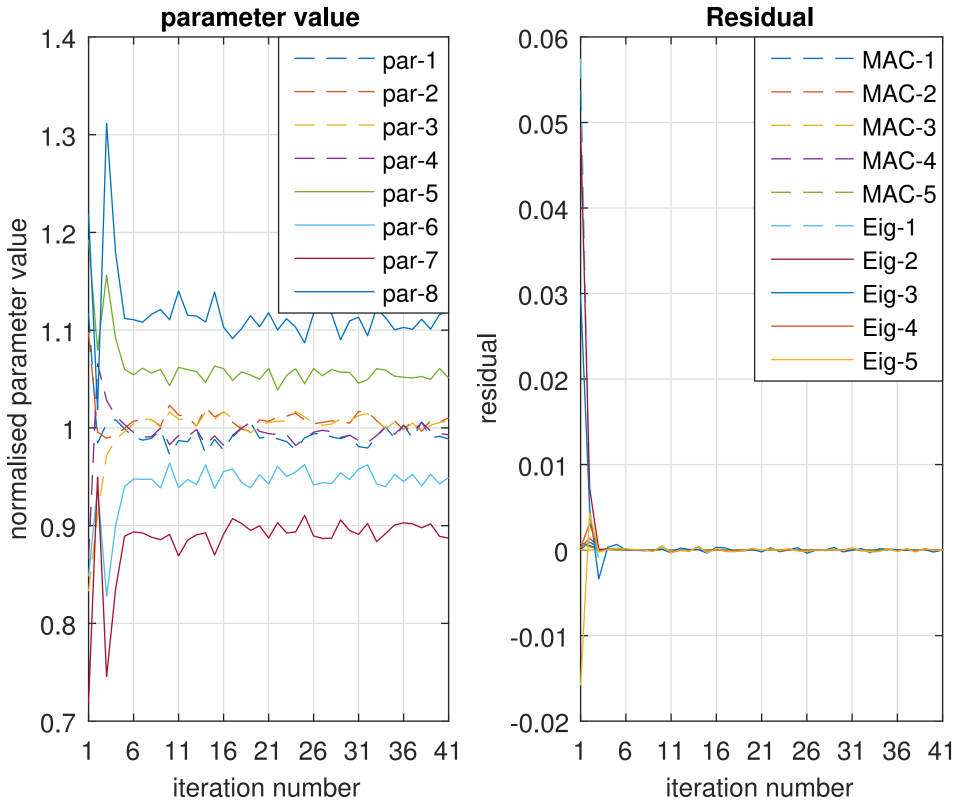

Figure 4.16: The parameter values and the residuals are shown at each iteration step. Updating using 5 modes, a noise level of $1e-5$ and the pseudo-inverse.

Table 4.7: Results of the dynamic updating procedure for different noise levels.

	noise level		
parameter	0.00E+00	1.00E-09	1.00E-06
1	1.00	1.00	1.00
2	1.00	1.00	1.00
3	1.00	1.00	1.00
4	1.00	1.00	1.00
5	1.00	1.00	1.01
6	1.00	1.00	0.99
7	1.00	1.00	0.98
8	1.00	1.00	1.02
	variance		
1	x	1.69E-20	1.37E-14
2	x	1.78E-20	1.61E-14
3	x	2.69E-20	2.46E-14
4	x	3.28E-20	3.01E-14
5	x	1.93E-20	2.48E-14
6	x	1.06E-20	1.59E-14
7	x	6.97E-21	7.94E-15
8	x	1.56E-20	1.92E-14

Discussion

The residual of the MAC values does not change much during updating, this indicates that mode shape changes reamain more or less the same. When the noise level is below a certain threshold the solution converges when the pseudo-inverse algorithms is used. If the noise is increased beyond a threshold level the condition for convergence - parameter change below a certain level - is not met after 41 iterations. The residual is close to zero. The condition number of the sensitivity matrix was found to be in the order of $1e4$, not particularly large. Still regularization was used to find a stable solution for the problem with noise level of $1.00E-5$. The parameters 1 to 4 are found close to their true value, this means that they are important in reducing the residual. These parameters thus influence the natural frequency of the modes. Looking at the mode shapes in figure 4.7 and the elements connected to these parametes it can be seen that these elements strain the most for these mode shapes. It was found that at least five modes were needed for the updating to work, apparently this amount of informations is needed. With these five modes all the four modes found using the wet FEMAP model are included.

4.5. Static updating to actual measurements

In this section the updating procedure applied to the beam model using actual measurement data. Only the static case is considered. First the sensitivity of the parameters is shown and then the results are given and discussed. Two ways of solving the least square problem are used the pseudo-inverse and regularization. The parameters used are those in table 4.4.

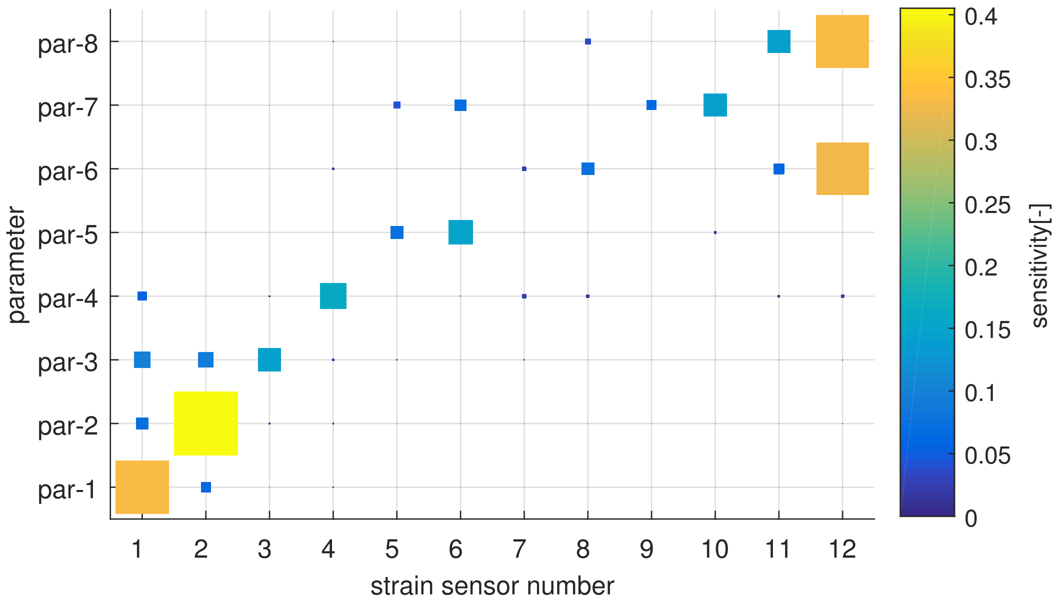

Figure 4.17: Sensitivity of the parameters for the neutral load case. Size of the squares is proportional to the sensitivity.

Sensitivity

The sensitivity of the parameters is shown in figure 4.17. The most sensitive parameters are: 1, 2, 6 and 8. The parameters are most sensitive for the sensor that is in the same area. The rows seem to be linearly independent. Notice that the sensitivities found here are different from those in figure 4.11, this is because the parameter values are different in these two analyses. In general the response is a non-linear function and as a result the sensitivities are dependent on the parameter setting.

Results

The result of the updating procedure using the pseudo-inverse is shown in figure 4.18. During the updating the condition number of the sensitivity matrix becomes very large. A solution is found but one that is not-physically feasible. Also the residual is zero after updating. Regularization was used in an attempt to find a physically-feasible solution see figure 4.19. This figure shows that the solution does not converge and parameter values also attain non-physical values.

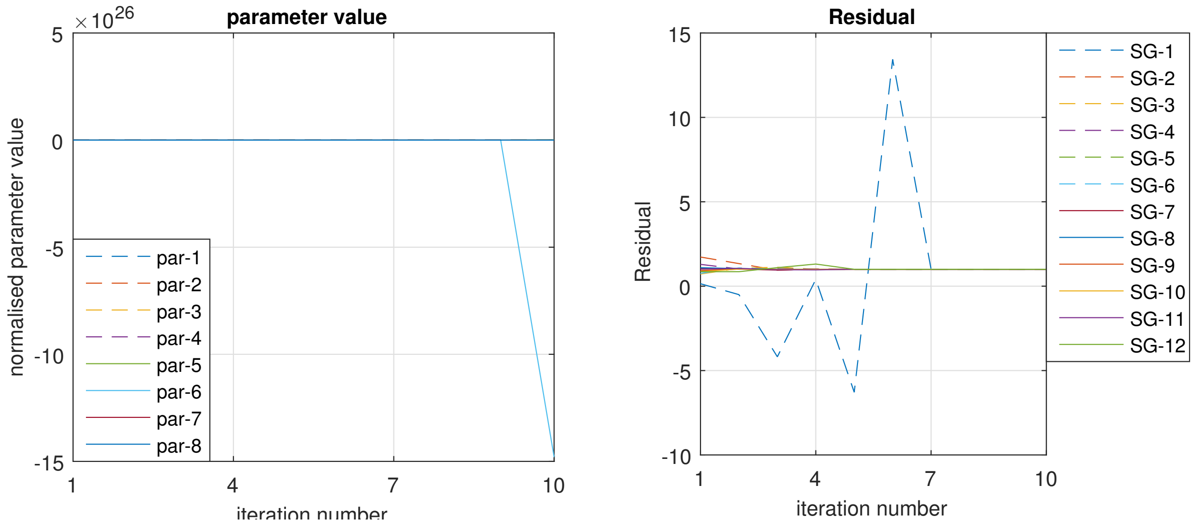

Figure 4.18: The parameter values and the residuals are shown at each iteration step. For updating using the strain measurements and the pseudo-inverse, the parameter values diverge.

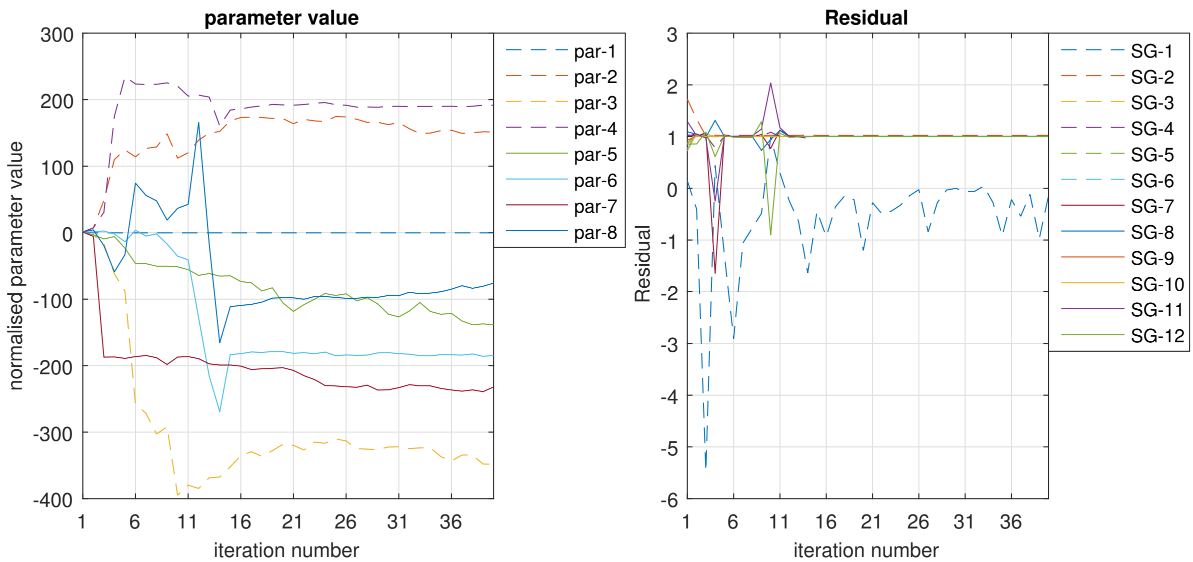

Figure 4.19: The parameter values and the residuals are shown at each iteration step. For updating using the strain measurements and regularization, the parameter values diverge.

Discussion

When updating the beam model to the actual measurements a non-physical solution is found using the pseudo-inverse. The condition number of the sensitivity matrix becomes very large during the updating. A large condition number can lead to wrong outcomes, see appendix A.2. Regularization can be used to overcome this. However when regularization is used no converging solution is found. The reason for the non-physical parameter estimates of the pseudo-inverse algorithm is thus not only due to the large condition number. It is most likely caused by the incorrect modeling of the strain in the beam model. In figure 4.20 the strain in the FEMAP model for the neutral loading condition is shown. From this figure it is apparent that the strain varies more or less continuously. Now look at figure 4.21 which gives the strain in x-direction[2] of the elements for the neutral loading condition. In this figure the strain shows big jumps across elements and is discontinuous. These big

[2] In the local element coordinate system.

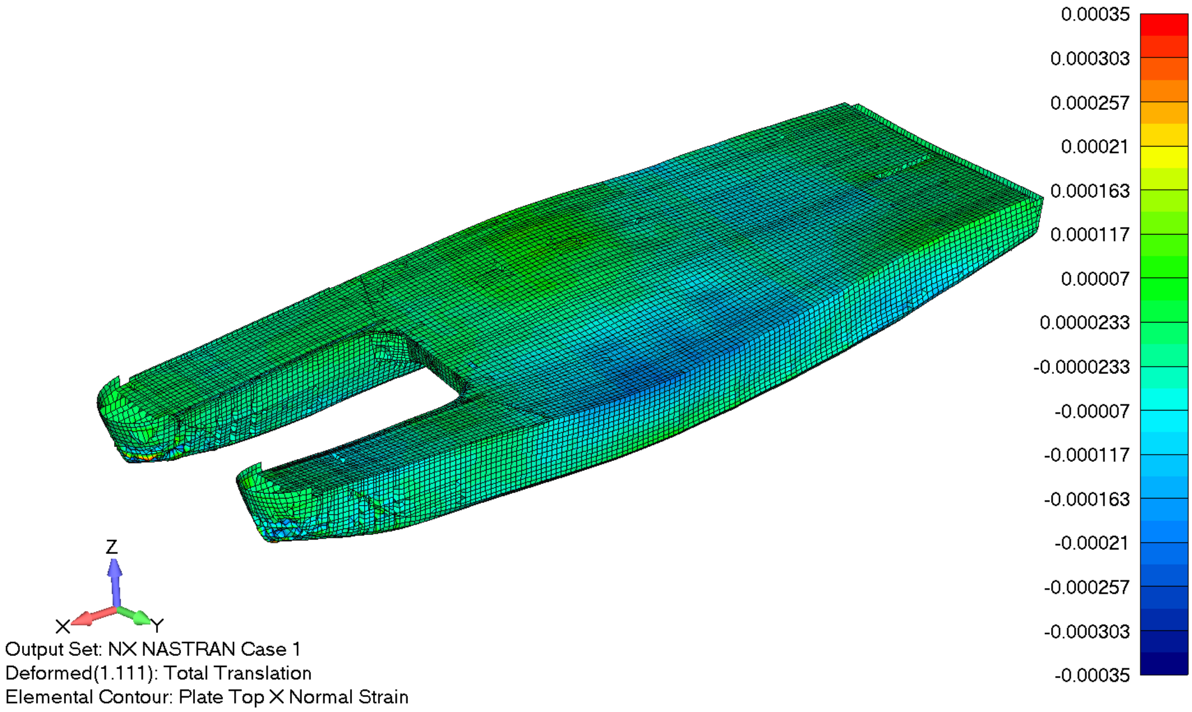

Figure 4.20: The strain in the plates of the FEMAP model in x-direction, for the neutral load case.

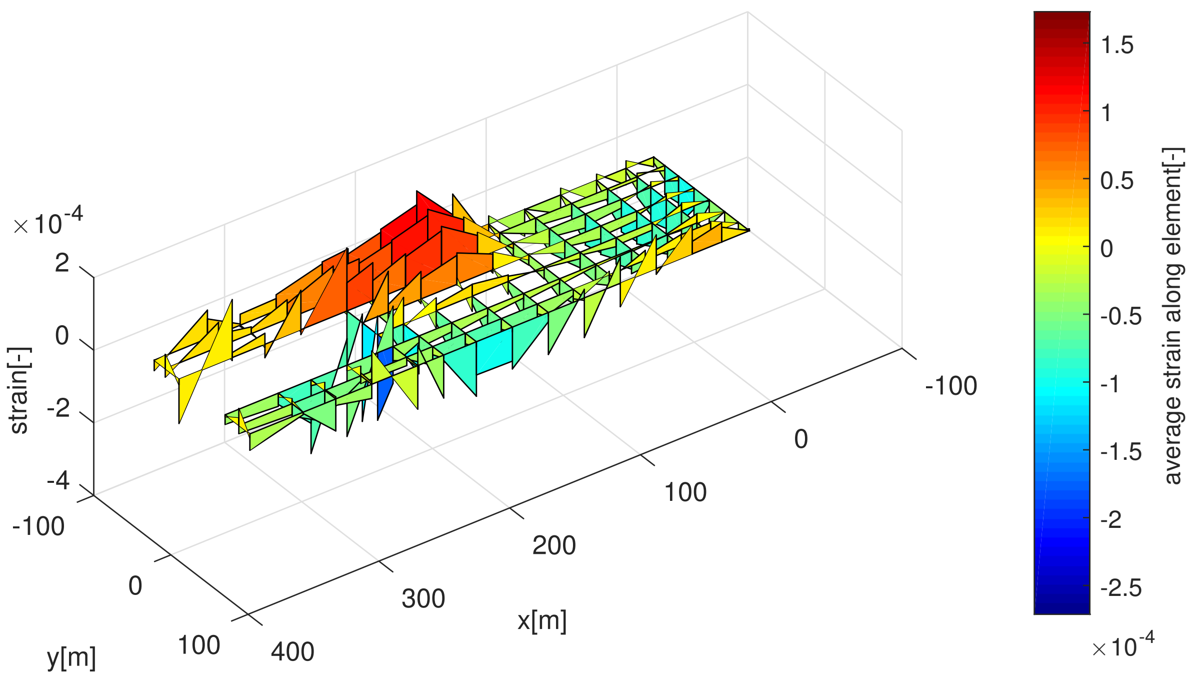

Figure 4.21: The strain at the deck along each element of the beam model. The color indicates the average strain over the element.

jumps are caused by the coarse distribution of the stiffness in the beam model, and more in particular the jumps are caused by the torsional stiffness in the elements perpendicular to an element. Although the deformation of the beam model show a good correlation with the FEMAP model. The strains are not modeled correctly by the beam model. And this is likely the cause of the diverging updating procedure. The average strain of the beam model does show some correlation with the strains of the FEMAP model. The modeling error $\boldsymbol{\eta}_{er}$

of the beam element model is too large. And in updating the beam model the residual - see (2.12) - is minimized. Updating only affects the parameter error $\boldsymbol{\eta}_\theta$. When minimizing the residual the parameter error increases to do away with the large modeling error. This causes the parameter estimates to be non-physical. When the modeling error is too large the union of the model space S_3 and S_2 is empty, see figure 2.6a , and changing the parameters can not result in a model that correlates with the structure.

4.5.1. Model validation

In this section the validation of the updated models is discussed. First the validation test is given, and then the results of its application to the updated models in this chapter are given.

Validation test

The final step in a FEMU procedure is to validate the updated model, see section 2.1.5. To do this the predicted behavior of the updated model is compared to the measured behavior not used during the updating. In this thesis virtual measurements were used to find an updated model. For the virtual measurements the true parameter values are known and these can be used to validate the updated model. To this end a test was devised to check whether or not an updated model can be considered a validated model. When noise is added to the virtual measurements the measured behavior will be different and as a result the true parameter values will not be found. However, these parameter values should not change significantly, if they do the problem is sensitive to noise and the updated model will most likely not be a validated model. Therefore a maximum of 10% change is allowed on each individual parameter and the sum of the absolute change of all the parameters, $\sum \delta\theta$, is smaller that 25%. The results of the test can be seen in table **??**. Where PI stands for Pseudo-inverse and Reg for regularization, referring to the algorithm that was used to find the parameter estimates.

Table 4.8: The validation test applied to the updated model.

	noise level	Algorithm	η_{er}	$\sum \Delta\theta$	max deviation	validated
Static	1.00E-02	PI	no	20%	8.0%	yes
Static	1.00E-1	PI	no	157%	69%	no
Static	1.00E-02	PI	yes	16%	10%	yes
Static	1.00E-1	PI	yes	105%	38%	no
Dynamic	1.00E-06	PI	no	6.0%	2.0%	yes
Dynamic	1.00E-05	Reg	no	94%	28%	no

Table 4.9: tab:val

Results

The the results show that for the static cases and a noise level of 1.00E-2 both the analyses yield a validated model. For a noise-level of 1.00E-1 the analyses do not yield a validated model. The dynamic case for a noise-level of 1.00E-6 yields a validated model, for a higher noise level the pseudo inverse algorithm does not converge see figure 4.16. Using regularization to find a solution does also not yield a validated model.

Discussion

For the static case it can be concluded that the stiffness of the PS can be validated using finite element model updating if the noise level does not exceed 1.00E-2. The same is true for the dynamic case, however, there the noise level is much smaller 1.00E-6. Because regularization has the effect of penalizing parameter changes, this does not help in finding the parameter estimates close to the true parameters. The test to for a validated model has been thought of by the author, and is open for debate. But it does give a quantifiable measure of the validity of an updated model. The above shows that below certain noise levels the updated model is a validated model. For the strain gauges the sensor noise is 0.25E-2. Assuming that the updating procedure works in the same way for the FEMAP model as it does for the beam model, it can be concluded that the structural stiffness of the Pioneering Spirit can be validated using the current sensor setup. Because the sensor noise of the strain gauges is below the above stated maximum noise. For the dynamic case the noise is added on the derived parameters, and how this translates to actual sensor noise is not investigated in this thesis. It is not known whether the noise level on the derived parameters translates to a sensor noise level not exceeded by the actual sensors. However, the identification method used to find the derived quantities puts limits on the accuracy with which these quantities can be identified. And the noise of 1.00E-6 is beyond that limit.

4.6. Summary

In this section the results of the analyses in this chapter are summarized. In this chapter the beam model of the PS was discussed and its properties were explained. Then the FEMU method - as presented in chapter 2 - was applied to the beam model of the PS. The beam model was shown to correlate with the global behavior of the PS, for both the static and the dynamic behavior. The results of the FEMU method using simulated data showed that the beam model can be updated using the current measurement setup. Using simulated data meaningful parameter estimates were found for the static case, even when a modeling error $\boldsymbol{\eta}_{er}$ and a measurement error $\boldsymbol{\eta}_m$ were introduced in the residual. Also for the dynamic case meaningful parameter estimates were found, here only a measurement error $\boldsymbol{\eta}_m$ was introduced in the residual. The quality of the parameter estimate depends on the noise level of the measurements $\boldsymbol{\eta}_m$, the modeling error $\boldsymbol{\eta}_{er}$ and the ability of the parameters to change the parameter error $\boldsymbol{\eta}_\theta$; as is apparent from figure 2.4. For the dynamic updating using simulated data it was found that at least 5 modes were needed to find a parameter estimate. Apparently that is the minimum amount of information needed to find a converging solution. For the dynamic case a smaller noise level was found to cause divergence in the algorithm using the pseudo-inverse as compared to the static case. Regularization was used to find a converging solution, however the original parameter settings were not found. The modes were measured at every node and all nodal DOF's, this results in very accurate mode shape measurements. In reality the mode shapes are measured using accelerometers at 4 locations and for 6 DOF's. Up to this point the dynamic behavior of the PS is identified using these 4 accelerometers, and four mode shapes were identified using this data. This would indicate the the current number of identified mode shapes would not be enough to update the model. Updating the beam model using actual strain measurement for a static case failed. The reason for this is most likely the discrepancy between the predicted strains of the beam model and the measured strains. It was shown that the strains in the FEMAP model and the beam model do not correlate. The beam model models the global behavior well but strains are local measures and are not modeled correctly by the beam model. The modeling error $\boldsymbol{\eta}_{er}$ is too great and because of this the unrealistic parameter estimates are found. If the modeling error is too large the union of S_3 and S_2 is empty and a model that correlates with the measurements can not be found using FEMU.

From here there are two ways to proceed adapt the model or the data:

1. Discard the beam model and construct a FE-model with a small modeling error $\boldsymbol{\eta}_{er}$, Such a model will correlate with the measured data, and the model will be in S_3 and S_2. Such a model will probably be constructed using plate elements, as is the case for the FEMAP model.

2. The strain measurements could be used to find nodal displacements, which are modeled correctly by the beam model. This would also result in a reduction of the modeling error $\boldsymbol{\eta}_{er}$. For this a method to transform strain measurements in to displacements should be developed, whether such a transformation exists is not known.

An updated model is not yet a validated model. A test was developed to check whether or not the simulated models are valid models. This test showed that for the static case the noise level should not exceed 1.00E-2 for the updated model to be a validated model. For the dynamic case the noise level should not exceed 1.00E-6.

“Life is the art of drawing sufficient conclusions from insufficient premises.”

Samuel Butler

5 Summary, Conclusion and Recommendation

In this chapter the summary, conclusion and recommendation are presented.

5.1. Summary

In this section thesis the results presented in this thesis are summarized.

Finite element model updating was identified as a way to validate the structural stiffness of the Pioneering Spirit using the current sensor setup. To check if this method would work and the Finite element model updating techniques were implemented and applied to a simplified model of the Pioneering Spirit. These techniques were first applied to a test case.

Test case

To gain insight in the concepts involved in finite element model updating it is applied to a test case, the cantilever beam. The results in section 3.5.2 show that for an Euler-Bernoulli beam the natural frequency sensitivity is constant for the first 6 natural frequencies beams when parameters are used that change all elements. Using the same parameters for a Timoshenko beam the natural frequency sensitivity changes per mode. In section 3.5.3 different methods are used to determine the mode shape derivative. Fox and Kapoor’s approximation method is not guaranteed to be accurate and taking into account more mode shapes does not necessarily lead to a better mode shape derivative. Nelson’s method to determine mode shapes is found to be the most accurate. The mode shape derivative is highly dependent on the parameter choice. There are parameterizations that affect the natural frequency more than the mode shape and vice-versa. In section 3.6 it is shown that the quality of the results of finite element model updating depend - in part - on the quality measured behavior. The quality of the measured behavior depends on the number, location and the noise in the measurements. If more parameter than measurements are used many different parameter estimates are possible, a solution is picked depending on the updating algorithm. Using more or the same number of measurements as parameters is desirable. The location of the measurements is important for the conditioning of the problem. Ill-conditioning can be resolved by using regularization in the updating algorithm, the original parameter setting was not found when regularization was used to alleviate ill-conditioning of a problem where no measurement error and modeling was present. The amount of regularization does not change the solution, only the number of iterations are affected. Noise introduces a measurement error, this makes that the measured behavior is different from the true behavior. As a results the original parameter values will not be found when noisy measurements are used. Parameters with a small sensitivity are most affected by noise. If too much noise is present the measured behavior is too distant from the true behavior, this may results in divergence. Applying regularization in this case will not result in a physically realistic parameter estimate.

Ships model
This insight was valuable when the FEMU techniques were applied to the beam model of the Pioneering Spirit. Using simulated strain measurements that mimic the sensors on the Pioneering Spirit it was shown that the beam model can be updated for the static case and for the parametrization in this thesis see section 4.4.2. This even when measurement error and modeling error was introduced. For the dynamic case the simulated measurements consisted of mode shapes and natural frequencies see section 4.4.3. At least 5 natural frequencies and 5 mode shapes were needed for the updating to work. The modeling error of the beam model was found to be too big for use with actual strain measurements. A test was devised to check if the updated models using virtual measurements were validated models see section 4.5.1. For the static case the maximum noise level of $1e-2$ was found for the updated model to be a validated model. For the dynamic case a noise level of $1e-6$ was found to be the maximum for the updated model to be a validated model.

5.2. Conclusion

The goal of this research is to investigate whether or not the structural model of the Pioneering Spirit can be validated using the current sensor setup. Finite element model updating was identified as the most suitable method to validate the structural model. This method was implemented and was applied to a simplified beam model of the Pioneering Spirit. The goal of this research has been reached. Now the research question is repeated and answered.

Can finite element model updating be used to validate the structural stiffness of the Pioneering Spirit using the current sensor setup?

The research question can be answered assuming that the updating method applied to the FEMAP model will work in the same way as it did for the beam model. For the static case the sensor noise should not exceed $1e-2$ to find a validated model. For the dynamic case the limit on the noise of the derived parameters is $1e-6$ to find a validated model, which is beyond the limits of the identification methods. For the static case it is possible to validate the structural stiffness of the PS using FEMU and the current sensor setup. For the dynamic case this is not possible.

5.3. Recommendation

The work presented in this thesis can be seen as a precursor to applying FEMU to the FEMAP model of the Pioneering Spirit some recommendation to successfully do this are presented here.

Model updating of the beam model using simulated data can be improved by:

1. Changing the number of measurements in the simulation and check what the effect is.
2. Use different parameterizations and see what the effect is on the parameter estimates.
3. Improve the parametrization method by using for example the force balance method. Also a careful study of the differences between the observed and predicted behavior can lead to a better understanding of which areas of the model are faulty and should be parametrized.
4. Better investigate the relationship between sensor noise and parameter estimates.

Model updating of the beam model using actual measurement data can be improved by:

1. Find an accurate transformation of the strain measurements to nodal displacements. Using such a transformation it is expected that the beam model can be updated to the real data.

2. Extracting modal parameters from the accelerometers and strain gauges. In doing this the actual measured data can be used to update the beam model.

3. For the dynamic case the hydrodynamic effects should be taken into account as they significantly affect the dynamic properties of the structure. This includes the added mass, added damping and the hydrostatic restoring stiffness. When hydrodynamic effects are not taken into account the modeling error $\boldsymbol{\eta}_{er}$ will most likely be significant resulting in parameter estimates that are non-physical.

When the first two recommendations are implemented it is expected that the simplified model can be updated to the actual measurement data. The third recommendation will allow for more parameters to be estimated.

Updating the FEMAP model of the Pioneering Spirit is more involved than for the beam model considered in this research, because the model has much more degrees of freedom. The following recommendations are given to validate the FEMAP model using FEMU:

1. Prior to any updating the model should be thoroughly checked by taking into account: assumptions made when constructing the current model and look for areas that are not modeled correctly. This information can be used to reduce the modeling error $\boldsymbol{\eta}_{er}$, making sure that for the initial model S_3 and S_2 overlap. This will also help to find the right parametrization of the model.

2. Adding more sensors will result in richer measurement data and a more accurate description of the measured behavior, reducing $\boldsymbol{\eta}_m$. If the number of parameters needed to update the model exceeds the number of measurements adding more sensors is required.

3. The PS is a structure that has a mass and stiffness that varies due to different ballast conditions, also several structural components are being added to the PS. In a updating procedure these should be taken into account.

4. The hydrodynamic effects should be taken into account properly to minimize the modeling error $\boldsymbol{\eta}_{er}$.

5. The number of DOF's in the FEMAP model can be reduced to lower the computational costs of updating.

6. The final step of FEMU is to check whether the behavior of the updated model correlates better with measured behavior not used in the updating than the initial model. Here care should be taken with selecting a measured to test the updated model as the behavior of the ship maybe dependent on the environmental conditions.

7. The strain gauges should be properly calibrated in order minimize the measurement error $\boldsymbol{\eta}_m$, so that the measured behavior is closer to the true behavior.

A

Non-linear Least squares

In this section the non-linear least-square problem and its solution is explained.

A.1. Non-linear least-squares

An unconstrained optimization problem minimizes a certain norm of a quantity $f(\mathbf{x})$ by finding the optimal value for $\mathbf{x}$ in (A.1), the functions $r_i(\mathbf{x})$ are non-linear functions of $\mathbf{x}$. The norm of a vector is given by (A.2).

$$\min_{\mathbf{x}\in\mathbb{R}^n} \quad f(\mathbf{x}) = ||r_i(\mathbf{x})||_p \tag{A.1}$$

In this case the Euclidean norm is used and $p = 2$. It is not necessary to use the Euclidean norm, well known applications exist for cases where $p = 1$ and $p = \infty$ [6]. The different values for p may be seen as a weighting of the values of r_i depending on their magnitude.

$$||r_i(\mathbf{x})|| = \left(\sum_{i=1}^{m} |r_i(\mathbf{x})|^p)\right)^{1/p} \tag{A.2}$$

Using $p = 2$ the minimization problem defined in (A.1) then becomes a non-linear least squares optimization problem. And can be restated as:

$$\min_{\mathbf{x}\in\mathbb{R}^n} \quad f(\mathbf{x}) = \frac{1}{2}\sum_{i=1}^{m} r_i^2(\mathbf{x}) \tag{A.3}$$

This problem can be solved using the Gauss-Newton method which uses a first order Taylor approximation of $r_i(\mathbf{x})$ at the current point, then solve the linearized problem to find a next point. This is repeated until a convergence criteria is met. The method needs an initial estimate of the vector $\mathbf{x}$ to start. The starting position may lead to different outcomes due to the non-linearity of $r_i(\mathbf{x})$. The method is locally convergent for nearly all non-linear problems and usually globally convergent[4]. Linearizing (A.3) turns it into a least-squares problem, a least-squares problem is thus solved each iteration.

The non-linear least-square problem is encountered in the field of data fitting. A model $g_i(\mathbf{x})$ with parameters $\mathbf{x}$ is fitted to data $\mathbf{d}$, with $i = 1..m$ where m is the number of measurements and with $j = 1..n$ where n is the number of model parameters. Then the residual r_i between the model and the data is given by (A.4).

$$r_i(\mathbf{x}) = d_i - g_i(\mathbf{x}) \tag{A.4}$$

The first order Taylor expansion of the residual is given in (A.5), where $J(\mathbf{x})_{ij}$ is the first derivative of the model g_i, and $\mathbf{x}_s$ some initial setting of the parameters.

$$r_i(\mathbf{x}) \approx r_i(\mathbf{x}_s) + \left.\frac{\partial r_i^2(\mathbf{x})}{\partial x_j}\right|_{\mathbf{x}_s} \delta\mathbf{x} = r_i(\mathbf{x}_s) + J(\mathbf{x})_{ij}\Big|_{\mathbf{x}_s} \delta\mathbf{x} \tag{A.5}$$

Substituting (A.5) into the minimization problem (A.3) leads to a least squares problem. To understand the non-linear least-squares solution a good understanding of a least-squares problems is needed.

A.2. The least-square problem

The solution of simultaneous linear equations (A.6) is a problem encountered in many areas of science, and it is fundamental in the study of linear algebra. With $\mathbf{A}$ a M by N real matrix, $\mathbf{x}$ a N by 1 vector and $\mathbf{b}$ a M by 1 vector.

$$\mathbf{Ax} = \mathbf{b} \tag{A.6}$$

10 cases for $\mathbf{Ax} = \mathbf{b}$

In general there are 10 different cases to consider when solving (A.6)[7]. They have to do with: the shape $\mathbf{A}$, the $r = rank(\mathbf{A})$, whether $\mathbf{b}$ is in $range(\mathbf{A})$.

1. $M = N = r$. $\mathbf{b} \in range(\mathbf{A})$. There is one solution with $\boldsymbol{\epsilon} = 0$.
2. $M = N > r$, $\mathbf{b} \in range(\mathbf{A})$. There are many solutions with $\boldsymbol{\epsilon} = 0$.
3. $M = N > r$, $\mathbf{b} \notin range(\mathbf{A})$. There are many solutions with the same $\boldsymbol{\epsilon}$.
4. $M > N = r$, $\mathbf{b} \in range(\mathbf{A})$. There is one solution with $\boldsymbol{\epsilon} = 0$.
5. $M > N = r$, $\mathbf{b} \notin range(\mathbf{A})$. There is one solution with minimum $\boldsymbol{\epsilon}$.
6. $M > N > r$, $\mathbf{b} \in range(\mathbf{A})$. There are many solutions with $\boldsymbol{\epsilon} = 0$.
7. $M > N > r$, $\mathbf{b} \notin range(\mathbf{A})$. There are many solutions with the same minimum $\boldsymbol{\epsilon}$.
8. $N > M = r$, $\mathbf{b} \in range(\mathbf{A})$. There are many solutions with $\boldsymbol{\epsilon} = 0$.
9. $N > M > r$, $\mathbf{b} \in range(\mathbf{A})$. There are many solutions with $\boldsymbol{\epsilon} = 0$.
10. $N > M > r$, $\mathbf{b} \notin range(\mathbf{A})$. There are many solutions with the same minimum $\boldsymbol{\epsilon}$.

These 10 cases can be split up into 3 categories:

- $\mathbf{A}$ is square:$M = N$. There are as many equations as unknowns
- $\mathbf{A}$ with $M > N$. There are more equations than unknowns, overdetermined.
- $\mathbf{A}$ with $N > M$. There are more unknowns than equations, underdetermined.

A solution to this problem only exist if $\mathbf{b}$ is in the range of $\mathbf{A}$, if not $\mathbf{A}$ no solution for $\mathbf{x}$ exists. The next best solution to is the one within the range of $\mathbf{A}$ with the smallest Euclidean norm $\sqrt{\boldsymbol{\epsilon}^T\boldsymbol{\epsilon}}$ to $\mathbf{b}$, the error, see (A.7) and (A.8), in this light the least-square method can be viewed as an optimization method. The solution can be found by the orthogonal projection of $\mathbf{b}$ onto the column space of $\mathbf{A}$, this projection is in the range of $\mathbf{A}$ and is the least square solution of (A.6). A visual representation of this problem in 3 dimensions can be seen in figure A.1 for case 5 in the list below, with $M = 3$ and $N = r = 2$.

$$\boldsymbol{\epsilon} = \mathbf{A}\hat{\mathbf{x}} - \mathbf{b} \tag{A.7}$$

$$Find \quad \hat{\mathbf{x}} \quad satisfying \quad min||\boldsymbol{\epsilon}||_2 \tag{A.8}$$

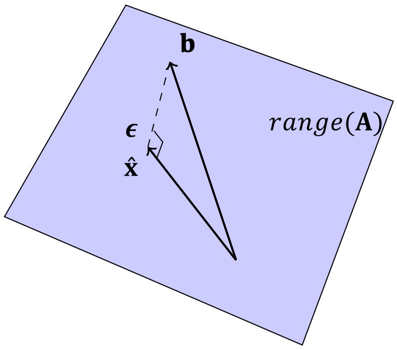

Figure A.1: The least squares problem visualized, for 3-dimensions.

For case 1, 4 and 5 a unique (least-square) solution exists to (A.6). For case 2, 3, 6, 7, 8, 9 and 10, this is not the case and many solutions exist. However a unique solution can be found for these cases if additional information is added, in the form of constraints;

- minimize the euclidean norm of error: $\boldsymbol{\epsilon}^T\boldsymbol{\epsilon}$.
- minimize the euclidean norm of the solution: $\mathbf{x}^T\mathbf{x}$.

The solution is then found by using the Pseudo-inverse of $\mathbf{A}$, which can be determined by using the singular value decomposition. Using the pseudo inverse is a form of regularization.

Apart from the possible non-uniqueness of the problem in (A.6), due to rank deficiency and under-determination, another problem is encountered when finding a solution to (A.6). This has to do with the linear dependency of the columns of $\mathbf{A}$, if the the columns are close to being linearly dependent the solution is very sensitive to small changes in the $\mathbf{b}$ and the problem is then called ill-conditioned.

Example: ill-conditioning & condition number

We have the matrix $\mathbf{D}$ defined by (A.9), it is clear that the columns of this matrix are close to being linearly dependent. If we try to find a solution for $\mathbf{Dx} = \mathbf{y}$ the solution will greatly vary when the parameter δ in $\mathbf{y}$ is changed slightly, see (A.11).

$$\mathbf{D} = \begin{bmatrix} 1 & 10 \\ 10 & 100.1 \end{bmatrix} \tag{A.9}$$

$$\mathbf{y} = \begin{bmatrix} 11 + \delta \\ 110.1 \end{bmatrix} \tag{A.10}$$

$$\mathbf{Dx} = \mathbf{y} \quad \begin{cases} \mathbf{x} = \begin{bmatrix} 1 \\ 1 \end{bmatrix} & \text{for } \delta = 0 \\ \mathbf{x} = \begin{bmatrix} 100.1 \\ -9 \end{bmatrix} & \text{for } \delta = 0.1 \end{cases} \tag{A.11}$$

In FEMU $\mathbf{y}$ represents measurements, these are inherently contaminated with noise. $\mathbf{y}$ thus contains small errors, obtaining a well-conditioned problem is important. A measure for how well a matrix is conditioned is the condition number defined in (A.12), it is the ratio between the spectral norm of $\mathbf{D}$ and the norm of the inverse of $\mathbf{D}$. The spectral norm is defined by (A.13), its value is the largest singular value of $\mathbf{D}$. Geometrically this can be interpreted as the maximum amount the unit sphere - given by $||\mathbf{z}|| = 1||$ - will be 'stretched'. The norm of $\mathbf{D}^{-1}$ - its biggest singular value - is the reciprocal of the smallest singular value of $\mathbf{D}$. Geometrically the smallest singular value of $\mathbf{D}$ is a measure for how much the unit sphere will be 'squeezed'.

$$condition\, number\ = ||\mathbf{D}|| \cdot ||\mathbf{D}^{-1}|| \tag{A.12}$$

$$||\mathbf{D}|| \equiv sup_{||\mathbf{z}||=1}||\mathbf{Dz}|| \tag{A.13}$$

The condition number is the ratio between the largest and the smallest singular value of a matrix. Geometrically it is the ratio between the squeezing and stretching of a linear transformation given by a matrix. How much a matrix will stretch a vector depends on the direction of the vector. If the direction of the vector changes the stretching changes, when a matrix has greatly varying stretch in certain directions a small change to the direction of a vector can lead to a big change in the transformed vector. Such a matrix would be considered ill-conditioned. In figure A.2 a linear transformation on the unit sphere is shown for a well-conditioned and a ill-conditioned transformation matrix. The black and green lines in this figure indicate two unit vectors. The stretching of the transformation is large in the ill-conditioned matrix, and as a result the absolute difference between the two matrices is great in case of an ill-conditioned matrix transformation. In case of a well-conditioned matrix transformation the absolute difference is of the same order of magnitude as before the transformation.

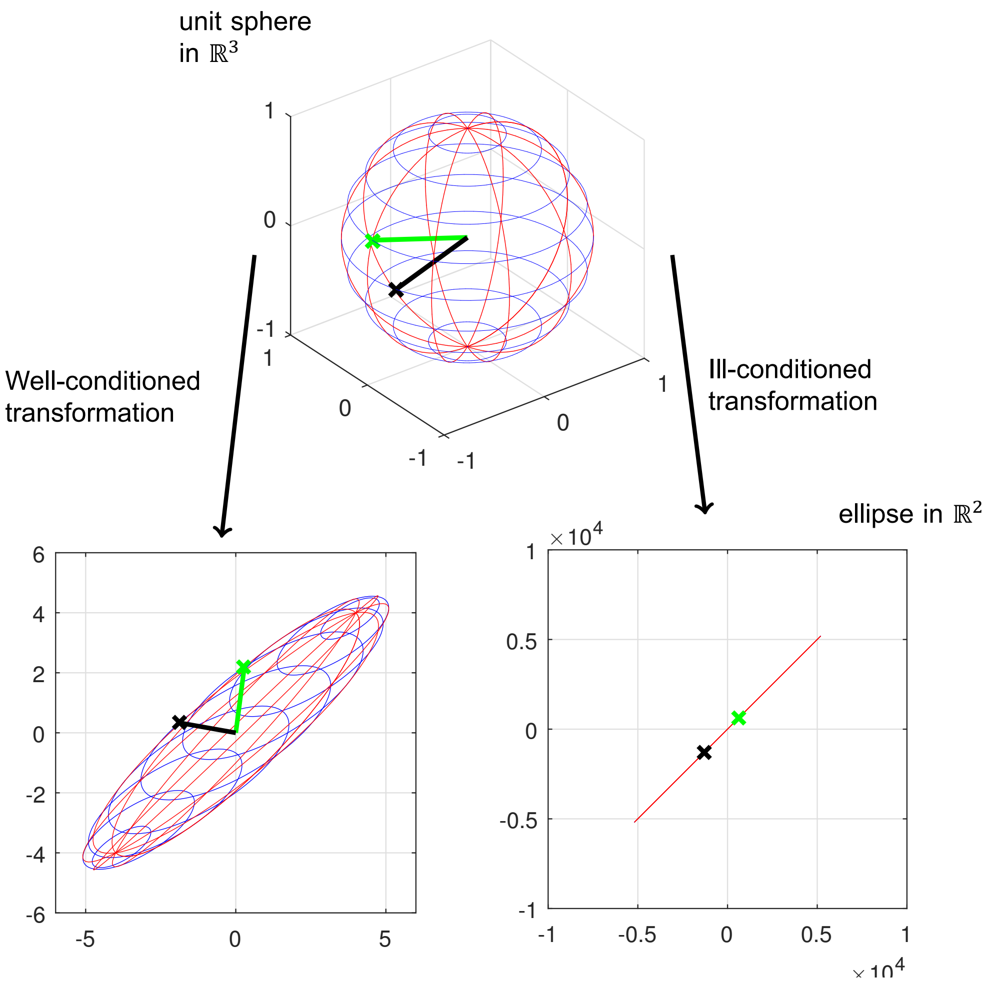

Figure A.2: Geometric view of two linear transformation of the unit sphere in $\mathbb{R}^3$ to $\mathbb{R}^2$, ill-conditioned and well-conditioned. Longitude(red) and latitude(blue) of the unit sphere are shown before and after the transformation.

A.2.1. Regularization

In order to overcome ill-conditioning the original problem (A.8) can be altered by adding a regularization term. The norm of the solution varies greatly for ill-conditioned problems, see (A.11). The regularization term takes into account changes in the solution norm, damping the otherwise big changes in the solution. In (A.14) the regularization term is shown, $\mathbf{I}$ is the identity matrix and J the new cost function. The regularization term turns the ill-conditioned problem in a well-conditioned problem, but there is a catch. The solution will depart form the true solution, as the magnitude of λ increases. Hence the magnitude regularization term requires some consideration. One method for choosing lambda using the L-curve is given in [19]. The particular form of regularization in (A.14) is called Tikonov regularization.

$$||\mathbf{A}\hat{\mathbf{x}} - \mathbf{b}||_2 + \lambda^2||\mathbf{I}\hat{\mathbf{x}}||_2 = J(\hat{\mathbf{x}}) \tag{A.14}$$

A.3. The least-square estimator

The least square problem can be used in estimation to find the estimate for the N parameters $\hat{\mathbf{x}}$ from M measurements $\mathbf{b}$, the measurements are contaminated with a measurement error $\boldsymbol{\mu}$.

$$\mathbf{A}\mathbf{x} = \mathbf{b} + \boldsymbol{\mu} \tag{A.15}$$

To find an estimate $\hat{\mathbf{x}}$ for the parameters we now assume the following on the statistical properties of (A.15):

1. The expected values of the measurements are linear combinations of the parameter (A.16).
2. The variances of the of measurements are uncorrelated and each measurement has the same variance σ^2 (A.17).
3. The mean of the measurement error $\boldsymbol{\mu}$ is zero.

$$E[\mathbf{b}] = \mathbf{A}\mathbf{x} \tag{A.16}$$

$$E[(\mathbf{b} - E[\mathbf{b}])(\mathbf{b} - E[\mathbf{b}])^T] = \sigma^2\mathbf{I} \tag{A.17}$$

$$E[\boldsymbol{\mu}] = \mathbf{0}; \tag{A.18}$$

For $rank(\mathbf{A}) = N$ the unbiased least square estimate is given by (A.19).

$$\hat{\mathbf{x}} = (\mathbf{A}^T\mathbf{A})^{-1}\mathbf{A}^T\mathbf{b} + (\mathbf{A}^T\mathbf{A})^{-1}\mathbf{A}^T\boldsymbol{\mu} \tag{A.19}$$

Now the estimated value of (A.19) is determined.

$$E[\hat{\mathbf{x}}] = E[(\mathbf{A}^T\mathbf{A})^{-1}\mathbf{A}^T\mathbf{b}] + E[(\mathbf{A}^T\mathbf{A})^{-1}\mathbf{A}^T\boldsymbol{\mu}] \tag{A.20}$$
$$E[\hat{\mathbf{x}}] = (\mathbf{A}^T\mathbf{A})^{-1}\mathbf{A}^T E[\mathbf{b}] + (\mathbf{A}^T\mathbf{A})^{-1}\mathbf{A}^T E[\boldsymbol{\mu}] \tag{A.21}$$
$$E[\hat{\mathbf{x}}] = (\mathbf{A}^T\mathbf{A})^{-1}(\mathbf{A}^T\mathbf{A})\mathbf{x} + (\mathbf{A}^T\mathbf{A})^{-1}\mathbf{A}^T\mathbf{0} \tag{A.22}$$
$$E[\hat{\mathbf{x}}] = \mathbf{x} \tag{A.23}$$

This shows that the expected value of (A.19) is unbiased.
The variance of the estimate $\hat{\mathbf{x}}$ is given by:

$$Var(\hat{\mathbf{x}}) = Var((\mathbf{A}^T\mathbf{A})^{-1}\mathbf{A}^T\mathbf{b}) \tag{A.24}$$
$$Var(\hat{\mathbf{x}}) = (\mathbf{A}^T\mathbf{A})^{-1}\mathbf{A}^T Var(\mathbf{b})\mathbf{A}(\mathbf{A}^T\mathbf{A})^{-1} \tag{A.25}$$
$$Var(\hat{\mathbf{x}}) = (\mathbf{A}^T\mathbf{A})^{-1}\mathbf{A}^T\sigma^2\mathbf{I}\mathbf{A}(\mathbf{A}^T\mathbf{A})^{-1} \tag{A.26}$$
$$Var(\hat{\mathbf{x}}) = \sigma^2\mathbf{I}(\mathbf{A}^T\mathbf{A})^{-1} \tag{A.27}$$

This shows how the variance of the estimate can be determined.

B

Beam element

B.1. Element validation

To validate the implementation of the Timoshenko beam element a comparison is made with the results from ANSYS, a commercial finite element software package. As a test case the cantilever beam and the static load cases presented in chapter 3 are used. The results are shown in B.1. This table shows that there is a small difference in the results for load case 1 and no difference for load case 2. The formulation of the Timoshenko beam element in ANSYS is not known to the author, it is assumed that the difference for load case 1 is due to the difference in the formulation of the effective shear area. The difference is small in the order of a promille.

Table B.1: Comparison of the static deflection from ANSYS and the code used in this thesis.

	ANSYS [mm]	code [mm]	difference [mm]
LC1	94.80	94.88	0.08
LC2	4.74	4.74	0.00

B.2. Element coordinate system

The beam element coordinate system is shown in figure B.1, together with the nodal degrees of freedom.

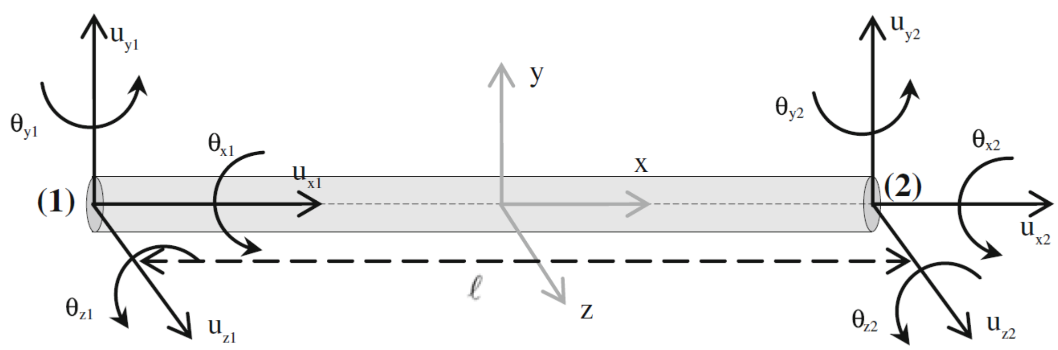

Figure B.1: The local element coordinate system from [16].

C

Ship coordinate system

The coordinate system fixed to the vessel is depicted in C.1. It is located at the centerline of the vessel, at the lowest point of the keel, and located 5.7m from the aft-most point of the stern. It is a right-handed-coordinate system.

- The x-axis is pointing from stern to bow.
- The y-axis is pointing from centerline to Port-side.
- The z-axis is pointing from keel to deck.

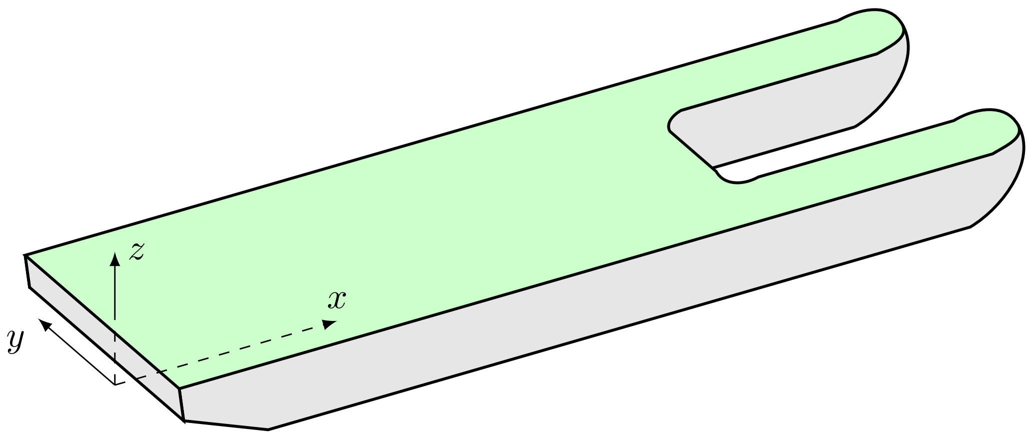

Figure C.1: The axis conventions, a right-handed coordinate system is located at the keel of the ship at the centerline.

D
Sensors

The Pioneering Spirit is equipped with a large number of sensors. The relevant sensors for this research are the strain-gauges. There are two types of strain-gauges on the vessel. One measures shear strain (SSG) and the other measures normal strain (LBSG). The sensor noise of the strain gauges is 0.25%.

The strains measured using the LBSG correlate well with the predictions of the FEMAP model see figure D.1, in this figure the stresses are shown but these are proportional to the strains. For the shear strain gauges in figure D.2 sensor 10 and 11 seem to correlate well with the predictions, and sensor 9 and 12 do not correlate well with the predictions.

Table D.1: Strain gauges and their positions.

type	sensor number	x [m]	y [m]	z [m]
LBSG	1	94.25	-65.58	28.60
LBSG	2	94.25	65.58	28.60
LBSG	3	206.75	-65.58	28.60
LBSG	4	206.75	65.58	28.60
LBSG	5	261.75	-65.58	28.60
LBSG	6	261.75	-26.33	28.00
LBSG	7	261.75	26.33	28.00
LBSG	8	261.75	65.58	28.60
SSG	9	261.75	-65.58	24.23
SSG	10	261.75	-26.33	24.23
SSG	11	261.75	26.33	24.23
SSG	12	261.75	65.58	24.23

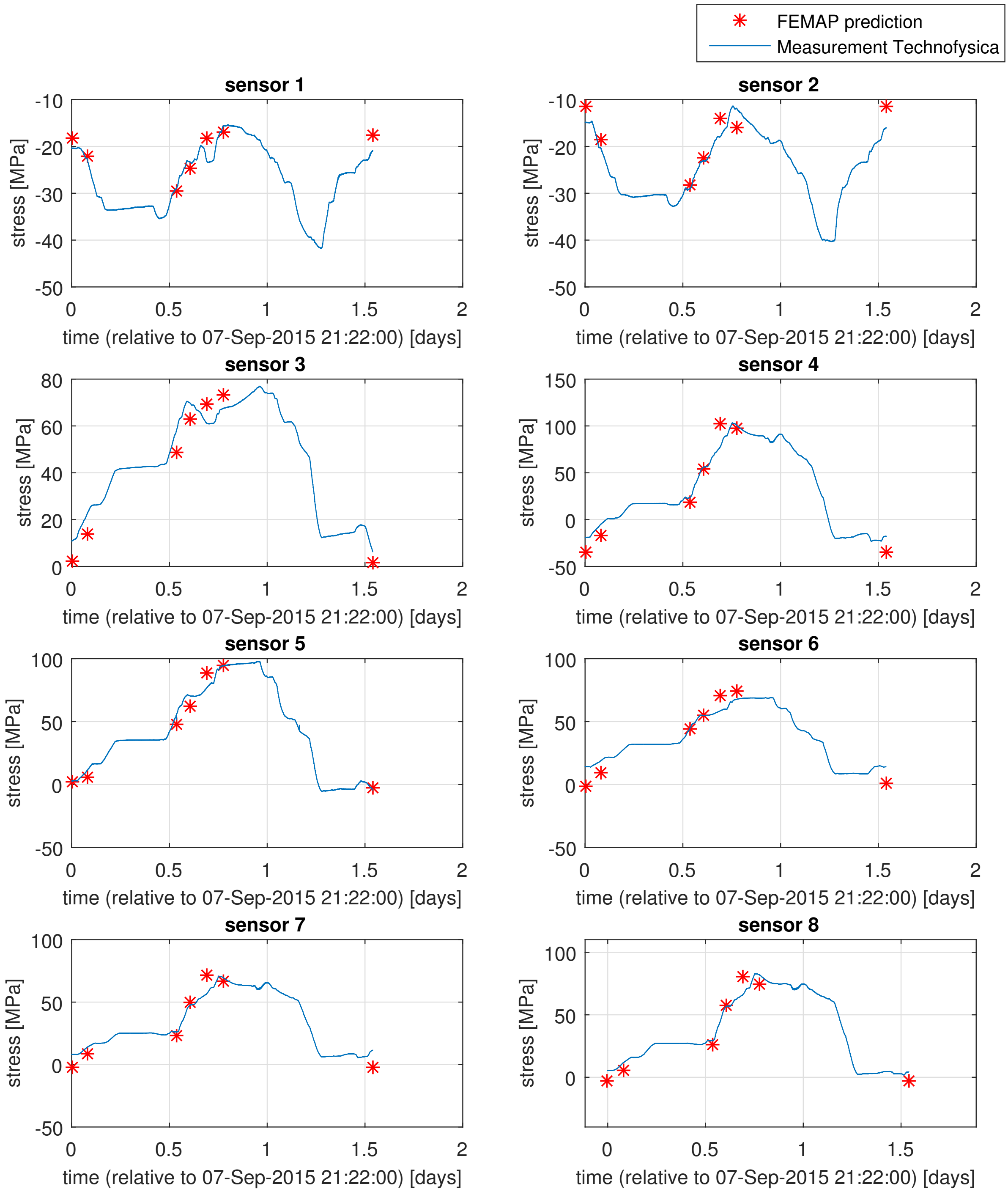

Figure D.1: Measured normal stresses and predicted stresses by the FEMAP model, for sensors 1 to 8.

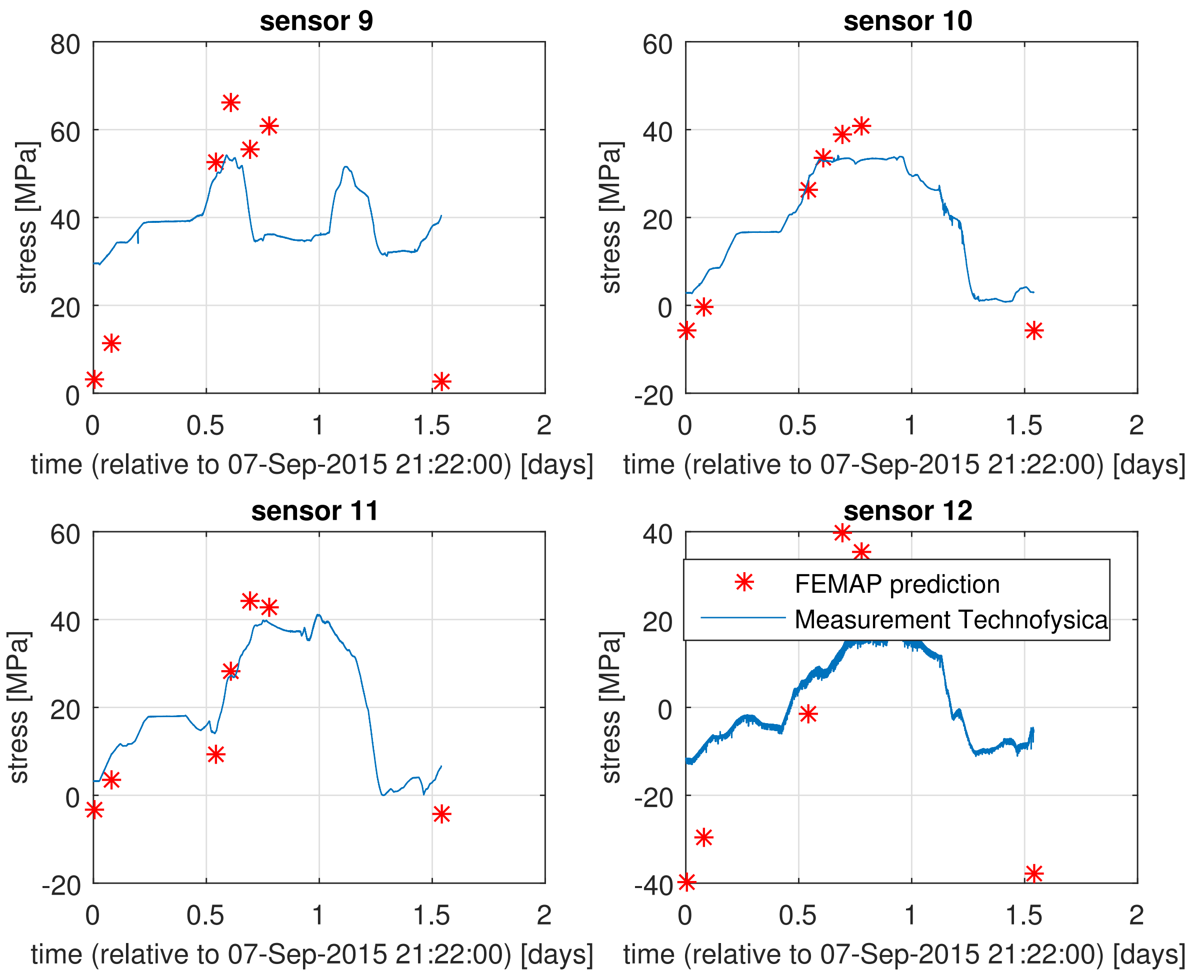

Figure D.2: Measured shear stresses and predicted stresses by the FEMAP model, for sensors 9 to 12.

E

Loading Conditioning Tool

Prior to any operation performed by the PS several analyses are performed. This is done to confirm that the vessels motions remain within bounds and at the same time to verify the structural integrity of both the cargo and the vessel during an operation. For these analysis input on the vessels mass distribution, ballasting condition etc. is needed. Every lifting operation performed by the PS is basically a one-off, since the cargo and operating location is different each time. This means that the input for the analyses change, to efficiently create this input a wide range of possible loading conditions a tool has been developed by Allseas, the Loading Conditioning Tool or LCT.

The LCT contains an accurate description of the mass distribution of the vessel in the longitudinal and the transverse direction, to do a preliminary check of the vessel strength when a ballast water distribution is determined. These distributions are used as input to determine the mass of the elements of the elements in the model in this report.

F Relative differences

In this appendix the relatives and maybe more mathematical expressions are explained

F.1. Relative differences

difference between Euler-Bernoulli and Timoshenko

$$\delta_{diff} = \frac{\delta_{EB} - \delta_{TIM}}{\delta_{EB}} \tag{F.1}$$

Frequency difference between Euler-Bernoulli and Timoshenko

$$f_{diff} = \frac{f_{EB} - f_{TIM}}{f_{EB}} \tag{F.2}$$

Relative differences between parameters

$$S_{diff} = \frac{S_{EB} - S_{TIM}}{S_{EB}} \tag{F.3}$$

F.2. noise on measurements

Noise is defined in the following manner: by drawing values from a uniform probability distribution $\mathcal{U}$ on the interval $(-1, 1)$ this value is then multiplied by a noise level and the measurement value, see equation (F.4). The noise level is defined as a percentage of the measured value, and it can be varied to increase the noisiness of the measurements. The values drawn from the uniform distribution results in white noise, and it is implemented by using the random generator of `MatLab`. The state of the random generator is reset every time a new set of numbers is drawn, to properly compare the results. The noisy measurement value is defined by summing the noise and the measured value as in equation (F.5). The variance of the uniform distribution is given by equation F.6.

$$Noise = \mathcal{U}(-1, 1) \cdot noise - level \cdot measurement \tag{F.4}$$

$$Noisymeasurement = measurement + noise \tag{F.5}$$

$$\sigma^2 = \frac{(b-a)^2}{12} = \frac{2^2}{12} \tag{F.6}$$

Bibliography

[1] Etienne Balmes. Parametric families of reduced finite element models. theory and applications. *Mechanical Systems and Signal Processing*, 10(4):381 – 394, 1996. ISSN 0888-3270. doi: https://doi.org/10.1006/mssp.1996.0027. URL http://www.sciencedirect.com/science/article/pii/S0888327096900278.

[2] Etienne Balmes. Efficient sensitivity analysis based on finite element model reduction. In *IMAC 98*, 05 1997. URL https://www.researchgate.net/publication/267824986_EFFICIENT_SENSITIVITY_ANALYSIS_BASED_ON_FINITE_ELEMENT_MODEL_REDUCTION.

[3] A. BERMAN. System identification of structural dynamic models theoretical and practical bounds. In *Structures, Structural Dynamics, and Materials and Co-located Conferences*, pages –. American Institute of Aeronautics and Astronautics, May 1984. doi: 10.2514/6.1984-929. URL https://doi.org/10.2514/6.1984-929.

[4] Ake Bjorck. *Numerical Methods for Least Squares Problems*. Society for Industrial and Applied Mathematics, 1996. doi: 10.1137/1.9781611971484. URL https://epubs.siam.org/doi/abs/10.1137/1.9781611971484.

[5] A.F. Bower. Lecture notes on continuum mechanics, 2012. URL http://www.brown.edu/Departments/Engineering/Courses/En221/Notes/Kinematics/Kinematics.htm.

[6] C. Sidney Burrus. Iterative reweighted least squares. URL http://cnx.org/content/m45285/1.12/.

[7] C. Sidney Burrus. Basic vector space methods in signal and systems theory, January 2013. URL http://cnx.org/content/col10636/1.5/.

[8] Robert D. Cook, David S. Malkus, Michael E. Plesha, and Robert J. Witt. *Concepts and Applications of Finite Element Analysis*. John Wiley & Sons, Inc., USA, 2007. ISBN 0470088214.

[9] S. Ibrahim E. Fissette, C. Stavrinidis. Error location and updating of analytical dynamic models using a force balance method. In *Proceedings of the 6th International Modal Analysis Conference*, page pp. 1183–1190, 1988.

[10] Guido De Roeck Ellen Simoen and Geert Lombaert. Dealing with uncertainty in model updating for damage assessment: A review. *Mechanical Systems and Signal Processing*, 56-57:123 – 149, 2015. ISSN 0888-3270. doi: https://doi.org/10.1016/j.ymssp.2014.11.001. URL http://www.sciencedirect.com/science/article/pii/S0888327014004130.

[11] R. L. FOX and M. P. KAPOOR. Rates of change of eigenvalues and eigenvectors. *AIAA Journal*, 6(12):2426–2429, December 1968. ISSN 0001-1452. doi: 10.2514/3.5008. URL https://doi.org/10.2514/3.5008.

[12] M. Friswell and J.E. Mottershead. *Finite Element Model Updating in Structural Dynamics*. Solid Mechanics and Its Applications. Springer Netherlands, 1995. ISBN 9780792334316. URL https://doi.org/10.1007/978-94-015-8508-8.

[13] MI Friswell and JE Mottershead. Physical understanding of structures by model updating. In *International Conference on Structural System Identification, Kassel, Germany*, pages 81 – 96, 9 2001. Conference Organiser: Conference on Structural Systems Identification Other: Keynote Address.

[14] DNV GL. Class guideline dnvgl-cg-0127 finite element analysis, October 2015. URL https://rules.dnvgl.com/docs/pdf/DNVGL/CG/2015-10/DNVGL-CG-0127.pdf.

[15] S E Hirdaris and P Temarel. Hydroelasticity of ships: Recent advances and future trends. *Proceedings of the Institution of Mechanical Engineers, Part M: Journal of Engineering for the Maritime Environment*, 223(3):305–330, 2009. doi: 10.1243/14750902JEME160. URL https://doi.org/10.1243/14750902JEME160.

[16] Halil Karadeniz. *Stochastic Analysis of Offshore Steel Structures: An Analytical Appraisal*. Springer Series in Reliability Engineering. Springer, London, 2013. URL https://doi.org/10.1007/978-1-84996-190-5.

[17] Gyeong-Ho Kim and Youn-Sik Park. An improved updating parameter selection method and finite element model update using multiobjective optimisation technique. *Mechanical Systems and Signal Processing*, 18(1):59 – 78, 2004. ISSN 0888-3270. doi: https://doi.org/10.1016/S0888-3270(03)00042-6. URL http://www.sciencedirect.com/science/article/pii/S0888327003000426.

[18] David C. Lay. *Linear algebra and it's applications*. Pearson/Addison-Wesley,, Boston :, 3rd ed. update. edition, 2006. Includes index.

[19] John E. Mottershead, Michael Link, and Michael I. Friswell. The sensitivity method in finite element model updating: A tutorial. *Mechanical Systems and Signal Processing*, 25(7):2275 – 2296, 2011. ISSN 0888-3270. doi: https://doi.org/10.1016/j.ymssp.2010.10.012. URL http://www.sciencedirect.com/science/article/pii/S0888327010003316.

[20] R. B. NELSON. Simplified calculation of eigenvector derivatives. *AIAA Journal*, 14(9):1201–1205, September 1976. ISSN 0001-1452. doi: 10.2514/3.7211. URL https://arc.aiaa.org/doi/abs/10.2514/3.7211.

[21] JINSIANG SHAW and SUHADA JAYASURIYA. Modal sensitivities for repeated eigenvalues and eigenvalue derivatives. *AIAA Journal*, 30(3):850–852, March 1992. ISSN 0001-1452. doi: 10.2514/3.10999. URL https://doi.org/10.2514/3.10999.

[22] Dynamic Design Solutions. *Short course on Verification, Validation and updating of Finite Element Model for Structural Analysis. Theory, practice and applications.* DDS, Interleuvenlaan 64 , 3001 Leuven, Belgium, march 2017.